Fall 2009

Depth evaluation of damage to aircraft fuselage skins using microwave and millimeter wave methods

Andrew Dale McClanahan

Department:

DEPTH EVALUATION OF DAMAGE TO AIRCRAFT FUSELAGE SKINS USING MICROWAVE AND MILLIMETER WAVE METHODS

by

ANDREW DALE MCCLANAHAN

A THESIS

Presented to the Faculty of the Graduate School of the

MISSOURI UNIVERSITY OF SCIENCE AND TECHNOLOGY

In Partial Fulfillment of the Requirements for the Degree

MASTER OF SCIENCE IN ELECTRICAL ENGINEERING

2009

Approved by

R. Zoughi, Advisor
R. DuBroff
D. Beetner

ABSTRACT

The depth of damage to metal surfaces is a particularly useful, sought after, and difficult to obtain piece of information, and is used to guide repair decisions. For this investigation such damage is represented as rectangular slots (cracks) or cylindrical pits. Several millimeter wave methods are presented to evaluate depth. The quarter-wavelength resonant response of cracks, excited by a probing rectangular waveguide, allows evaluation of depth using the phase of reflection coefficient. A theoretical derivation is also supplied, modeling the system as the junction of two rectangular waveguides, the probing waveguide and the crack. If the crack is filled with a dielectric material, shallower cracks may be evaluated and the magnitude of reflection coefficient may be used instead of phase. This approach has the advantage of low sensitivity to crack width and probe position, but has some limitations in the minimum depth and the smallest openings which can be evaluated. The depth of pits and shorter cracks may be evaluated using the phase in a non-resonant approach, by comparison with reference curves. A dielectric slab-loaded waveguide probe is also developed which theoretically would allow measurement of smaller damages, of both opening and depth, as a resonance perturbation. Sensitivity to very small damage is apparent, but high sensitivity to probe position is also evident.

Extensive simulation results are presented for each approach, with supporting measurements. Evaluation of the depth of filled cracks, using the quarter-wavelength resonance approach, is, in particular, demonstrated in measurements for depths from 0.7-2.7 mm for three frequency bands and three filling materials.

ACKNOWLEDGMENTS

Thanks to Dr. Zoughi for his consistent efforts at making me better at whatever I put my hand to do; and for his long patience, particularly with my writing. Thanks to Dr. Kharkivskiy, who spent long hours pouring over data with me and whose knowledge of resonators was invaluable. Thanks to Tayeb, AK, and Kristen for the many second opinions and encouragement. Thanks to Andy for his many hours of measurements, without which this work would not be complete. Thanks to my committee members for being a part of my graduate studies. Thanks to Frank Hepburn, of the NASA Marshall Space Flight Center, and Emilio Nanni for facilitating V- and W-band PNA measurements.

Thanks to my parents, David, and Julie for the encouragement and support, and for the good food always waiting at home. Thanks to all the family and friends who lifted me up in prayer and asked about my progress.

And, finally, thanks to my Lord Jesus, who makes life worth living.

This work has been supported by a grant from the Air Force Research Laboratory (AFRL) under contract no. FA8650-04-C-5704 in conjunction with the Center for Aerospace Manufacturing Technologies (CAMT).

TABLE OF CONTENTS

LIST OF ILLUSTRATIONS

LIST OF TABLES

Page

1. INTRODUCTION

1.1. PROBLEM STATEMENT

Aircraft fuselage skins are susceptible to damage from a number of sources. Impact damage, corrosion and incidental damage caused by maintenance operations can affect the long-term structural integrity of fuselage skins. Even minor damage such as scratches and pits can negatively impact corrosion resistance and/or fatigue life. Impact of the loose ends of broken cables is one source of such damage and commonly produces openings of 0.13-0.76 mm, depths that are microscopic to 1 mm, and lengths from 0.13 to 250 mm (which will be modeled as cylindrical pits and rectangular slots or cracks).

Geometrical information about the damage can be used for maintenance, repair decisions and structural integrity evaluation of panels that are under stress while in service. Evaluation of damage depth is a particularly important piece of information since aircraft fuselages are made of relatively thin panels and any such damage may: a) be a considerable percentage of the panel thickness which may be critical from a structural integrity point of view (i.e., source of crack initiation), and b) protrude through a thin cladding layer used as a corrosion preventative agent. For instance, if damage has penetrated only slightly beyond the cladding layer the repair may be to burnish the damaged area; however, if the damage extends significantly beyond the cladding layer then the area will be blended, which requires an additional (ultrasonic) inspection to map the area and ensure that the material removed has not created negative margins in the skin. Determining whether damage has penetrated the cladding layer presents a particularly difficult case since the cladding layer often has thicknesses in the range of 0.04-0.08 mm.

Nondestructive evaluation (NDE) methods capable of rapidly detecting these damages and, more importantly, characterizing their dimensions can be very useful and are sought. Much research has been performed in the area of crack detection and evaluation, but typically for deeper and narrower cracks. For instance, methods for evaluation of crack depth have been developed for eddy-current [1-2], ultrasonic [3-4], AC field measurement [5], and microwave techniques using coaxial probes [6-8] and

rectangular waveguides (described in detail later). Methods of pit sizing have also been developed using eddy-current [9] and radiography [10] methods.

1.2. DAMAGE TYPES AND SAMPLES

For the purpose of evaluating damage dimensions three models were used to represent common damage geometries: long (i.e. the length of the sample) rectangular slots, finite rectangular slots, and cylindrical pits. It is important to note that an alternative definition of a long crack, related to the probe size, will be given in Section 1.3, and that definition will be used from that point on. Figure 1.1 shows schematics of the three damage types.

A variety of samples were available or prepared for this investigation with various dimensions and types of damage. All preparation methods allowed very accurate control of the width or diameter of damage due to the physical dimensions of the machining tools; however, the depth (and length for finite cracks) is dependent on the control of the machining tools and a wide range of depths were observed in the prepared samples with respect to the intended depths. Consequently, the depth of all damage (except as noted) was measured using a micrometer (with a precision of 0.025 mm) and those values are reported.

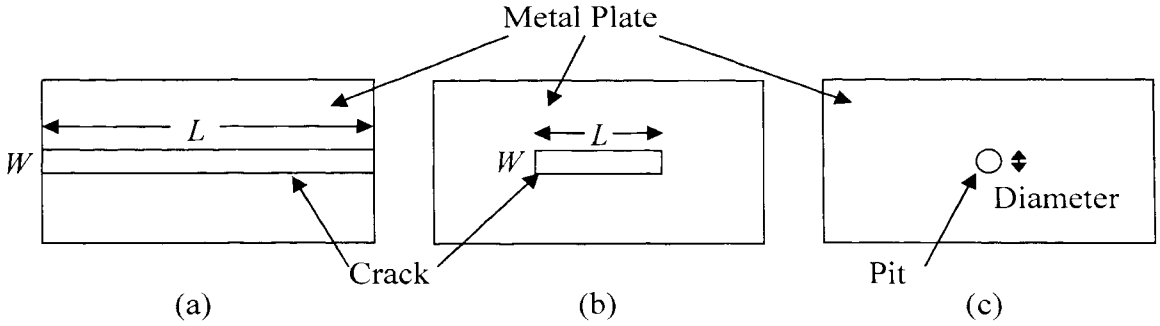

Figure 1.1. Plan view of three types of damage: a) long crack, b) finite crack, and c) pit (not-to-scale).

Three aluminum plates were prepared with long crack samples. The cracks were cut across the length of the plate with a saw, leaving a rectangular slot with a flat bottom,

one with $W = 0.5$ and 13 depths from 0.29-6.38 mm, another with $W = 0.85$ mm and 10 depths from 0.3-1.72 mm, and the third with two sets of cracks, three cracks with $W =$ 0.75 and three depths from 0.51-1.51 mm and three cracks with $D \sim 1$ mm and widths from 0.75-1.50 mm.

Two aluminum plates were prepared with finite crack samples. The cracks were machined, and have rounded ends and rounded bottoms. For the first plate three relatively large cracks were produced. The dimensions of the three cracks are given in Table 1.1.

Table 1.1. Actual crack widths, depths, and lengths for the large finite cracks sample.

Width (mm)	Depth (mm)	Length (mm)
0.88	0.55	4.70
0.88	2.00	6.48
2.00	2.00	7.62

The second finite crack plate was prepared with shallower cracks, and is shown in Figure 1.2. Figure 1.2a shows the schematic of this plate. The cracks were machined, leaving rounded ends, but milling bits were used for this sample to create flat-bottomed cracks. The cracks were cut to $L = 38$ mm, with widths of 0.25-2.54 mm and desired depths of 0.05-0.25 mm. The smallest bit broke while cutting the first crack so only one of the narrowest cracks was actually cut, and for only a portion of the intended length. A picture of the final plate is shown in Figure 1.2b. The actual (measured by micrometer) crack depths are given in Table 1.2.

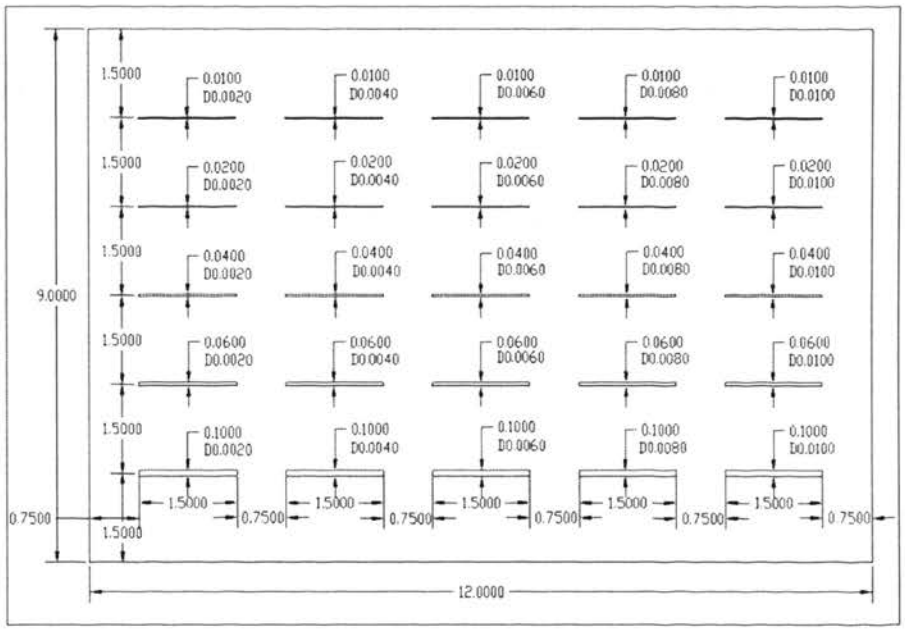

(a)

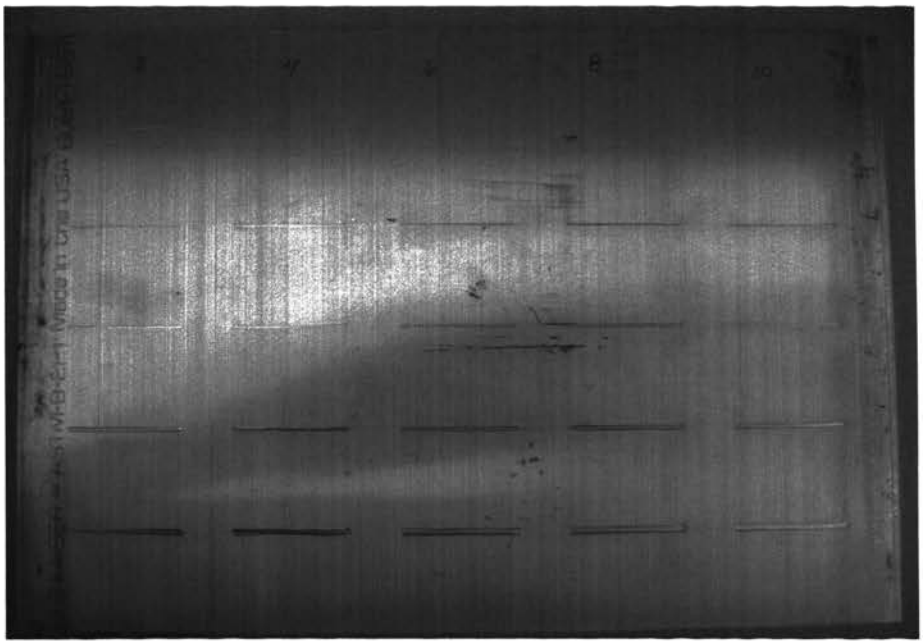

(b)

Figure 1.2. Shallow machined finite cracks sample: a) schematic and b) picture. In a), dimensions are in inches and "*D*" denotes the depth of the crack.

Table 1.2. Actual crack widths and depths for shallow machined finite cracks sample.

Desired Depth (mm) / *Width (mm)*	0.05	0.10	0.15	0.20	0.25
0.25	0.12	-	-	-	-
0.51	0.12	0.36	0.46	0.42	0.33
1.02	0.03	0.32	0.49	0.44	0.29
1.52	0.07	0.38	0.51	0.41	0.28
2.54	0.05	0.20	0.26	0.36	0.22

Three aluminum plates were prepared with pit samples. For the first plate relatively large pits were drilled, leaving a rounded bottom. The pits had a diameter of 2.75 mm and five depths from 0.48 to 2.51 mm. The second plate was prepared with shallower pits as shown in Figure 1.3. Figure 1.3a shows the schematic of the plate. The pits were machined using milling bits and have flat bottoms. The pits were cut with diameters from 0.25-2.54 mm and desired depths from 0.05-0.25 mm. A picture of the final plate is shown in Figure 1.3b. The actual measured pit depths are given in Table 1.3.

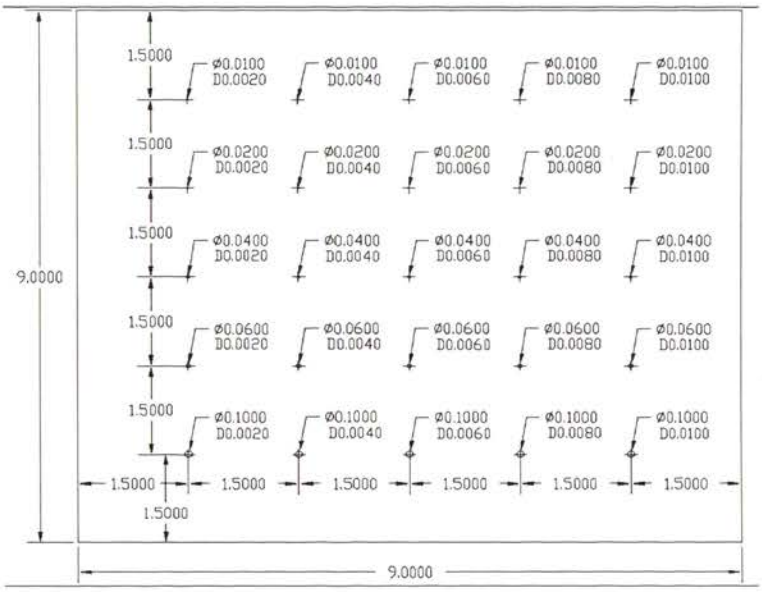

(a)

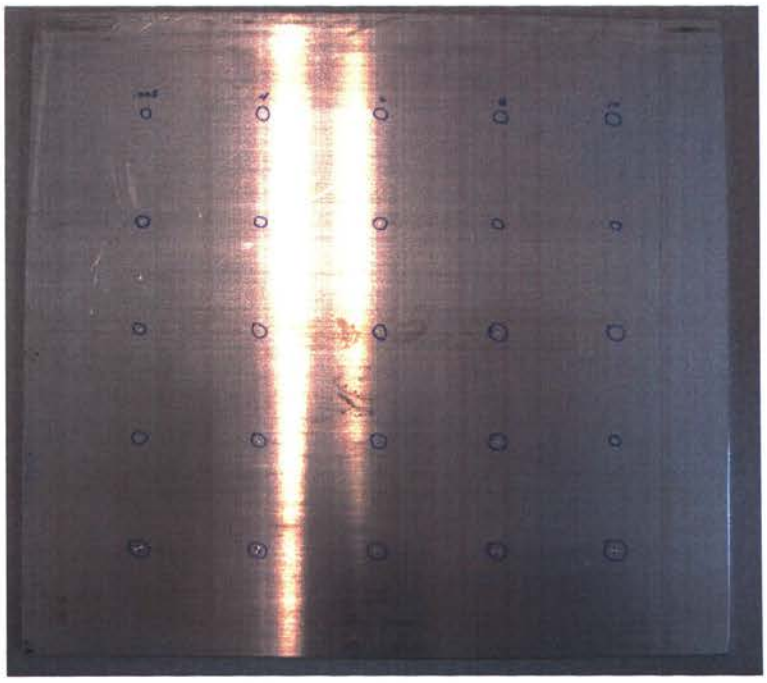

(b)

Figure 1.3. Shallow machined pits sample: a) schematic and b) picture. In a), dimensions are in inches and "*D*" denotes the depth of the pit.

Table 1.3. Actual pit widths and depths for shallow machined pit sample.

Desired Depth (mm) / *Width (mm)*	0.05	0.10	0.15	0.20	0.25
0.25	0.06	0.13	0.19	0.19	0.27
0.51	0.08	0.14	0.21	0.25	0.17
1.02	0.05	0.13	0.26	0.24	0.25
1.52	0.07	0.16	0.19	0.23	0.26
2.54	0.07	0.14	0.22	0.26	0.25

The third plate was prepared using laser machining, and is shown in Figure 1.4. Figure 1.4a shows the schematic of this plate. Visual inspection under magnification showed that these pits had irregular bottoms. Two sets of forty eight pits were cut with diameters from 0.2-1.0 mm and desired depths from 0.15-0.4 mm. A picture of the final plate is shown in Figure 1.4b. Accurate readings with the micrometer could not be achieved for pits with diameters smaller than 0.5 mm on this sample, so the desired depths are used for these pits. The measured pit depths are given in Table 1.4.

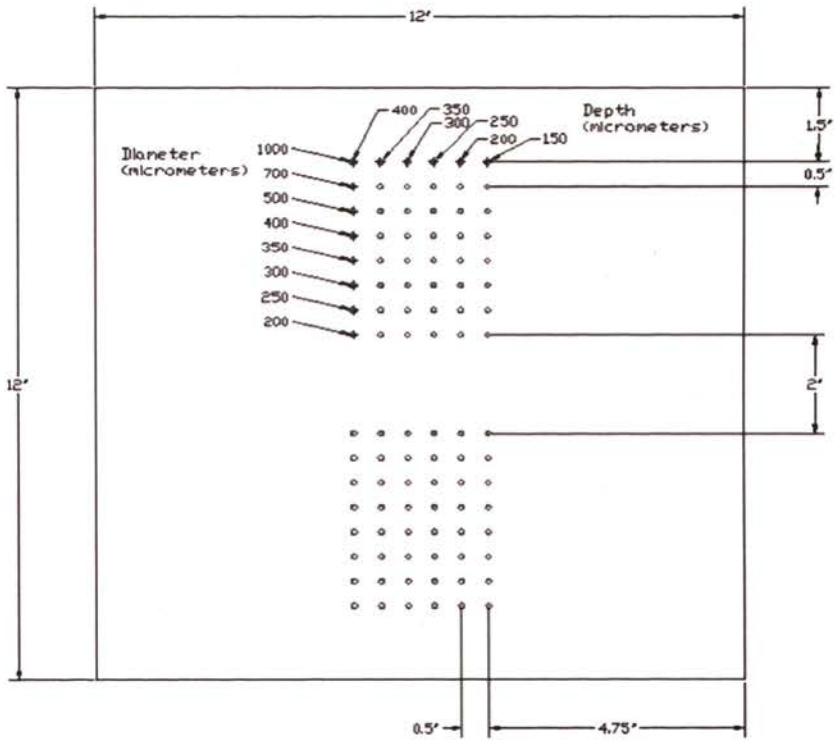

(a)

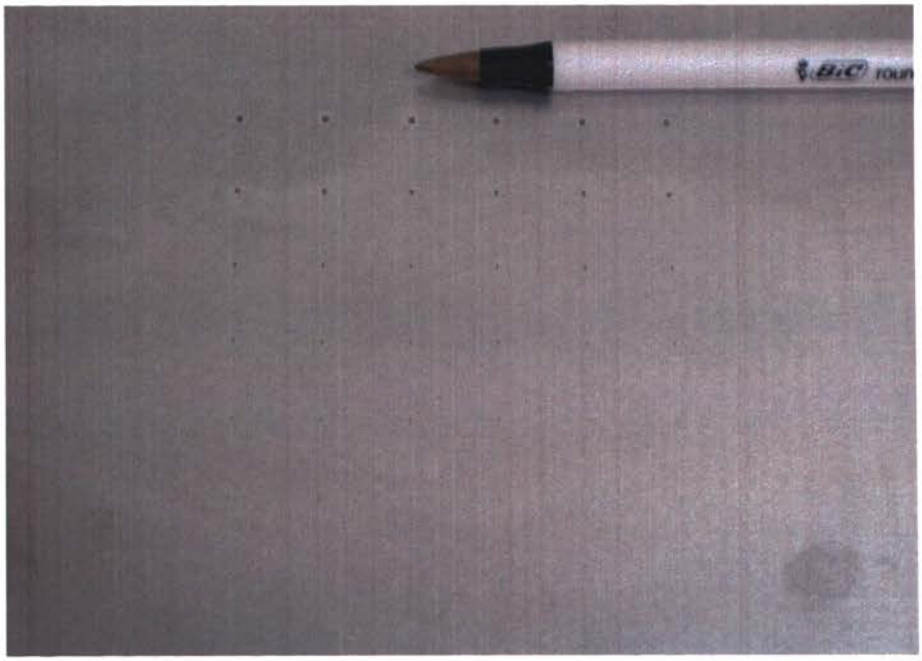

(b)

Figure 1.4. Laser cut pits sample: a) schematic and b) picture.

Table 1.4. Actual pit diameters and depths in laser cut sample.

Desired Diameter (mm) / *Width (mm)*	0.40	0.35	0.30	0.25	0.20	0.15
1.00	0.50	0.48	0.49	0.33	0.23	0.18
0.70	0.47	0.37	0.36	0.33	0.25	0.28
0.50	0.41	0.35	0.34	0.29	0.25	0.23

1.3. MICROWAVE AND MILLIMETER WAVE NDE FOR CRACKS

Nondestructive evaluation is defined as the science and practice of evaluating various properties of a material without compromising its utility and usefulness [11]. The properties of interest may be physical, chemical, mechanical, or geometrical in nature. In general, an interrogating signal is generated which interacts with the material under test and either the reflection or transmission of the signal is detected and analyzed to extract the relevant properties of the material [12-14].

For the current investigation a probing rectangular waveguide is used to deliver an electromagnetic signal to the damage and pick up the reflected signal. Signals are generated in the microwave (300 MHz to 30 GHz, with corresponding wavelengths of 1,000-10 mm) and millimeter wave (30-300 GHz, with corresponding wavelengths of 10-1 mm) frequency ranges. The reflection coefficient (complex ratio of reflected signal to transmitted signal) is then analyzed for obtaining geometrical information about the crack.

Extensive work has been previously performed in electromagnetically modeling the interaction of an open-ended rectangular waveguide with a crack at microwave frequencies and the consequent uses of such a waveguide for crack detection, sizing, tip location, and imaging [12-29]. However, for these investigations a crack was generally assumed to be a *through* crack or have a relatively large depth and narrow width compared to the damage of interest in this investigation. Work has also been performed in using rectangular waveguides for detection and evaluation of pits [30-33].

It was shown in [17], that the reflection coefficient is maximally disturbed by a crack when that crack is oriented parallel to the broad dimension of the probing

waveguide. The relative orientation of a crack is shown in Figure 1.5 with the dimensions of a crack (with width W, length L and depth D), and the probing rectangular waveguide (with broad and narrow dimensions of a and b, respectively) in contact with the metal plate. The probing waveguide is assumed to be operating in its dominant TE_{10} mode [34]. The crack is placed near the middle of the waveguide narrow dimension (i.e. centered in the waveguide). It has been shown that once such a crack is located near the middle of the probing waveguide aperture, the reflection coefficient measured at the probing waveguide aperture remains fairly constant as a function of the location of the crack [15], so precise placement is not critical. In addition, for a relatively narrow crack ($W << b$), whether its length is exactly equal to a, or longer than a, the reflection coefficient remains relatively unchanged [15]. Thus for simulations (unless otherwise noted), the crack length, L, is set equal to the broad dimension of the probing waveguide, a, as shown in Figure 1.5a. The cylindrical pits used are symmetric so orientation is not an issue for them. They are positioned, as much as possible, in the exact center of the waveguide, similar to cracks.

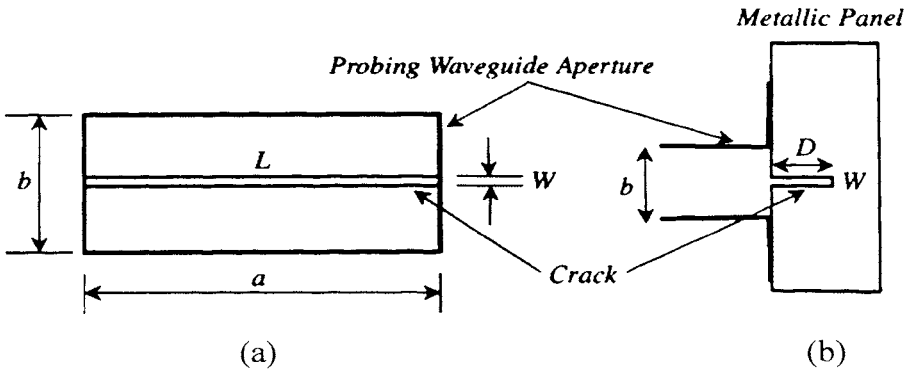

Figure 1.5. Schematic of a probing rectangular waveguide and a crack in a metal plate: a) plan-view and b) side-view (not-to-scale).

CST Microwave Studio® was used to perform simulations and obtain the complex reflection coefficient (referenced to the probing waveguide aperture),

$$\Gamma = \Gamma' + j\Gamma'' = |\Gamma| e^{j\Phi_\Gamma} \tag{1}$$

as a function of crack dimensions, material properties of the metal plate, frequency of operation, and material properties of dielectric filling the crack (in Section 3); where Γ', Γ'', $|\Gamma|$, and Φ_Γ are the real part, imaginary part, magnitude, and phase of the reflection coefficient, respectively.

X-band (8.2–12.4 GHz) and K-band (18–26.5 GHz) measurements were performed by tightly placing an open-ended rectangular waveguide probe over a crack, while the crack was as much as possible placed in the middle of the narrow dimension of the waveguide aperture, as shown in Figure 1.5a. The waveguide probe was then attached to an Agilent 8510C VNA and was calibrated at its aperture prior to the measurements. The measurements which will be shown were averaged 16 times using the internal averaging feature of the VNA. V-band (50–75 GHz) and W-band (75–110 GHz) measurements are also presented which were performed in the same fashion using an Agilent E8361A PNA (at the NASA Marshall Space Flight Center).

Swept frequency Ka-band (26.5–40 GHz) measurements were conducted using a custom-designed reflectometer whose dc output voltage is related to the magnitude of reflection coefficient measured at the probing waveguide aperture, as shown in Figure 1.6. A swept frequency oscillator and a frequency doubler are used to generate a swept frequency signal covering Ka-band frequencies. The signal is then fed through an isolator and a directional coupler to the probing waveguide. The reflected signal is then rerouted to a detector and a digital voltmeter (DVM). The dc output voltage is then proportional to

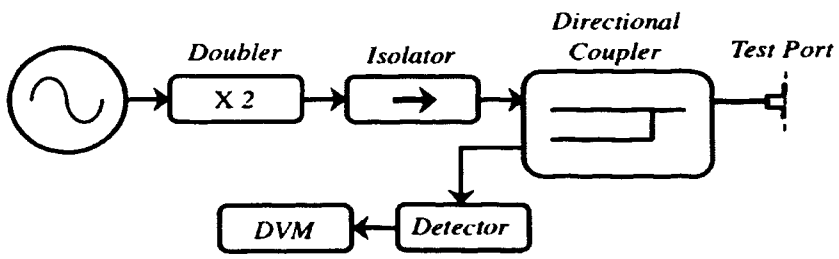

Figure 1.6. Schematic of Ka-band magnitude reflectometer.

the squared magnitude of reflection coefficient at the probing waveguide aperture. The measured data was smoothed across frequency and normalized per frequency point to a measurement of an aluminum plate without a crack (i.e. a short), to remove some of the frequency dependent variations in the measurement system due to the various components.

The thesis, including the present section, contains five sections. The second section provides an analysis of an empty waveguide used to probe an empty crack. A detailed discussion of the quarter-wavelength resonance of the crack is included as well as consideration of depth evaluation outside of the resonance. The third section analyzes an empty waveguide used to probe a dielectric-filled crack, with the resulting considerable change in the resonant properties. The measurement and estimation of the dielectric properties of water, corn oil and barium titanium oxide, which were used as filling materials, is also discussed. The forth section details the development of a dielectric slab-loaded waveguide probe, which was used to increase sensitivity to small damage, and its uses in depth evaluation. The fifth section gives a summary of the work performed, potential further uses of this work, and the steps that still need to be taken to prepare this work for its final use in depth evaluation.

2. EMPTY DAMAGE

2.1. LONG CRACKS

2.1.1. Approach/Theoretical Background. It has been noted that for a probing waveguide centered on a crack an abrupt transition occurs in the phase of reflection coefficient when the crack depth is approximately equal to one quarter of the guide wavelength, and then every half-guide wavelength thereafter [18]. The long crack and the probing waveguide structure, as presented in Section 1.3, can be viewed as a junction of two waveguides with different narrow dimensions or widths; namely, the probing waveguide and the crack. Subsequently, the bottom of the crack acts as a short-circuit. The short-circuited quarter-wavelength line is a well-known resonator [34] and these abrupt transitions are indications of the resonance.

The resonant response of the crack can be characterized by its resonant frequency, f_o, and its Q-factor. With the crack modeled as a rectangular waveguide the relationship between crack depth and the resonant frequency, f_o, is given by [34]:

$$D = \frac{\lambda_{go}}{4} = \frac{1}{4\sqrt{\left(\frac{f_o}{c}\right)^2 \varepsilon_r' - \left(\frac{1}{2L}\right)^2}}, \tag{2}$$

where λ_{go} is the guide wavelength in the crack waveguide at the resonant frequency, c is the speed of light in free-space, and $\varepsilon_r' = 1$ for an empty crack. If the frequency is swept then the phase transitions (resonances) will occur at different frequencies for different depths. Therefore, a swept frequency measurement can be used to obtain the resonant frequency for a crack, and the crack depth can be calculated from that frequency.

The loaded Q-factor of a resonator, Q_{Lo}, as a measure of the losses in the system is given by [34]:

$$\frac{1}{Q_{Lo}} = \frac{1}{Q} + \frac{1}{Q_e}, \tag{3}$$

where Q is the unloaded Q-factor due to the resonator itself and Q_e is the external Q-factor which is related to losses in the external feeding circuit (the probing waveguide in this case). The unloaded Q-factor results from the conductor loss in the crack walls such that:

$$Q = Q_c, \tag{4}$$

where Q_c is the Q-factor due to conductor (wall) loss (this distinction is needed in Section 3 when dielectric losses are introduced and influence the unloaded Q-factor as well).

The Q-factor related to conductor losses, Q_c, for the rectangular crack can be estimated from the well-known equations for a short-circuited quarter-wavelength resonator by [34]:

$$Q_c = \frac{\pi}{\lambda_{go}\rho_c\alpha_c}, \tag{5}$$

where α_c is the attenuation constant due to conductor losses and ρ_c is the electric field filling-factor for the crack (ratio of the electric field energy stored in the crack to the electric field energy stored in entire resonant volume). The filling-factor accounts for the portion of the resonant field which may extend into the probing waveguide.

The attenuation constant due to conductor losses in the crack walls can be calculated in the same manner as that for a rectangular waveguide (assuming a non-ferromagnetic conductor) as [34]:

$$\alpha_c = \frac{\sqrt{\pi}}{\sqrt{\sigma\mu_0\left(4\varepsilon_r'\left(\frac{f}{c}\right)^2 - \left(\frac{1}{a}\right)^2\right)}}\left(\frac{1}{L^3} + \frac{2}{W}\varepsilon_r'\left(\frac{f}{c}\right)^2\right), \tag{6}$$

where σ is the wall conductivity and μ_0 is the permeability of free-space.

The coupling between the crack resonator and the probing waveguide can have a significant impact on the obtained results, as will be shown in the following sections. It can be denoted by a coefficient of coupling given by [34]:

$$g = \frac{Q}{Q_e}. \tag{7}$$

From (7) three cases of the coupling between the resonator (crack) and the probing waveguide can be distinguished; namely the region where, 1) the resonator is undercoupled, $g < 1$; 2) the resonator is critically coupled, $g = 1$; and 3) the resonator is overcoupled, $g > 1$, to the probing waveguide [34].

2.1.2. Simulation Results. To demonstrate the influence of crack width and depth in the absence of dielectric and conductor losses, first an empty shallow crack in a perfectly conducting plate is considered. The crack length is set equal to a, as shown in Figure 1.5a. As a result of the absence of any losses, the magnitude of reflection coefficient measured at the probing waveguide aperture remains constant (i.e., $|\Gamma| = 1$) while the phase of the reflection coefficient changes primarily as a function of crack depth. When the crack width is equal to the narrow dimension of the probing waveguide, b, (an unrealistic situation but only discussed here for demonstrating the phase variation characteristics) the crack simply becomes a shorted waveguide section extending the reference plane. In this case, the phase varies linearly as a function of crack depth with a change of 180° from a short (the case of D = 0) when the crack depth is equal to a quarter-wavelength ($\lambda_g/4$). As the crack width decreases, the phase variation is no longer linear and the phase reversal may not occur at exactly at $\lambda_g/4$. Figure 2.1 shows the phase of reflection coefficient as a function of crack depth (normalized to λ_g) for three crack widths of $W = b$, $b/5$ and $b/25$, respectively, simulated at X-band. It can be observed that for all three widths there is a 360° phase transition in the crack depth range of 0-0.5λ_g. The most significant feature is that the linearity in the phase variation becomes less and less as width decreases. Moreover, the resonant frequency shifts from $\lambda_g/4$ as a function of crack width, and this will be considered in detail later.

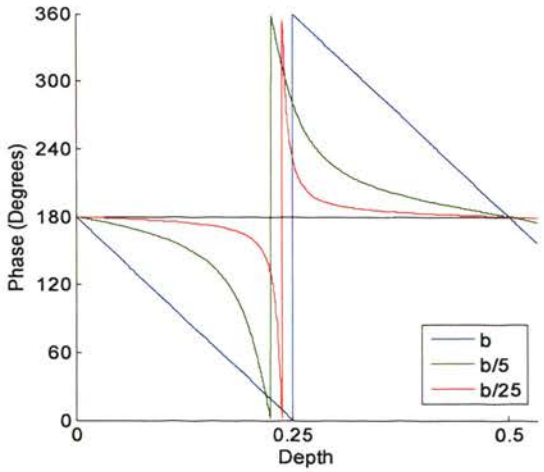

Figure 2.1. Simulated phase of reflection coefficient as a function of electrical depth (depth is given relative to wavelength) for empty cracks in a perfect electric conductor with three widths (including $W = b$, matched waveguide case). Simulations were performed at 10.3 GHz (X-band) with varying physical depth.

Figure 2.2 shows the phase of reflection coefficient as a function of frequency for cracks with several depths and widths at V-band. Figure 2.2a shows the phase of reflection coefficient for cracks with $W = 0.25$ mm and four different depths. The variation of the depth shifts the resonant frequency; in particular, shallower scratches cause the transition to occur at higher frequencies. This shift of resonant frequency occurs as described in (2) and is the foundation of this depth evaluation approach. Figure 2.2b shows the phase of reflection coefficient for cracks with $D = 1.27$ and four different widths, indicating that cracks with smaller widths have a more abrupt or sharper phase transition. These relationships have also been previously observed [18].

It was shown in [35] that the magnitude of reflection coefficient for a quarter-wavelength short-circuited waveguide changes slightly (decreases) if the conductor losses in waveguide walls are taken into account. In this investigation several cracks in metal plates with different conductivities were investigated and it was observed that *narrow* quarter-wavelength short-circuited cracks exhibit resonant behavior in the magnitude of reflection coefficient as well as in the phase. For instance, Figure 2.3 shows the simulated frequency dependence of the complex reflection coefficient, for cracks with $D = 1.03$ mm and five different widths, in an aluminum plate with a conductivity of

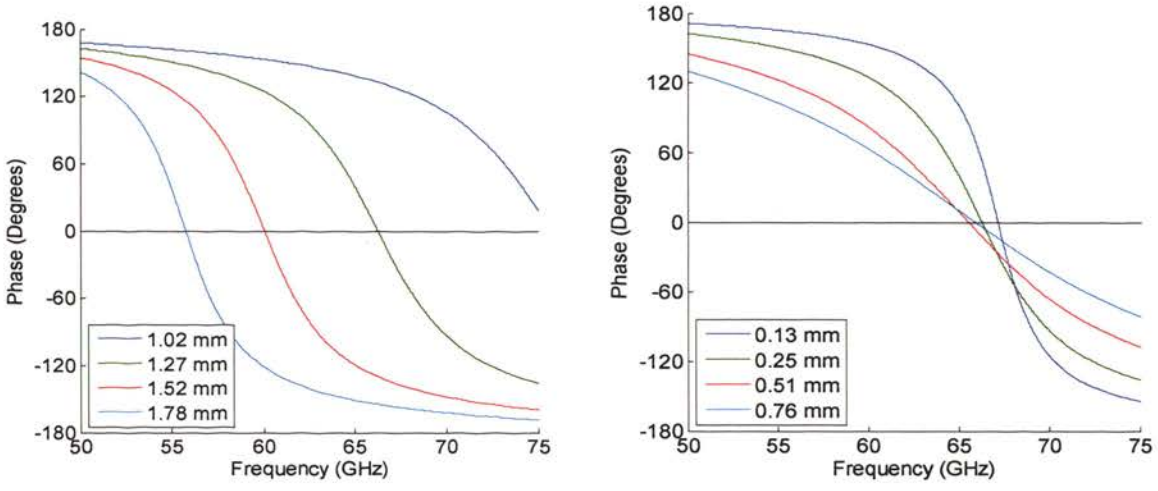

Figure 2.2. Simulated phase of the reflection coefficient as a function of frequency for empty cracks with several depths and widths at V-band: a) $W = 0.25$ mm and four depths, and b) $D = 1.27$ mm and four widths.

$\sigma = 3.72x10^7$ (S/m) at W-band. The probing waveguide dimensions for this band are $a =$ 2.4 mm and $b = 1.3$ mm, respectively. As shown in Figure 2.3a, the magnitude of reflection coefficient no longer remains constant (e.g., $|\Gamma| = 1$) and exhibits a resonant response for narrow crack widths. This resonant response has a minimum at the resonant frequency corresponding to the quarter-wavelength resonance. At least two important observations can be made from Figure 2.3a. First, the resonant frequency of the quarter-wavelength short-circuited crack may be found from the magnitude of reflection coefficient, and its depth can then be evaluated using (2). Second, the Q-factor and magnitude at the resonance are highly dependent on crack width and must be considered in determining the measurability of the resonant frequency. In particular, Figure 2.3a shows that $|\Gamma|$ at the resonance is non-monotonically dependent on width. For instance, for the widest cracks ($W = 1.3$ and 0.2 mm), $|\Gamma|$ is close to 1. However, as the width decreases, $|\Gamma|$ initially decreases and approaches zero (shown by the crack with $W = 0.022$ mm). As the width is further decreased, $|\Gamma|$ increases (e.g., $|\Gamma| = 0.65$ for the crack with $W = 0.01$) and approaches 1 as the width is reduced to zero (not shown in Figure 2.3a). It should be noted that the resonant frequency is relatively insensitive to crack width for the

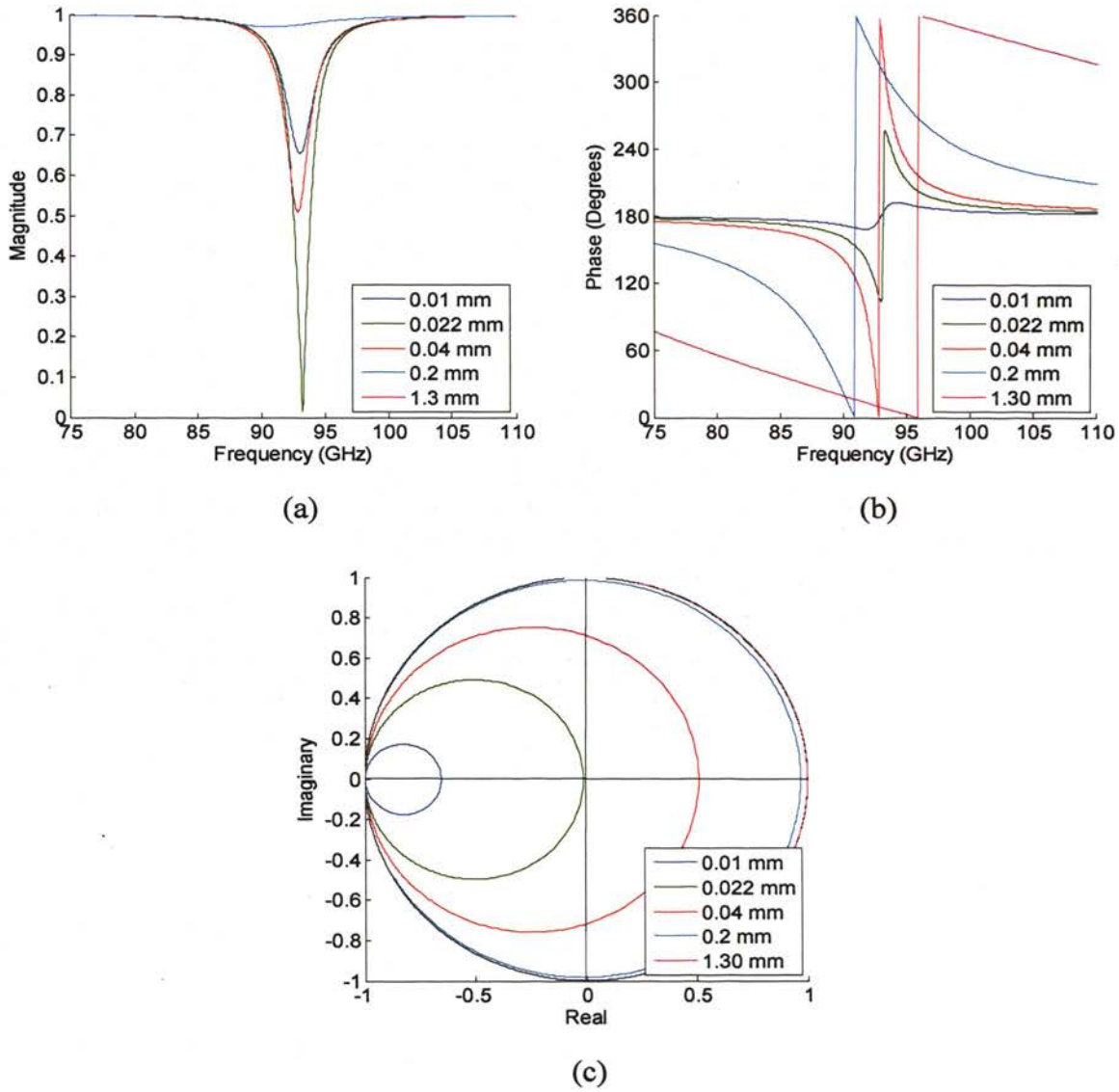

Figure 2.3. Simulated complex reflection coefficient of empty cracks in aluminum with $D = 1.03$ mm and five widths at W-band: a) magnitude and b) phase of the reflection coefficient as a function of frequency, and c) reflection coefficient in the complex polar plane.

range of 0.01–0.04 mm, as shown in Figure 2.3a. This observation is confirmed by the phase of reflection coefficient, shown in Figure 2.3b.

Plotting the results in the complex polar plane provides some additional insight to the resonance behavior, as shown in Figure 2.3c. In this format where the complex

reflection coefficient crosses the real axis ($\Gamma'' = 0$) indicates the minimum associated with $|\Gamma|$ (in Figure 2.3a) and thus also the resonant frequency. At $\Gamma'' = 0$ if the width is smaller than 0.022 mm, Γ' is negative (e.g., $\Gamma' = -0.65$ at the resonance for $W = 0.01$ mm) and as the width decreases the circle traced by the resonant response approaches a point located at $\Gamma = \Gamma' = -1$ which is the same effective reflection as a metal plate without a crack. If the width is greater than 0.022 mm, Γ' is positive (e.g., $\Gamma' = 0.51$ at the resonance for $W =$ 0.04 mm) and as the width increases the resonant response approaches a circle of (radius) $\Gamma' = 1$, which corresponds to the lossless case. This represents when the crack is overcoupled, as explained below.

Figure 2.4 shows two characteristics of the resonant response as functions of width for a crack with $D = 1.03$ mm in plates of four different metals ($\sigma_{Brass} = 1.57x10^7$, $\sigma_{Aluminum} = 3.72x10^7$, $\sigma_{Copper} = 5.8x10^7$, and $\sigma_{Silver} = 6.17x10^7$ (S/m)). In Figure 2.4a the curve for the aluminum plate, for example, demonstrates the magnitude of reflection coefficient as shown in Figure 2.3a for the full range of considered widths (0 – 1.3 mm) at the resonant frequency (i.e. the magnitude minimum). These results show that the crack exhibits measurable resonant behavior for a narrow range of widths, from about 0.005–0.1 mm (assuming that it is measurable if at the resonance $|\Gamma| \leq 0.9$). Change in the conductivity of the metal plate shifts the width at which critical coupling (magnitude of zero) occurs, with lower conductivities resulting in larger widths.

The loaded Q-factor, Q_L, can be defined as the ratio of the resonant frequency, f_o, to the 0.7 (3-dB) bandwidth, Δf, such that:

$$Q_L = \frac{f_o}{\Delta f}. \tag{8}$$

Figure 2.4b shows the loaded Q-factor as a function of width. The solid lines are calculated from simulated resonant responses, similar to those shown in Figure 2.3a, according to (8). By comparison with Figure 2.4a the Q-factor maximums correspond to critical coupling. The Q-factor drops off quickly to either side. The Q-factor in the overcoupled region does not depend on the conductivity of the metal, while in the

undercoupled region the loaded Q-factor is related to the conductor Q-factor, as will be shown.

The condition of critical coupling is $Q_e = Q$, so the loaded Q-factor at critical coupling can be determined from (3) – (6) and is shown in Figure 2.4b as the dashed curves. A filling factor of 0.55 was used to match this curve to the points of critical coupling, which implies that a large portion of the resonant field extends into the probing waveguide.

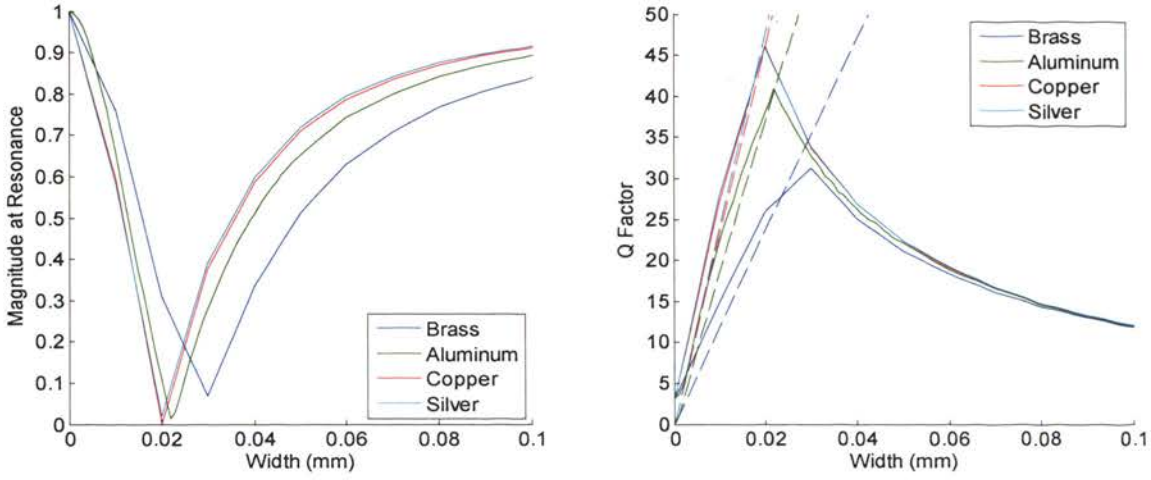

(a) (b)

Figure 2.4. Simulated characteristics of resonant response as functions of width for empty cracks in four metals with $D = 1.03$ mm at W-band: a) magnitude of reflection coefficient at resonant frequency and b) Q-factor. In b) the solid lines are from simulation and the dotted lines are $Q_C/2$ from (3) – (6).

The described features of the resonant responses can be explained by the coupling between the probing waveguide and the crack. From (7) it can be seen that at critical coupling ($g = 1$) the resonator is matched to the probing waveguide ($Q_c = Q_e$). If the aluminum conductor case is considered, the results for $W = 0.022$ mm correspond to critical coupling in which $\Gamma = 0$ at the resonant frequency (Figure 2.3a) and the loaded Q-factor is also maximum at this width (Figure 2.4b). As the width decreases the conductor

loss increases (Eq. (6)) and the resonator becomes undercoupled ($g < 1$, e.g., $W = 0.01$ mm) resulting in a reduction in the Q-factor. When $W > 0.022$ mm the resonator is overcoupled ($g > 1$, e.g., $W = 0.04$ mm), approaching the case when the entire signal is coupled into the crack (e.g., at $W = 0.2$ mm). In this case the external (to the crack) loss becomes dominant, causing the decrease in the loaded Q-factor.

2.1.3. Sensitivity Analysis. Using (2) to evaluate crack depth, by measuring the resonant frequency, shows no dependence on crack width since it is a close approximate form for evaluating crack depth (i.e., only considers the crack geometry). However, the simulations which include the entire structure, and are hence more accurate, showed some dependency between crack width and its resonant frequency. Therefore, to determine the sensitivity of evaluating crack depth using (2) to crack width, the following was considered. Simulations were conducted for several combinations of crack widths and depths (i.e., "actual" widths and depths). Subsequently, the resonant frequencies from the simulations (in effect representing actual measurements) were used in conjunction with (2) to estimate the depth. Three depths of $D = 0.92$, 1.1, and 1.41 mm, were used with varying widths in W-band. Figure 2.5 shows the error in depth estimation (compared to the depth used in simulation) as a function of crack width normalized to b, for three

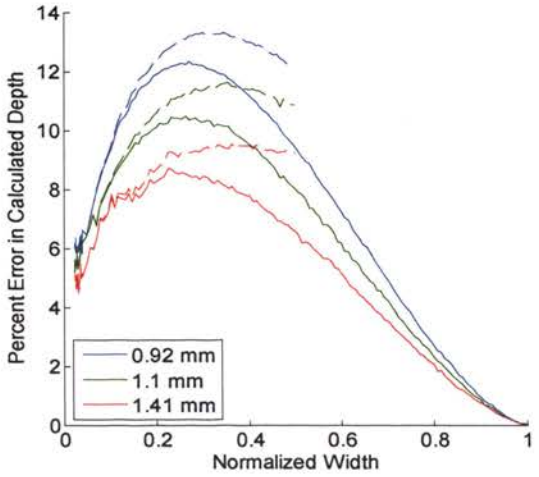

Figure 2.5. Simulated error in depth evaluation as a function of width (normalized to b) for empty cracks in aluminum with three depths at W-band: using phase (solid) and magnitude (dashed) of reflection coefficient.

depths using the phase (solid) and magnitude (dashed) of reflection coefficient to find the resonant frequency. The results show that using phase there is a maximum of 12.5% error in overestimating crack depths for the entire range of widths, as shown in Figure 2.5. The error also depends on the actual value of crack depth (i.e., error is less for deeper cracks). Using the magnitude the results agree well with the phase results for narrow cracks, up to a normalized width of about 0.2. At larger widths the error is higher for magnitude than phase; and for widths larger than 0.5 the magnitude dip is so small it cannot be used. The effect of the difference in widths between two waveguides (i.e. probing waveguide and crack) has been described as a parallel "junction capacitance" [36-37].

A correction factor was derived from these curves by matching to a polynomial such that:

$$D_{corrected} = \left[\left(0.62 f_n\right)\left(-0.43 W_n^3 + 0.85 W_n^2 - 0.37 W_n - 0.05\right) + 1 \right] D_{calculated}, \qquad (9)$$

where f_n is the resonant frequency normalized to the waveguide cutoff frequency and W_n is the crack width normalized to b. If (9) is applied to the phase results in Figure 2.5 the error is reduced to an average of 0.24%, with a maximum of 1.6%. The largest remaining error occurs for the narrowest cracks and if the crack width is restricted to $\geq 0.11b$ the average error is reduced to 0.15%, with a maximum of 0.5%.

In the derivation of (2), it was assumed that cracks with lengths longer than the broad waveguide dimension, a, would behave as if the length was equal to a. Simulations were performed with crack lengths greater than a to test this assumption. For the range of lengths used in these simulations (a–$2a$), the entire crack is still within the waveguide flange. Simulations were conducted for several combinations of crack widths and lengths, and the resonant frequency was found using the phase of reflection coefficient. Figure 2.6 shows the change in resonant frequency (compared to a crack with $L = a$) as a function of crack length, normalized to a, for a depth of 1 mm and five widths at W-band. The results show that there is a maximum of 5.5% change in resonant frequency over this range of lengths. Once the crack length exceeds $1.7a$ there is no further change in the resonant frequency. The change in the resonant frequency is similar between the six crack widths, and thus insensitive to width. Since this behavior is insensitive to length greater than $1.7a$

and width, for a crack with $L \geq 1.7a$ this error could be corrected by multiplying the measured resonant frequency by a constant.

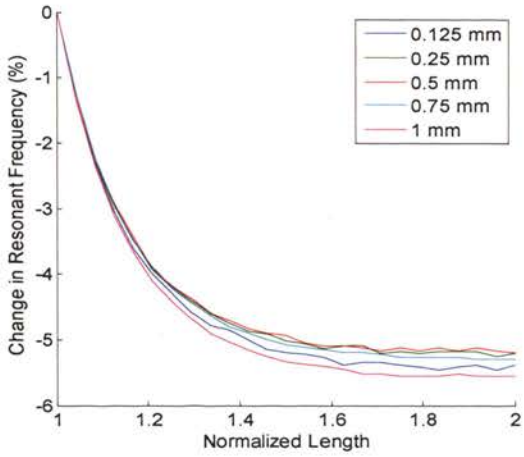

Figure 2.6. Simulated percentage change in resonant frequency as a function of crack length (normalized to a) for empty cracks in aluminum with $D = 1$ mm and five widths at W-band.

2.1.4. Measurement Results. Measurements were performed on cracks with $W =$ 0.5 mm and three depths in an aluminum plate at K-band using a VNA. Figure 2.7 shows the measured and simulated frequency dependence of the complex reflection coefficient for cracks with $W = 0.5$ mm and three depths at K-band. Figure 2.7a shows the phase of reflection coefficient with accompanying simulations (the simulations were performed using cracks in a perfect electric conductor). The measurements match the simulation results quite well, with similar curves for each depth and the resonant frequencies differing by less than 3%. The measurement results show the resonant response for all three cracks. The resonant frequency is clearly shifted as a function of crack depth, as expected. Figure 2.7b shows the measured magnitude of reflection coefficient for the same cracks. Dips can be observed in the magnitude for each crack which by comparison to Figure 2.7a, occur at the resonant frequencies. These are the consequence of conductor losses, as described previously, and are small since these cracks are much wider than the width for critical coupling. Figure 2.7c shows these measurements in the complex plane.

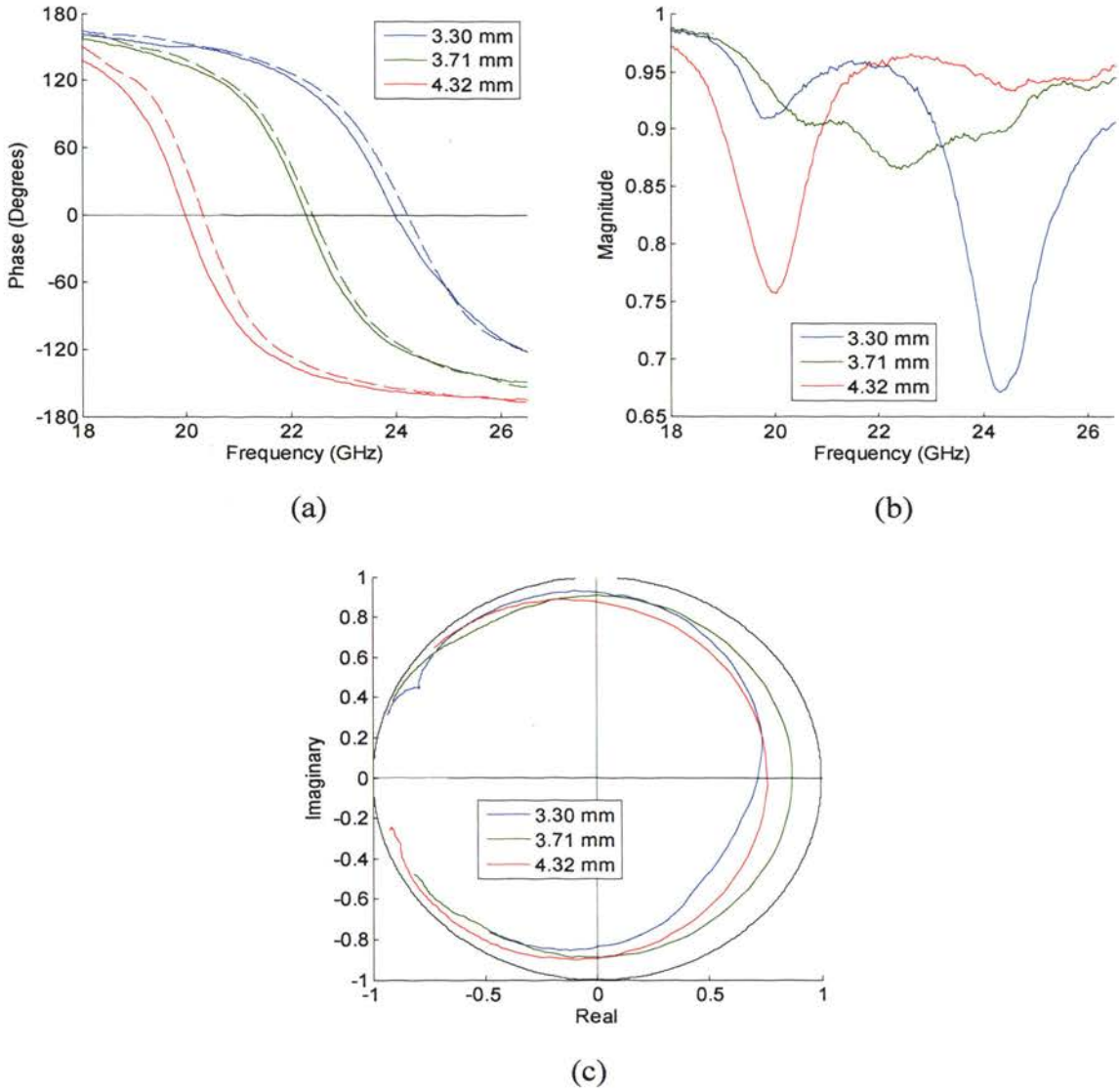

Figure 2.7. Measured (solid) and simulated (dashed) complex reflection coefficient of empty cracks in aluminum with $W = 0.5$ mm and three depths at W-band: a) magnitude and b) phase of the reflection coefficient as a function of frequency, and c) reflection coefficient in the complex polar plane.

The resonant circles are clearly seen and have a radius close to one, indicating that the cracks are highly overcoupled.

Figure 2.8 shows a comparison of the estimated depth using the described method and the actual crack depth (measured by a micrometer), for the K-band measurements shown in Figure 2.7. The resonant frequencies were found from the zero in the phase of

reflection coefficient, and the depth was estimated using (2). Figure 2.8a clearly shows the ability of this method to estimate crack depth. However, error in depth estimation may be as much as 20%. Figure 2.8b shows the estimated depth with the correction factor (from (9)) for width, which reduced the error to 12%. Sources of this error may include the positioning of the waveguide over the crack, the approximation of the crack length to equal the waveguide *a* dimension used in the derivation of (2), and error in the measurement of "actual" crack depth.

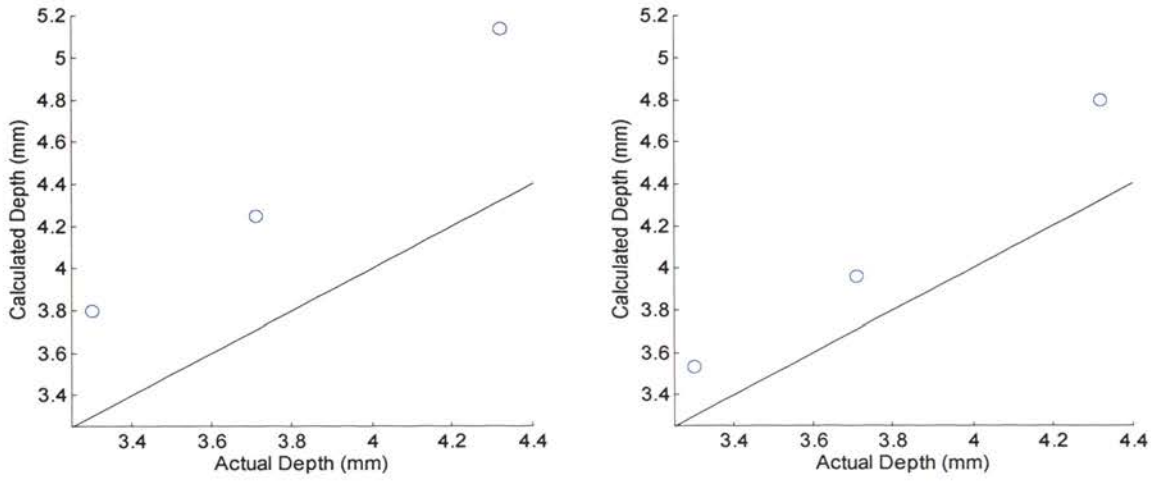

Figure 2.8. Comparison of depth calculated from measurements (using Equation (2)) to actual depth (as measured by micrometer) for K-band measurements: a) without and b) with correction factor for width.

2.1.5. Cracks Shallower than a Quarter-Wavelength. It may not be possible to provide very high frequency measurements to observe the quarter-wavelength resonance for very shallow damage. It may also be desirable for ease of measurement or design of measurement systems to use single frequency measurements. Consequently, the use of the phase of reflection coefficient to evaluate depth was investigated for cracks shallower than a quarter-wavelength.

Figure 2.9 shows the measured (solid) and simulated (dashed) phase of reflection coefficient for cracks with two widths and several depths at W-band. For each of the cracks in Figure 2.9 the depth is less than a quarter-wavelength and, consequently, the resonant frequency will be higher than the operating frequency band. The measured data show some variance from the simulations, with in general a greater phase change in measurement than simulation. However, for each width, in both simulation and measurement, the curves are sorted by depth with deeper cracks resulting in a larger phase change. This is expected since the resonant frequency will be lower, and thus closer to the operating frequency band, for the deeper cracks than for the shallower cracks. Since the resonant frequency is closer more of the tail of the resonant response is seen. The cracks in Figure 2.9a have a diameter of 0.51 mm while the cracks in Figure 2.9b have a diameter of 1.02 mm. The wider cracks in Figure 2.9b result in a larger phase change than in Figure 2.9a, which is also expected since wider cracks have a more gradual phase change in the resonant behavior (Figure 2.2b), the effects of which will extend further in frequency. If two curves of different width but a common absolute phase of ~150° at 75 GHz, e.g. 0.46 mm in Figure 2.9a and 0.29 mm in Figure 2.9b, are

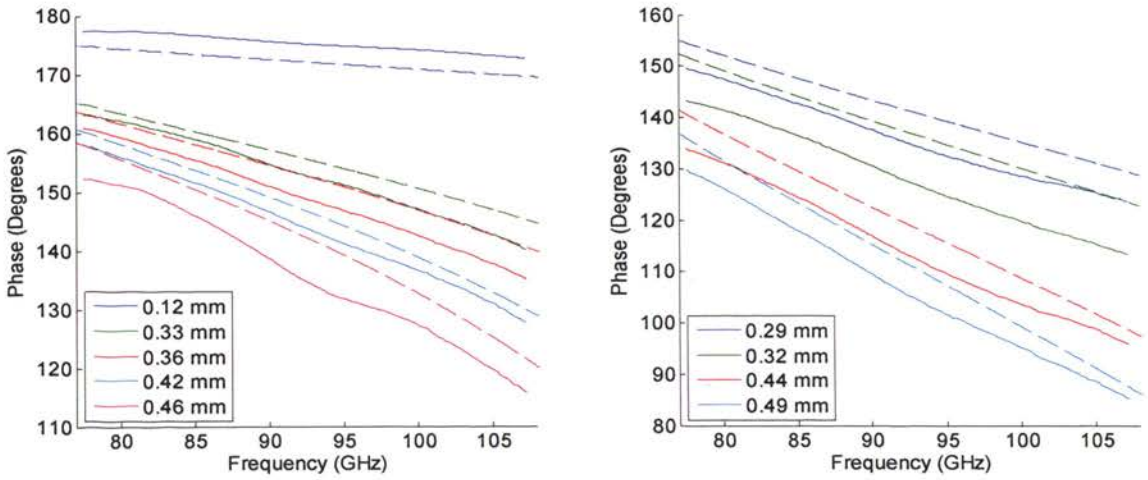

(a) (b)

Figure 2.9. Measured (solid) and simulated (dashed) phase of reflection coefficient as a function of frequency for empty cracks in aluminum with two widths and several depths at W-band: a) $W = 0.51$ mm with five depths and b) $W = 1.02$ mm with four depths.

compared it can be observed that the slopes are different. So it should be possible to distinguish between the effects of depth and width if the phase is known for at least two frequency points, and crack depth could then be evaluated.

2.2. FINITE CRACKS

Finite cracks present a more complex electromagnetic problem than long cracks, since several additional boundaries are introduced and the length of the crack becomes important as an additional geometrical parameter. The behavior can be somewhat similar to long cracks, however, if the crack length is sufficient to support a propagating mode for a portion of the frequencies within the band. Equation (2) is a valid approximation as long as a propagating mode is supported; otherwise the quarter-wavelength resonance cannot exist.

Simulations were performed to determine the frequencies that can be propagated for various crack lengths, as shown in Figure 2.10. Figure 2.10a shows the simulation geometry. The signal coupled from port 1 to port 2 will be very small if no propagating mode is supported in the crack since in that case the signal will be significantly

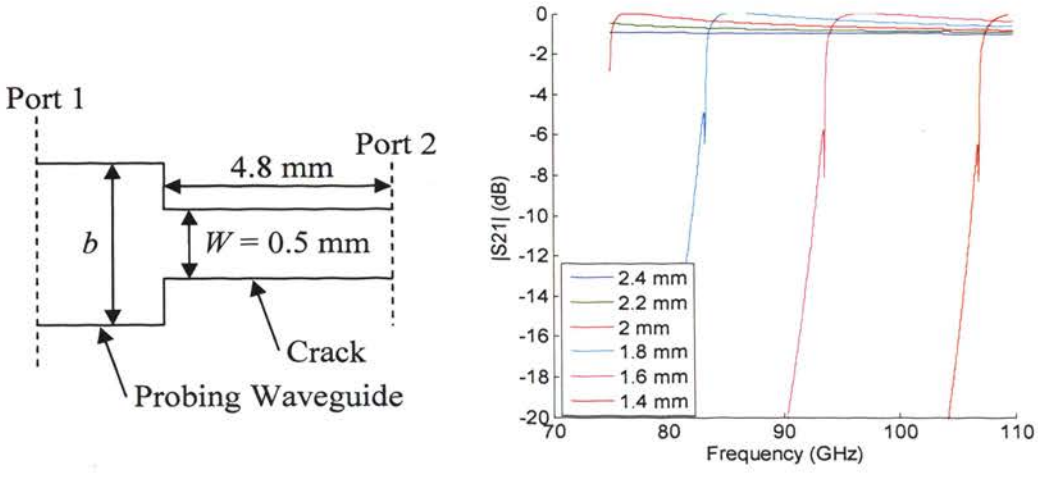

(a) (b)

Figure 2.10. Simulated signal transfer from a probing waveguide to an empty finite crack at W-band: a) side-view of simulation schematic (not-to-scale) and b) $|S_{21}|$ for 6 crack lengths.

attenuated as it travels the 4.8 mm in the crack to port 2. Figure 2.10b shows $|S_{21}|$ for cracks in a perfect electric conductor with 6 different lengths at W-band. It is observed that $|S_{21}|$ is reasonably high for the 2.4 and 2.2 mm long cracks over the entire frequency band, so these cracks will support a propagating mode for the full band. The 2, 1.8, 1.6, and 1.4 mm long cracks each have a sharp drop in $|S_{21}|$, where for lower frequencies a propagating mode is not supported and for higher frequencies one is supported. Following the trend of this figure, and according to well-known waveguide equations, for cracks with $L \leq 1.2$ mm = $a/2$ no propagating mode will be supported within the frequency band.

Figure 2.11 shows the simulated phase of reflection coefficient for cracks with D = 1.4 mm, W = 0.5 mm, and ten different lengths, starting from $L = a$ = 2.4 mm, at W-band. It is seen that the frequency where the phase crosses zero (the resonant frequency) shifts to the right (higher frequencies) as the crack length decreases, as would be expected from (2). Furthermore, this shift accelerates as the length is reduced. For sufficiently long cracks where a propagating mode is supported for some portion of the frequency band, with a proper depth, a resonance may be observed, as shown in Figure 2.11a. If the length is further reduced the resonance first shifts out of the frequency band

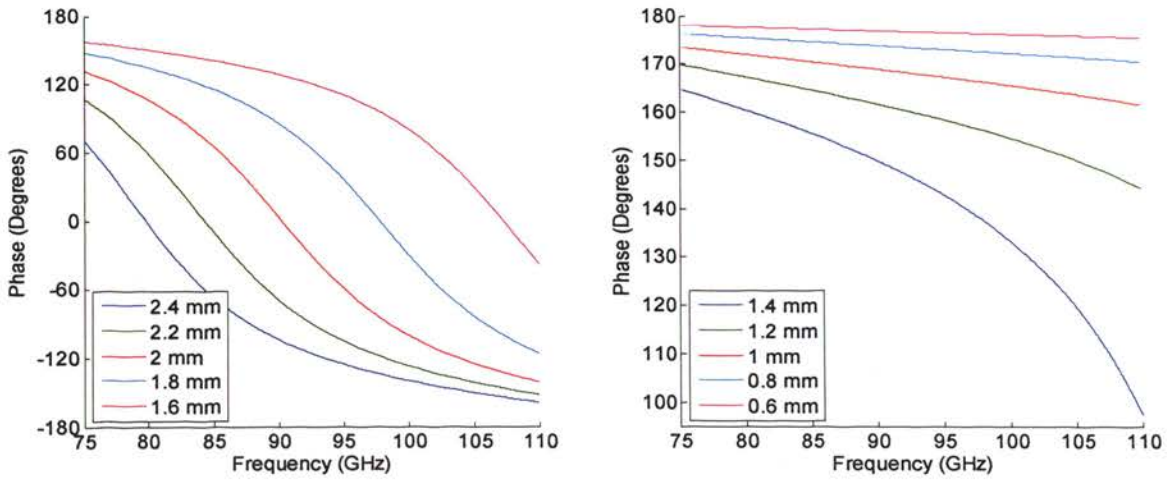

(a) (b)

Figure 2.11. Simulated phase of reflection coefficient as a function of frequency for empty cracks in aluminum with D = 1.4 mm, W = 0.5 mm, and ten lengths at W-band.

(e.g., 1.4 mm crack in Figure 2.11b), and at some shorter length the crack will cease to support propagating modes for the entire frequency band (1.2–0.6 mm cracks in Figure 2.11b). For cracks where the resonant frequency can be evaluated it is possible to use the quarter-wavelength resonance and (2) to estimate depth (as will be shown). For shorter cracks the phase change which is still observed may contain some information about the crack depth.

Figure 2.12 shows the percent error in depth estimation using (2) and the simulations shown in Figure 2.11a. It is seen that the error is relatively small, and in fact offsets some of the error from the previously-described width dependency. This is reasonable since when the crack length is reduced current can flow around the edges of the crack, which would tend to have an inductive effect. The capacitive effect of the crack width, as described previously, would then be partially cancelled by this inductive effect. It is important to note that this method can only be applied to cracks with a known length which is greater than $a/2$.

Figure 2.13 shows the simulated phase of reflection coefficient as a function of crack depth for cracks with $W = 0.5$ and 4 lengths which will not support a propagating mode at 92.5 GHz (W-band). For each length the phase converges to a minimum value, and the depth beyond that point cannot be seen. This is due to the limited penetration of

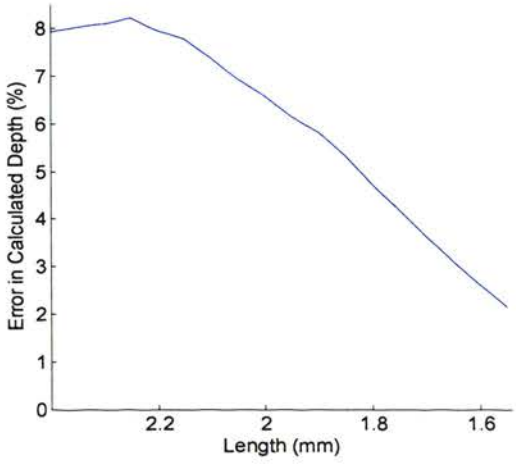

Figure 2.12. Percent error in depth calculated from the measurements shown in Figure 2.11a using (2) compared to the actual simulation depth.

evanescent modes. It is also observed that shorter cracks converge for smaller depths and to a lesser phase change than longer cracks, e.g., the phase of the 0.6 mm long crack levels off around a depth of 0.4 mm, while the phase of the 1.2 mm long crack is continuing to change at a depth of 1 mm. Consequently, if the crack length is known (the width will likely be needed as well, as shown in Figures 2.9a-b for long cracks) the phase can be used to find the depth if the crack is sufficiently shallow or, if the crack is not sufficiently shallow, to know that the crack width is greater than some depth which is the maximum penetration of the signal.

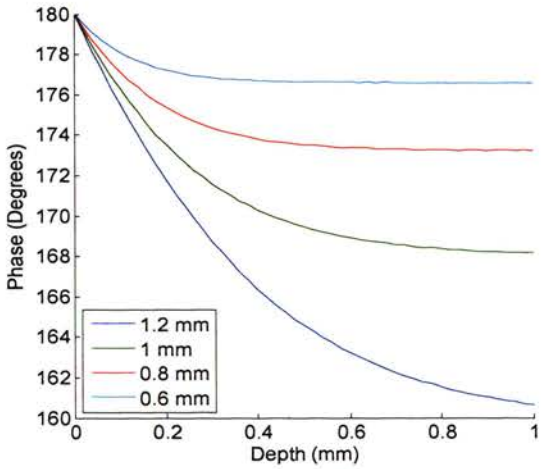

Figure 2.13. Simulated phase of reflection coefficient as a function of crack depth for empty cracks in aluminum with $W = 0.5$ and 4 lengths at 92.5 GHz (W-band).

The sensitivity to position, within the probing waveguide aperture, is an important consideration for finite cracks. The crack position may be varied in two dimensions and it may also be more difficult to accurately position the probing waveguide over the crack, since for finite cracks no portion of the crack extends outside the waveguide aperture. A rectangular crack with $L = a/2 = 1.2$ mm, $W = 0.5$ mm, and $D = 1$ mm was simulated with the crack center at various locations in the waveguide aperture at W-band. The setup and results are shown in Figure 2.14. The position was varied along three directions as shown in Figure 2.14a. Only one quadrant was considered since the waveguide is

symmetric in both directions. Figure 2.14b shows the phase at 92.5 GHz as a function of the normalized offset for each of the three paths. The shift along path *a* has a significant and immediate effect upon the measured phase, indicating that this measurement is strongly dependent on variations along this direction. The change in phase is more gradual and much smaller along path *b* so the position along this dimension is not critical, which is expected since the electric field in the probing waveguide is uniform in this direction. A greater effect is observed as the crack nears the edge of the waveguide. The change in phase along path *c* is very close to that along path *a*, indicating that in the presence of shifts in both dimensions the shift along *b* has no discernable effect and only the shift along *a* is significant.

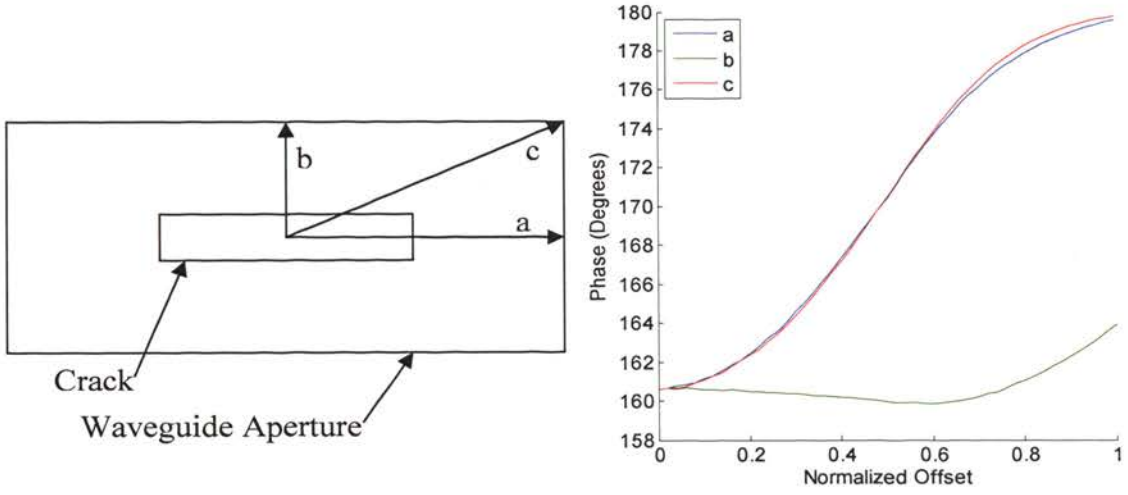

(a) (b)

Figure 2.14. Simulated empty finite cracks in aluminum with $D = 1$ mm, $W = 0.5$ mm, and $L = a/2 = 1.2$ mm at 92.5 GHz (W-band): a) Plan-view of finite crack in waveguide aperture and three paths of shifting crack position (not-to-scale), and b) simulated phase of the reflection coefficient along each path as a function of position along the path (each path is normalized to its length).

2.3. PITS

Pits with openings that can be contained within the waveguide aperture will have diameters much less than *a* and, thus, will not support propagating waves. Consequently,

the quarter-wavelength resonance phenomenon cannot be used. However, the presence of a pit changes the reflection coefficient and information about the damage depth may be extracted from this change.

Figure 2.15 shows the phase of reflection coefficient as a function of frequency for pits with diameter of 1.0 mm and four different depths. The simulation results in Figure 2.15a not only show the presence of a pit (i.e., phase different than 180°), but also that the phase is a function of pit depth. Figure 2.15b shows measurement results of pits with similar dimensions. It can be seen that the behavior of the pits with respect to depth is similar for simulation and measurement. There is an absolute shift of a few degrees between measurement and simulation, but this is likely from error in the measurement calibration. The measured results for the 0.33 mm-deep pit show a localized dip in phase around 100 GHz, but this is not seen in simulation or the other measurements and is likely measurement error due to the probe position shifting during the measurement.

Figure 2.16 shows measurement results of pits at a different frequency band or with a different diameter than those shown in Figure 2.15. Figure 2.16a shows measurement results of the same pits as shown in Figure 2.15b, but at V-band. The phase

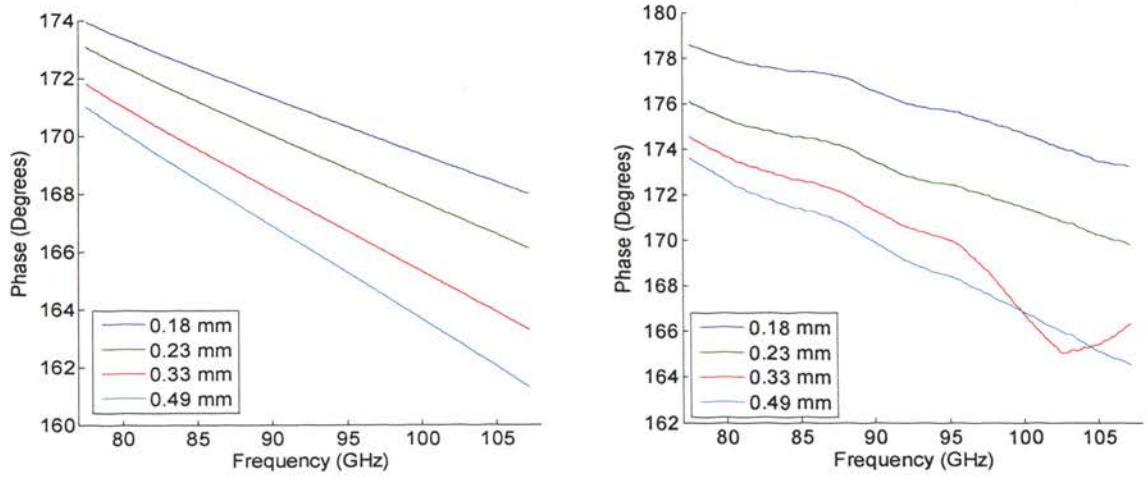

Figure 2.15. Simulated and measured phase of reflection coefficient as a function of frequency for pits in aluminum with a diameter of 1.0 mm and four depths at W-band: a) simulated and b) measured.

change is much smaller at V-band, as expected since at lower frequencies the pits are electromagnetically smaller in both depth and diameter. However, the curves are still ordered by depth, with greater phase change caused by the pits with larger depths. The one exception is the 0.49 mm-curve for the lower half of the frequency band. The difference between the measured phase for this crack and that expected from comparison with the other curves is consistent with a change in the phase of reflection coefficient associated with the probing waveguide not being exactly flat on the aluminum plate (i.e. tilted), which was observed in several measurements (not shown). Figure 2.16b shows measurement results of pits with a diameter of 0.7 mm and five different depths at W-band. As expected for the smaller pit diameter, the phase change is also smaller than for the 1 mm-diameter pit results shown in Figure 2.15b. The curves are not sorted by depth in this case, which suggests that for this small of pits measurement error from sources such as probe position may be more significant than the influence of depth.

Figure 2.17 shows the simulated phase of reflection coefficient as a function of pit depth for pits in an aluminum plate with six different diameters at 92.5 GHz. For each

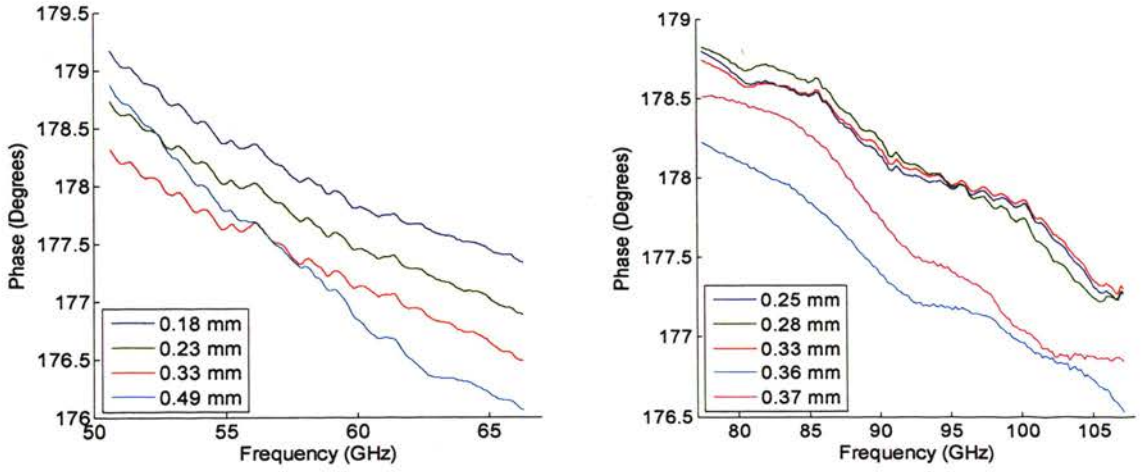

Figure 2.16. Measured phase of reflection coefficient as a function of frequency for empty pits in aluminum with two diameters and several depths at V-band and W-band: a) pits with diameter of 1.0 mm and four depths at V-band and b) pits with diameter of 0.7 mm and five depths at W-band.

diameter the phase quickly converges to a minimum value, and the depth beyond that point cannot be seen (as mentioned before, pits with openings significantly smaller than the waveguide cannot support propagating waves and thus penetration is limited for deeper pits as in the case of finite cracks [16]). It is also observed that smaller diameter pits have less effect on the phase. The 0.125 mm-diameter pit has no effect on the phase and cannot even be detected. The 0.75 mm-diameter pit has a maximum of 5° phase shift and for depths less than 0.5 mm the phase can be directly related to pit depth.

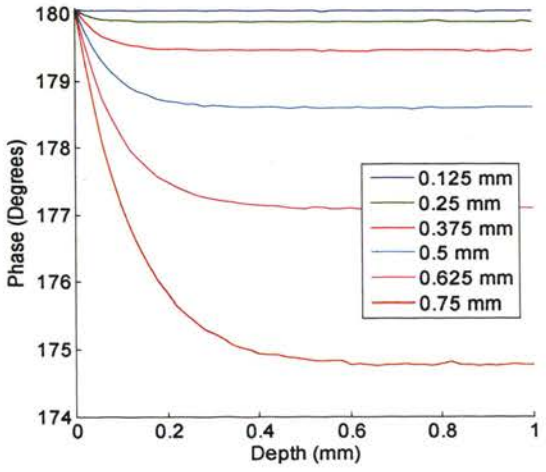

Figure 2.17. Simulated phase of reflection coefficient as a function of depth at 92.5 GHz (W-band) for empty pits in aluminum with six diameters.

3. DIELECTRIC-FILLED DAMAGE

3.1. LONG CRACKS

3.1.1. Approach/Theoretical Background. If a crack is filled with a dielectric material having a relative (to free-space) complex dielectric constant, $\varepsilon_r = \varepsilon_r' - j\varepsilon_r''$ (the real part indicates relative permittivity and the imaginary part indicates relative loss factor), there are two primary differences with respect to an empty crack. First, the crack geometry changes electromagnetically; in particular from (2) it is evident that the guide wavelength in a crack filled with a material with a relative permittivity, $\varepsilon'_r > 1$, is reduced, which makes a shallow crack appear electrically deeper. Consequently, the depth of a crack can be evaluated at a lower resonant frequency in a filled-crack than when it is empty. The electrical crack length and width may be increased as well. Second, losses associated with the dielectric material are introduced to the system, and these are in addition to the conductor losses described previously. The dielectric losses are expected to be more significant than the conductor losses for typical dielectric materials and crack dimensions. For a filled-crack, then, the unloaded Q-factor is related to both conductor and dielectric losses and (4) must be replaced with [34]:

$$\frac{1}{Q} = \frac{1}{Q_c} + \frac{1}{Q_d}, \tag{10}$$

where Q_d is the Q-factor due to dielectric loss associated with the material filling the crack and can be estimated as [38]:

$$Q_d = \frac{1}{\rho_d \tan\delta} \tag{11}$$

where

$$\tan\delta = \varepsilon_r'' \Big/ \varepsilon_r' \tag{12}$$

is the loss tangent of the filling material and ρ_d is the electric field filling-factor for the crack (ratio of the electric field energy stored in the dielectric to the electric field energy stored in entire resonant volume). The filling-factor accounts for the portion of the resonant field (in the filled-crack) which may extend into the probing waveguide. Equation (11) is applicable to any waveguide or transmission line filled with a homogeneous dielectric material [34], which is a useful feature for crack depth evaluation since crack shape may not be perfectly rectangular.

3.1.2. Simulation Results. Simulations of dielectric-filled cracks in an aluminum plate were performed for several dielectric materials. Figure 3.1 shows the frequency dependence of the complex reflection coefficient for a crack with $D = 0.25$ mm and $W = 0.25$ mm filled with five dielectric materials, each with $\varepsilon_r' = 10$ but different loss tangents, at W-band. The specific loss tangents were chosen to include under, over and critical coupling, and the lossless dielectric case ($\tan\delta = 0$) as a reference. Figure 3.1a shows, as expected, a resonance behavior in the magnitude of reflection coefficient. It is important to note that the resonant frequency remains constant for all loss tangents, which is expected since the loss tangent does not appear in (2). The results also show that the resonance response minima changes non-monotonically as a function of loss tangent. For instance, if there are only conductor losses in the crack (i.e., $\tan\delta = 0$), the resonance response is barely detected in Figure 3.1a. On the other hand, when dielectric loss is introduced in the crack, $|\Gamma|$ initially decreases, approaching zero at $\tan\delta = 0.06$, and then increases, slowly approaching 1. It should also be noted that there is a slight asymmetry associated with the responses as a function of frequency. This is due to the increased signal attenuation at higher frequencies as the crack becomes electrically deeper. The phase of reflection coefficient, shown in Figure 3.1b, also changes as a function of loss tangent. For $\tan\delta = 0.02$ the phase is very close to the lossless case with a 360° phase transition, for $\tan\delta = 0.06$ it has a more gradual transition except for a very sharp 180° jump at the resonance, for $\tan\delta = 0.18$ it has some variation in phase but does not have the 360° phase transition, and by $\tan\delta = 0.5$ the phase variation has mostly disappeared.

Consideration of the complex reflection coefficients in polar format, as shown in Figure 3.1c, along with the influence of dielectric loss on the coefficient of coupling (as in (7)) allows for a more comprehensive understanding of the resonant behavior of the

dielectric-filled crack. The results for tan $\delta = 0.06$, shown in Figure 3.1c, correspond to (near) critical coupling, where there is no reflection from the crack at the resonant frequency. As tan δ increases from 0.06 the resonator becomes undercoupled ($g < 1$) and the resonant response shrinks towards $\Gamma' = -1$, approaching the case of reflection from a metal plate since the signal does not penetrate inside high-loss dielectrics. On the other

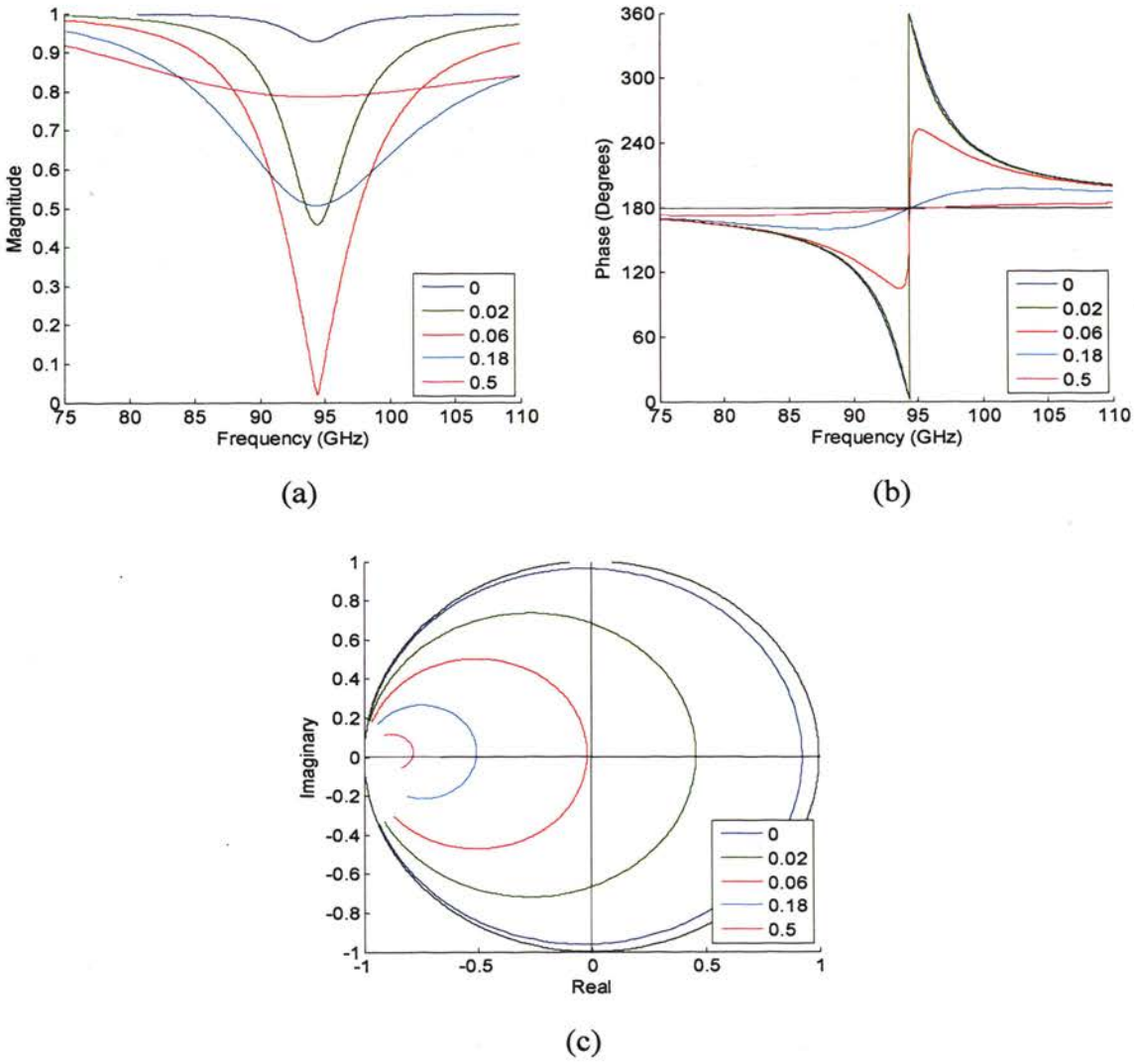

(a) (b)

(c)

Figure 3.1. Simulated complex reflection coefficient of dielectric-filled cracks in aluminum with $W = 0.25$ mm, $D = 0.25$ mm, $\varepsilon_r' = 10$, and five loss tangents at W-band: a) magnitude and b) phase of the reflection coefficient as a function of frequency, and c) reflection coefficient in the complex polar plane.

hand, when the tan δ decreases beyond 0.06 the resonator is overcoupled ($g > 1$) and the resonant response approaches the case where only conductor loss is considered (i.e., $\Gamma' \sim 1$).

Figure 3.2 shows characteristics of the resonant response as functions of loss tangent for cracks with $D = 0.25$ mm and six different widths. In Figure 3.2a the curve for $W = 0.25$ mm, for example, demonstrates the magnitude of reflection coefficient shown in Figure 3.1a for the full range of considered loss tangents (0 – 0.5) at the resonant frequency (i.e. the magnitude minimum). Figure 3.2a shows that dielectric-filled cracks exhibit resonant behavior for a wide range of widths, from small ($W = 0.06$ mm) all the way to $W = b = 1.3$ mm, with the use of a proper loss tangent (e.g., at tan $\delta = 0.06$ the resonance will be evident for all these widths). Increasing crack width shifts the loss tangent at which critical coupling (magnitude of zero) occurs, and this shift is approximately linear.

Figure 3.2b shows the loaded Q-factor as a function of loss tangent. For each of these curves, as the loss tangent increases the Q-factor smoothly decreases, with a distinct

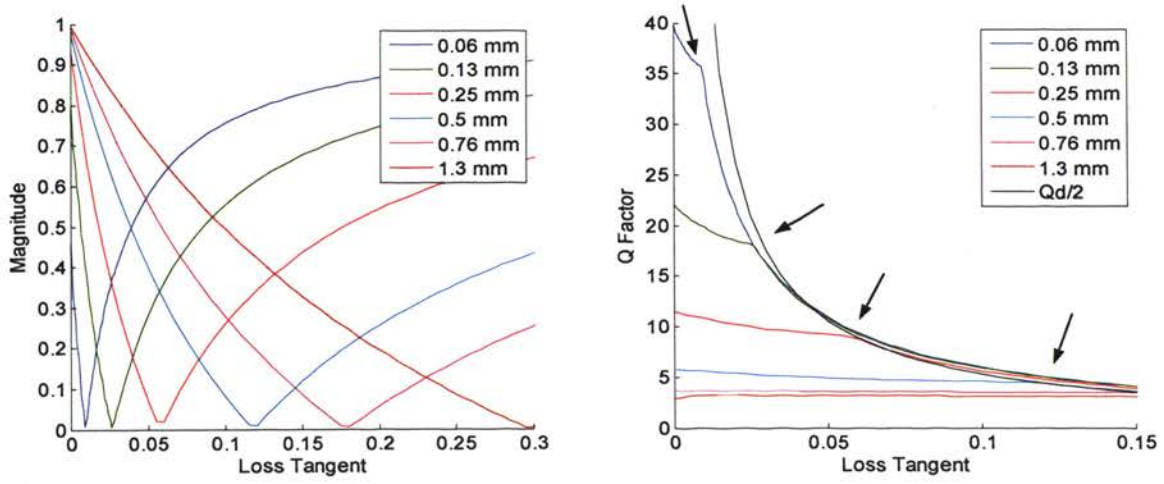

(a) (b)

Figure 3.2. Simulated characteristics of resonant response as functions of loss tangent for dielectric-filled cracks in aluminum with $D = 0.25$ mm, $\varepsilon_r' = 10$, and six widths at W-band: a) magnitude of reflection coefficient at resonant frequency and b) loaded Q-factor. In b) the points of critical coupling are indicated by arrows and the curve $Q_d/2$ from (13) is included.

change in slope at one point (indicated by arrows). By comparison with Figure 3.2a these points correspond to critical coupling. It should be noted that the loaded Q-factor in the overcoupled region is higher than in the undercoupled region, as is also evident in Figure 3.1a (i.e., evaluating using (8)). The Q-factor in the overcoupled region is highly dependent on the width of the crack, whereas in the undercoupled region the contribution of dielectric losses in the loaded Q-factor is dominant, as will be shown.

If conductor losses are neglected (for the moment) so that only dielectric losses are considered, and the condition of critical coupling $Q_e = Q$ is used, then the loaded Q-factor at critical coupling can be determined from (3), (10)–(12) as:

$$Q_L = \frac{Q_d}{2} = \frac{1}{2\rho_d \tan\delta} \tag{13}$$

The loaded Q-factor, calculated from (13), is shown in Figure 3.2b as the curve corresponding to $Q_d/2$. A filling factor of 0.95 was used to match this curve to the points of critical coupling, which is a practical value since the field will be concentrated in the dielectric. The curve matches well for the cracks with $W \geq 0.25$ mm shown in Figure 3.2b, which shows that the contribution of conductor loss is negligible in that case, but a difference is seen for the 0.13 and 0.06 mm wide cracks, since conductor losses will be greater for those cracks (according to (6)).

3.1.3. Sensitivity Analysis. The sensitivity of this method to variations in the crack length and width, relative permittivity and loss tangent of the filling material, and probe position were investigated. The case of a crack with $D = 0.26$ mm and $W = 0.5$ mm filled with a dielectric material having $\varepsilon_r' = 10$ and $\tan\delta = 0.06$ at W-band was selected as the initial case. This case results in a magnitude of reflection coefficient minimum of 0.3 at a resonant frequency of 90.7 GHz.

The effect of crack length greater than the waveguide broad dimension, a, was simulated for lengths from a to $2a$. The maximum observed change in the resonant frequency over this range was 0.15%. It was also observed that once the crack length exceeds $1.1a$ there is no further change. So the resonant frequency is not sensitive to

cracks lengths greater than a. Crack lengths smaller than the broad waveguide dimension will be considered as finite cracks in a separate section.

Using (2) to evaluate crack depth, by measuring the resonant frequency, shows no dependence on crack width since it is a close approximate form for evaluating crack depth (i.e., only considers the crack geometry). However, as for empty cracks, the simulations which include the entire structure, and are hence more accurate, showed some dependency between crack width and its resonant frequency. Therefore, to determine the sensitivity of evaluating crack depth using (2) to crack width, the following was considered. Simulations were conducted for several combinations of crack widths and depths (i.e., "actual" widths and depths). Subsequently, the resonant frequencies from the simulations (in effect representing actual measurements) were used in conjunction with (2) to estimate the depth. Three depths of D = 0.23, 0.26, and 0.31 mm, were used with varying widths at W-band. Figure 3.3 shows the error in depth estimation (compared to the depth used in the simulation) as a function of crack width normalized to b, for three depths using the phase (solid) and magnitude (dashed) of reflection coefficient to find the resonant frequency. The results using the phase show that there is less than 3.5% error in

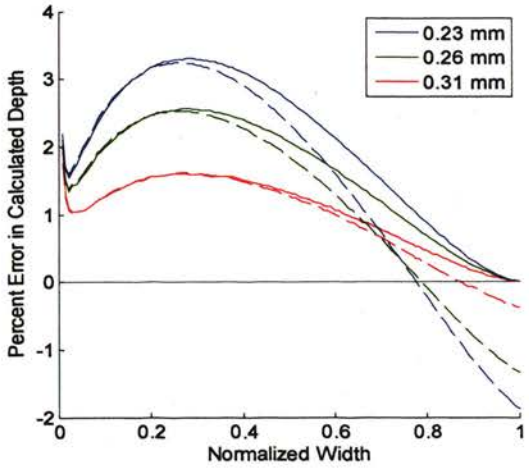

Figure 3.3. Percent error in depth estimation as a function of crack width using phase (solid) and magnitude (dashed) of reflection coefficient for simulated cracks in aluminum filled with a dielectric ($\varepsilon_r' = 10$, $\tan\delta = 0.06$) and with three depths at W-band. Widths are normalized to the probing waveguide b dimension.

overestimating crack depths for the entire range of widths, as shown in Figure 3.3, which is significantly less than for empty cracks. The error also depends on the actual value of crack depth (i.e., error is less for deeper cracks). Using the magnitude, increased signal attenuation at higher frequencies is a second source of error which biases the resonance towards higher frequencies and shallower depths (see Figure 3.1a). For narrower cracks with a higher Q-factor (see Figure 3.2b) this has a negligible shift in the resonant frequency and the curves using the phase match well to the curves using the magnitude. For wider cracks, with lower Q-factors, this causes an underestimation in crack depth evaluation by up to 2%. At normalized widths around 0.8 the two effects mostly cancel each other and the error as a function of crack width is minimized.

A correction factor was derived from the magnitude-based curves by matching to a polynomial such that:

$$D_{corrected} = \left[\left(1.5 f_n - 1.38\right)\left(-0.087 W_n^3 + 0.207 W_n^2 - 0.093 W_n - 0.013\right) + 1\right] D_{calculated} \qquad (14)$$

If (14) is applied to the magnitude results in Figure 3.3 the error is reduced to an average of 0.11%, with a maximum of 0.85%.

The sensitivity of the resonant frequency to various parameters is shown in Figure 3.4. In practice the dielectric properties of the filling material may only be measured with a certain accuracy, or may vary due to porosity as it is packed in the crack. Consequently, the sensitivity of the resonant frequency to the dielectric properties of the filling material was investigated. Figure 3.4a shows the change in resonant frequency as a function of the change in relative permittivity. As expected from (2), the resonant frequency is strongly dependent on the relative permittivity, with a nearly linear dependency. The results show that a 5% change in the relative permittivity causes a 2.4% change in the resonant frequency. Thus, the more accurately the relative permittivity is known (or measured) the more accurately crack depth may be evaluated. Figure 3.4b shows the change in resonant frequency as a function of loss tangent. As expected from Figures 3.1a–b, there is no noticeable shift of the resonant frequency due to changes in the dielectric loss.

As described previously, in this section damage is considered which is longer than or equal to the waveguide aperture broad dimension, a, and in simulations crack length

was set equal to a. Consequently, if the position of the damage, while still extending outside of the probing waveguide aperture, is shifted along its length there is no change to the crack in the simulation. However, the influence of positioning of the crack along b needs to be investigated. Figure 3.4c shows the change in the resonant frequency as a

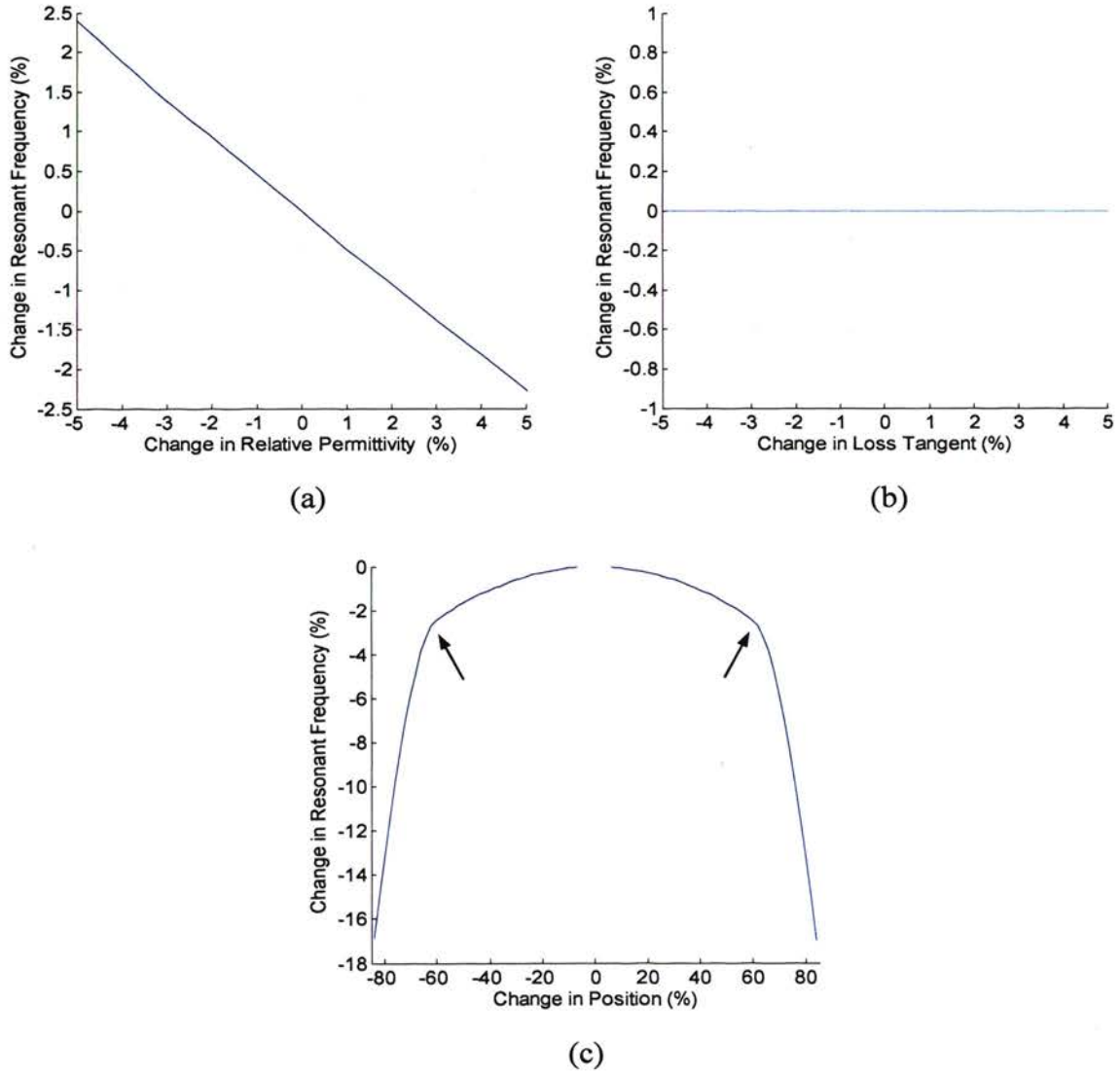

Figure 3.4. Simulated sensitivities of resonant frequency for cracks in aluminum plate with $D = 0.26$ mm and $W = 0.5$ mm at W-band and, except as perturbed for the analysis, filled with a dielectric of $\varepsilon_r' = 10$ and $\tan\delta = 0.06$: sensitivity to a) relative permittivity, b) loss tangent, and c) position of crack in waveguide aperture.

function of the crack position along the narrow dimension of the waveguide, normalized to $b/2$ (i.e., at a position of 100% the crack is centered on the edge of the waveguide aperture). It can be seen that for a shift of 50% in either direction from the center of the narrow waveguide dimension, the resonant frequency changes by ~2%. The shift is not significant until the edge of the crack reaches the edge of the waveguide, indicated by the arrows. At that point the resonant frequency changes sharply as a function of position, as expected and previously shown [20]. Consequently, as long as the entire crack width is within the waveguide aperture only a small error will be introduced by variations in its position. Additionally, since the maximum resonant frequency occurs when the crack is exactly in the center of the waveguide, the probe position may be varied and the resonant frequency used to position the crack in the center of the probing waveguide aperture.

3.1.4. Dielectric Materials. For measurement of dielectric-filled cracks (and pits) three materials were used: barium titanium oxide, corn oil, and water. Each has different advantages and disadvantages when used to fill cracks for depth evaluation. As was described previously, higher permittivity materials, used to fill a crack, allow the evaluation of shallower damage, and as such are desirable. It is also desired to have a low-loss material which provides near-critical coupling for cracks.

Barium titanium oxide ($BaTiO_3$, barium titanate) 325-mesh powder was the primary material used to fill cracks. Barium titanate is a high permittivity and low loss material [39-40] and since it is in the form of a fine powder it can be easily compacted into a tight crack; however the dielectric properties are very dependent on frequency in the range of use. For the purpose of these experiments the dielectric properties of barium titanate powder were measured using a completely-filled waveguide technique [41] at X-band and Ku-band (12.4 – 18 GHz) and were then extrapolated to obtain the K- and Ka-band values. It was also observed that cracks could be packed much more tightly with the powder than the waveguide sample holders that were used for the dielectric properties measurements, so the properties measurement results were scaled such that the measured resonant frequency of a 2.22 mm-deep crack (shown later) was matched to the simulation results with the same crack dimensions. Table 3.1 shows the final average relative permittivity and loss factor for the barium titanate powder used for evaluating crack depths.

Table 3.1. Average dielectric properties of barium titanium oxide powder for four frequency bands. K- and Ka-band are extrapolated.

Frequency Band	ε_r'	$\tan\delta$
X-Band	11.05	0.066
Ku-Band	9.14	0.060
K-Band	8.18	0.060
Ka-Band	7.71	0.060

Barium titanate-filled crack samples were prepared by filling the crack with a small amount of powder and packing it, repeating the process until the crack was totally filled flush with the surface of the plate. Any porosity in the powder will be filled with air, so clearly the filling or packing factor will affect the dielectric properties, and consequently, the measured results. Two independent measurements were conducted (shown later) on several cracks at K-band and each time the process of filling the crack was repeated in an attempt to experimentally evaluate the variations in the measurements due to any inconsistency in filling the crack. The results showed a maximum of 8% shift in the measured resonant frequency as a result of variations in the packing factor.

Corn oil, at millimeter wave frequencies, has dielectric properties of $\varepsilon_r = 2.5 - j0.1$ which are fairly stable as a function of frequency [42]. The permittivity is less than barium titanate, so there is a higher minimum crack depth which can be evaluated. The loss is reasonably small so the resonance should be easily observed. Since this is a liquid, cracks can be more completely filled. After cracks were filled with corn oil a piece of thin tape was placed over the crack to keep the oil in place and flush with the crack surface during measurement.

Distilled water, at millimeter wave frequencies, like barium titanate exhibits a large change in permittivity, from 75 at 10 GHz to 8 at 89 GHz [43-45]. The permittivity is greater than barium titanate in this range, which allows the evaluation of shallower crack depths. The loss is rather large ($\tan\delta \sim 1.9$ at 89 GHz [44-45]), so the resonance will be much smaller. As with corn oil, water can be used to completely fill cracks and

after cracks were filled a piece of thin tape was placed over the crack to keep the water in place and flush with the crack surface during measurement.

3.1.5. Measurement Results. Figure 3.5 shows the measured and simulated frequency dependence of the complex reflection coefficient for cracks filled with barium titanate powder, with $W = 0.5$ mm and three depths, at X-band. As expected, in Figure 3.5a the resonant response magnitude dips are clearly shown and the measured results closely match the simulation results. For the shallowest crack the minimum of the resonant dip occurs outside of the measured frequency band and only half of the resonant dip is seen. The trend in increasing resonant frequency for shallower cracks is also evident. The measured phase of reflection coefficient, as shown in Figure 3.5b, also shows good agreement with the simulation results. The phase only varies by about 20°, which (by comparison with Figure 3.1b) shows that these cracks are in the undercoupled mode. The differences between the measured and simulated results are primarily attributed to dielectric property measurements, dielectric packing factor, and accuracy of positioning the probe over the crack. Figure 3.5c shows the results in the complex polar plane. The points where the curves cross the real axis correspond to the magnitude minima in Figure 3.5a. These points are to the left of the origin, again indicating that these cracks are in the undercoupled region. There is also a key difference between Figure 3.5c and Figure 3.1c which is informative. In Figure 3.1c the loss tangent, and thus coupling, was varied and this was manifested as a change in the radius of the resonant circle. In Figure 3.5c the depth of the crack is varied, which has a less significant influence on the coupling but a direct influence on the resonant frequency. The shift of the resonant frequency results in different portions of the resonant circle being observed within the measured frequency band for each crack.

Figure 3.6 shows the measured frequency dependence of the complex reflection coefficient for barium titanate-filled cracks with $W = 0.85$ mm and three depths at K-band. Two sets of measurements are shown in Figures 3.6a-b. The cracks were emptied and repacked with powder between measurements. The difference between the measurement sets is attributed to differences in porosity between the two packings, and is significant (e.g. the 0.92 mm crack resonant frequency is shifted by 8% between measurements). The magnitude of reflection coefficient results again shows the resonant

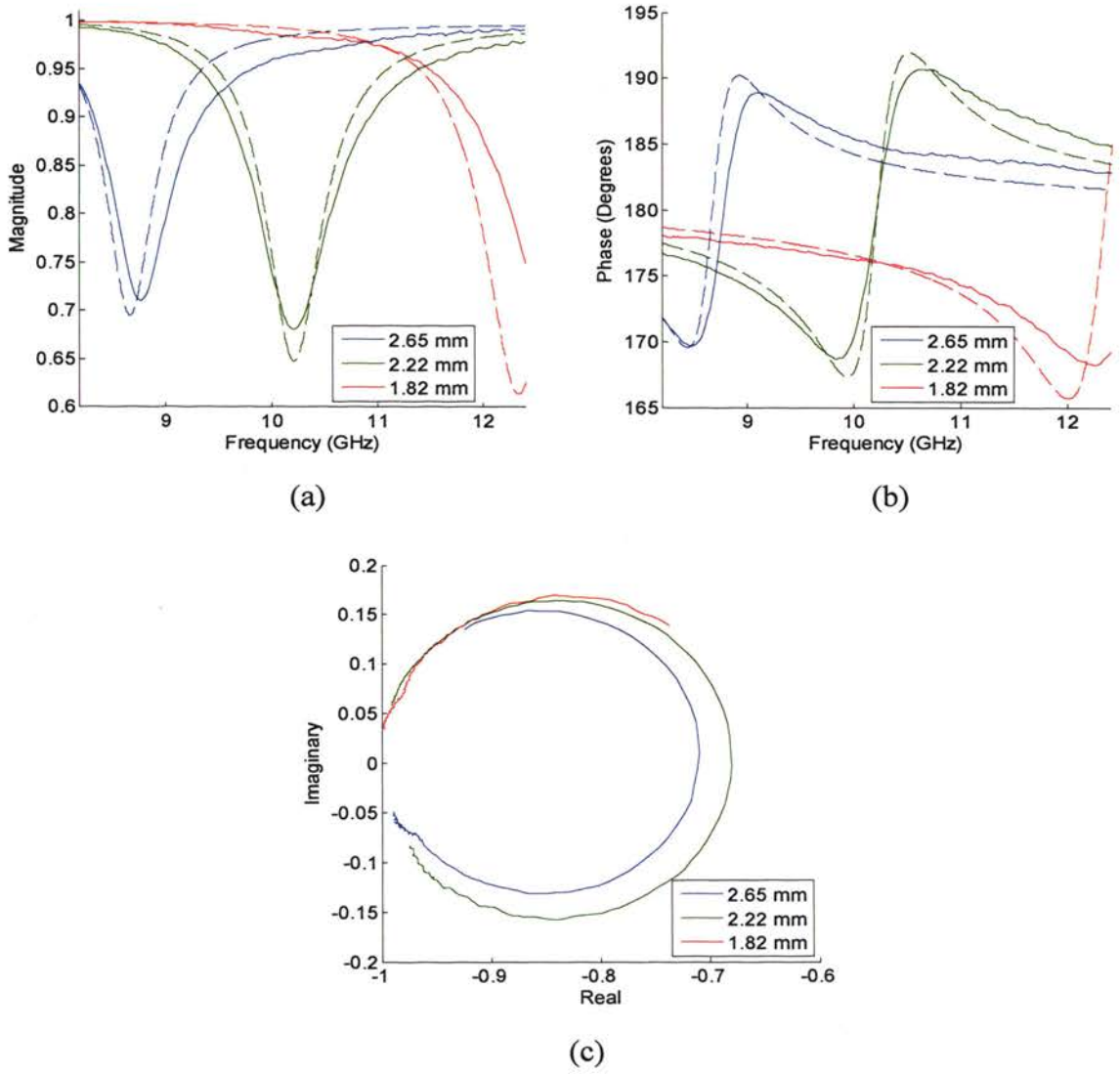

Figure 3.5. Measured (solid) and simulated (dashed) complex reflection coefficient of barium titanate-filled cracks in aluminum with $W = 0.5$ mm and three depths at X-band: a) magnitude and b) phase of the reflection coefficient as a function of frequency, and c) reflection coefficient in the complex polar plane.

effect and the trend between the resonant frequency and crack depth. Figure 3.6c shows the results in complex polar plane. The circular responses are again clearly evident and again the circles all cross the real axis ($\Gamma'' = 0$) to the left of the origin, though much closer to the origin than for the X-band measurements since b is smaller and these cracks are, thus, relatively wider. Consequently, it can be concluded that these cracks are also

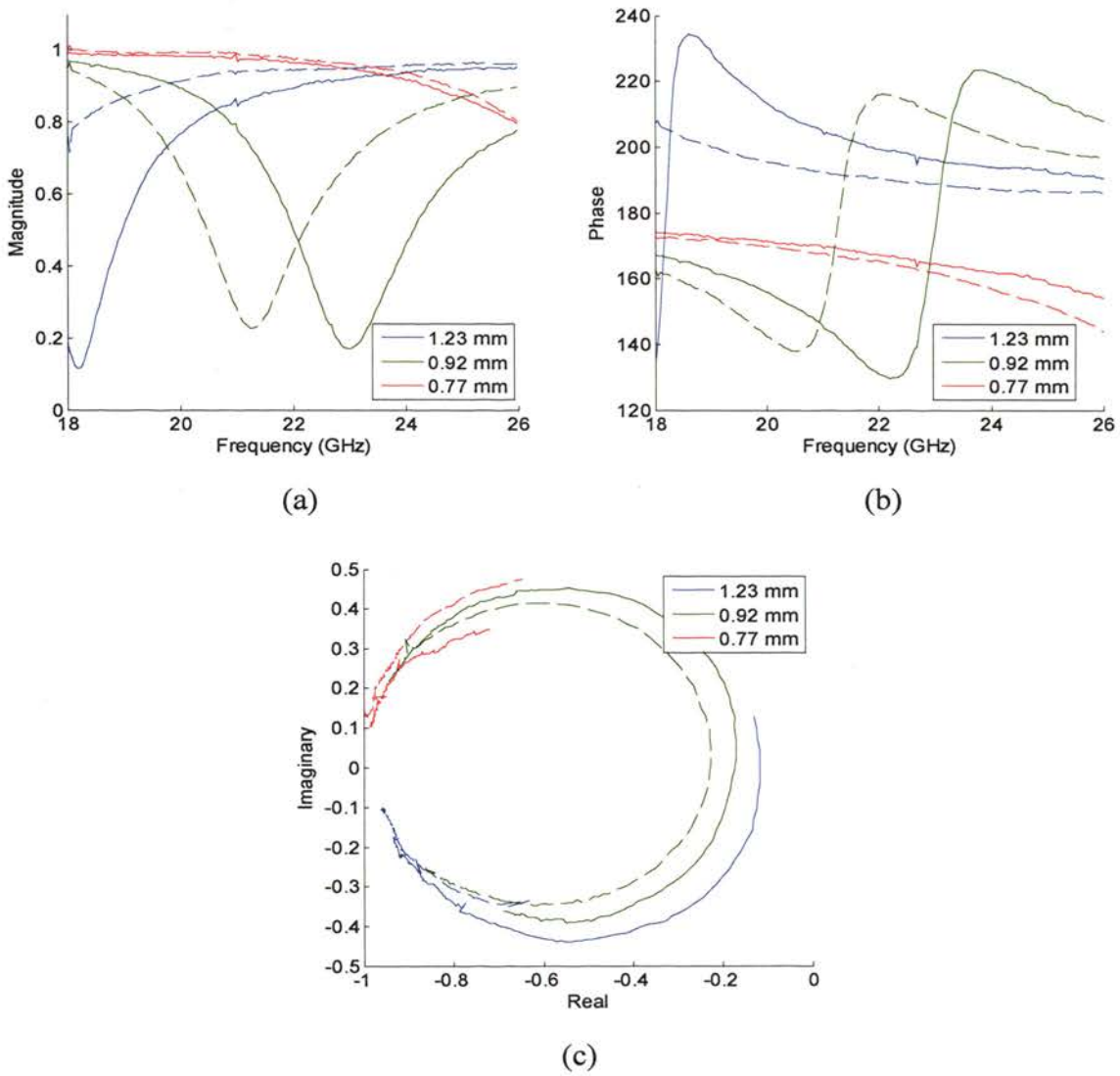

Figure 3.6. Two measurements (solid and dashed) of complex reflection coefficient of barium titanate-filled cracks in aluminum with $W = 0.85$ mm and three depths at K-band: a) magnitude and b) phase of the reflection coefficient as a function of frequency, and c) reflection coefficient in the complex polar plane.

undercoupled, but much nearer to critical coupling than the cracks measured at X-band, resulting in a somewhat larger magnitude dip and phase variation (compare to Figure 3.5a-b).

Figure 3.7 shows the resonant response for barium titanate-filled cracks at Ka-band, with respective depths of 0.74, 0.87, 0.88, and 1.19 mm and with $W = 0.5$ mm for

the 0.88 mm-deep crack and $W = 0.85$ mm for the others. Figure 3.7a shows the simulated magnitude of reflection coefficient and Figure 3.7b shows the measured reflectometer output voltage (the reflectometer system and post-processing is explained in Section 1.3) so curves cannot be directly compared between the figures. However, the resonant frequency (at the signal minimum) and level of the minimum relative to the other cracks should be the same for both figures (these parameters are unchanged by the non-linear characteristics of the detector and the smoothing of the curves), and can be compared. There are also frequency dependencies introduced by imperfections of the reflectometer system, but the crack resonance can still be easily determined. The measured resonant frequency of the 1.19 mm-deep crack is shifted about 1 GHz (~3%) from simulation. The 0.87 and 0.88 mm-deep cracks are similarly shifted and their resonant frequencies remain close to one another, which is expected since even though there is a significant difference in widths the resonant frequency is primarily dependent on depth, and those are very close. It is also interesting to note that the difference in widths (and, consequently, coupling) is manifested in the different levels of the minima

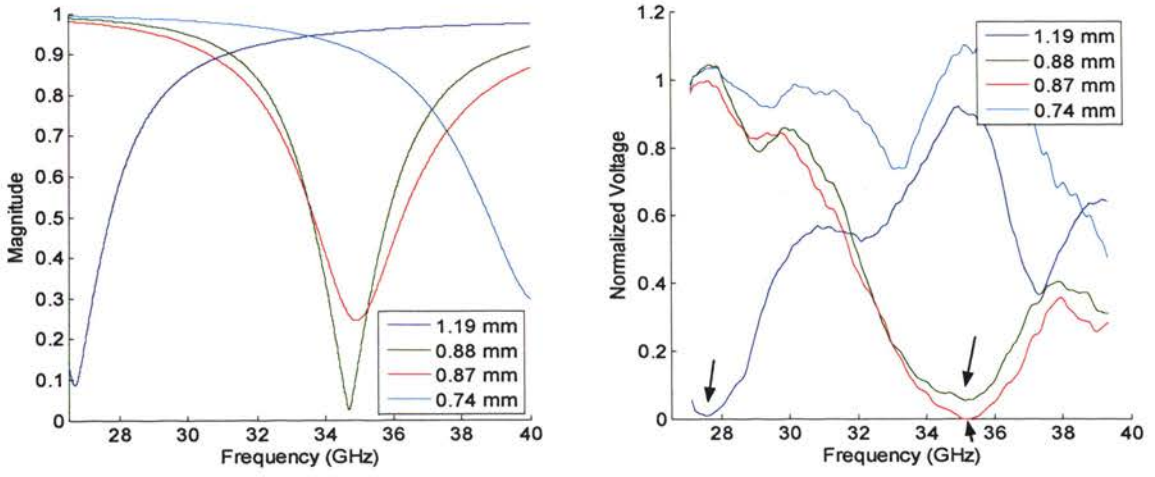

(a) (b)

Figure 3.7. Resonant response as a function of frequency for barium titanate-filled cracks with four depths at Ka-band: a) simulated magnitude of reflection coefficient and b) measured reflectometer output. The 0.88 mm-deep crack has $W = 0.5$ mm and all others have $W = 0.85$ mm. In b) smoothing and normalization to a no crack measurement (per frequency point) have been applied and the resonances are indicated by arrows.

for both simulation and reflectometer measurements, but the levels are reversed. Since in the simulations the 0.88 mm-deep crack is undercoupled and the others are overcoupled (from phase of reflection coefficient, not shown) this suggests that the actual loss tangent is greater than that used in the simulations and in the measurement both the 0.88 and 1.19 mm-deep cracks are undercoupled and the 0.87 mm crack is critically coupled (the observed reflectometer output of zero corresponds to a reflection coefficient magnitude of zero, which indicates critical coupling).

Figure 3.7 shows the resonant response for barium titanate-filled cracks at Ka-band, with respective depths of 0.74, 0.87, 0.88, and 1.19 mm and with $W = 0.5$ mm for the 0.88 mm-deep crack and $W = 0.85$ mm for the others. Figure 3.7a shows the simulated magnitude of reflection coefficient and Figure 3.7b shows the measured reflectometer output voltage (the reflectometer system and post-processing is explained in Section 1.3) so these curves cannot be directly compared. However,

Figure 3.8 shows the resonant response for corn oil-filled cracks at Ka-band, with respective depths of 1.82, 1.72, and 1.27 mm and with $W = 0.5$ mm for the 1.82 and 1.27 mm-deep cracks and $W = 0.85$ mm for the 1.72 mm-deep crack. Figure 3.8a shows the simulated magnitude of reflection coefficient and Figure 3.8b shows the measured reflectometer output voltage so, as for Figures 3.7a-b, curves cannot be directly compared between the figures. However, the resonant frequency (at the signal minimum) and level of the minimum relative to the other cracks should again be the same for both figures, and can be compared. There are again frequency dependencies introduced by imperfections of the reflectometer system, but the crack resonances can still be identified and the resonant frequencies determined. The resonant frequencies all match within about 1 GHz (~3%) between measurement and simulation and are all lower in measurement, which indicates that the actual real part of the permittivity for the corn oil may be a little lower than that used in the simulations. The curve from the 1.82 mm-deep crack has a second dip at 31 GHz that could be mistaken for the resonance, but is likely a frequency dependency of the system (also seen in the 1.27 mm curve) combined with a magnitude of reflection coefficient which is already low since it is near the resonant frequency. A third dip in the 1.82 mm-curve is also evident, which is likely also from a magnitude

dependency of the system. This curve has a wider resonant dip (i.e. lower Q-factor) than the other cracks, which would make it more sensitive to these frequency dependencies.

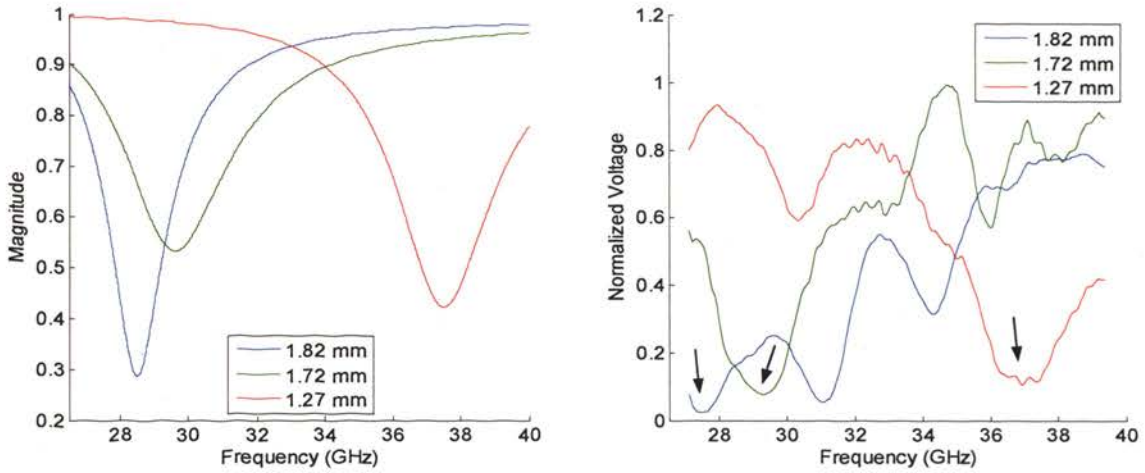

(a) (b)

Figure 3.8. Resonant response as a function of frequency for corn oil-filled cracks with three depths at Ka-band: a) simulated magnitude of reflection coefficient and b) measured reflectometer output. The 1.82 and 1.27 mm-deep cracks have $W = 0.5$ mm and the 1.72 mm-deep crack has $W = 0.85$ mm. Smoothing and normalization to a no crack measurement (per frequency point) have been applied in b), and the resonances are indicated by arrows.

Figure 3.9 shows the measured frequency dependence of the complex reflection coefficient for cracks with widths of 0.75, 1.13, and 1.5 mm and corresponding depths of 1.03, 1.01, and 0.99 mm, respectively, filled with distilled water at X-band. As expected, due to the high loss of the water, the change in magnitude and phase (Figures 3.9a-b) are small. Small frequency dependent measurement error (i.e., the ripples in the magnitude and phase) is also much more significant since the overall change is small. The resonant frequencies are close for the three samples, which is expected since the depths are similar. Figure 3.9c shows the results in complex polar plane. The circular responses are clearly evident and the circles cross the real axis ($\Gamma'' = 0$) well to the left of the origin,

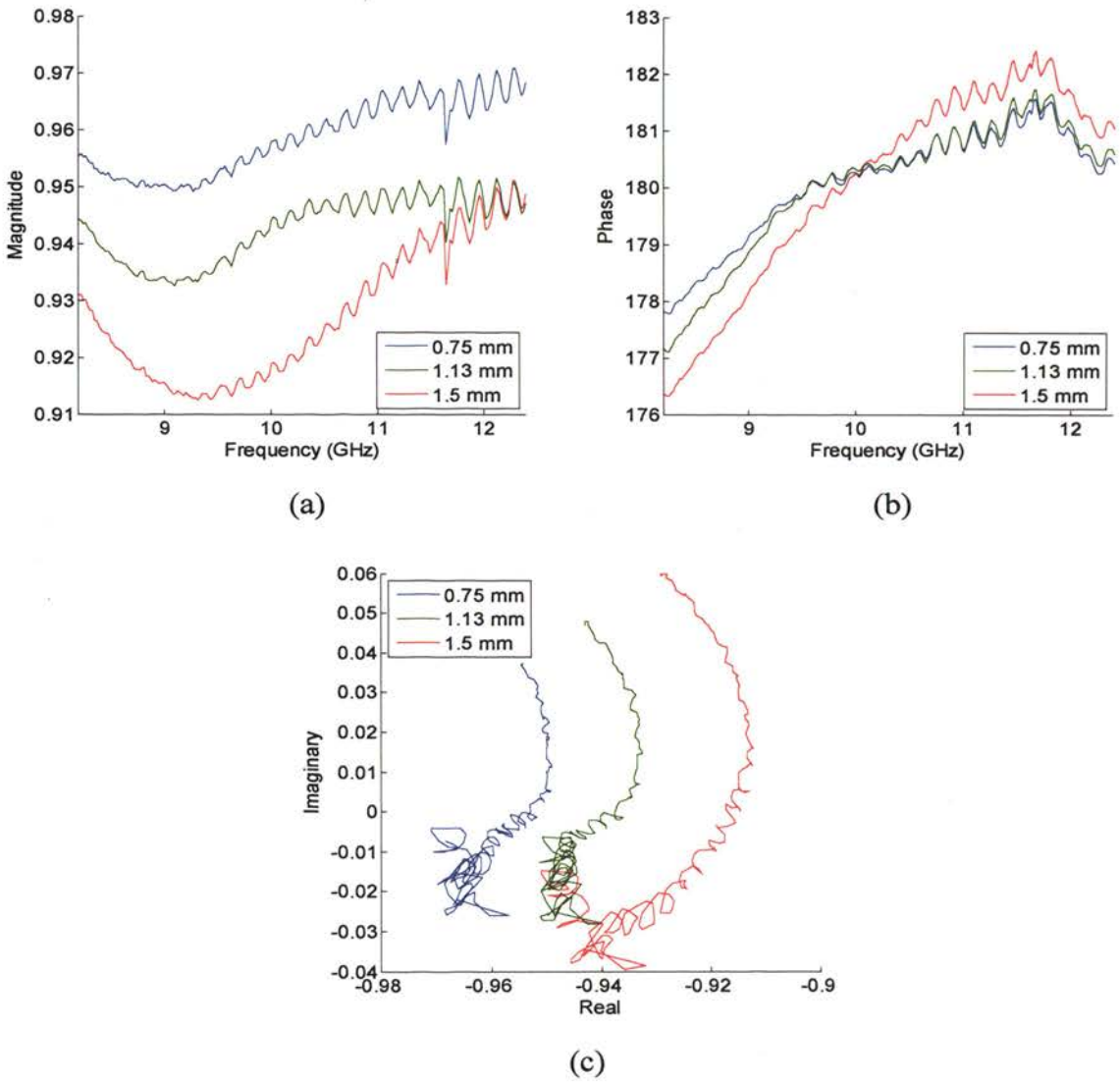

Figure 3.9. Measured complex reflection coefficient of distilled water-filled cracks in aluminum with widths of 0.75, 1.13, and 1.5 mm and corresponding depths of 1.03, 1.01, and 0.99 mm, respectively, at X-band: a) magnitude and b) phase of the reflection coefficient as a function of frequency, and c) reflection coefficient in the complex polar plane.

indicating that these cracks are highly undercoupled. The measurement error is again clearly seen due to the small overall change in the reflection coefficient.

Figure 3.10 shows a comparison of the estimated depth and the actual crack depth for simulations of cracks filled with barium titanate and measurements of cracks filled

with barium titanate, corn oil, and distilled water. The dielectric properties given in Table 3.1 were used for the barium titanate in the simulations and the depth calculation for both simulations and measurements; a value of $\varepsilon_r' = 2.5$ [42] was used for the corn oil and a value of $\varepsilon_r' = 66$ [43] was used for the distilled water. For the simulations, a crack with $W = 0.5$ mm was used and the (actual) depth was varied. The measurements include a mix of cracks with widths from 0.5 to 1.5 mm, and the "actual depth" was measured by a micrometer. For both simulation and measurement the resonant frequencies were found from the minimum of the magnitude of reflection coefficient, and the depth was estimated using (2). Figure 3.10 clearly shows the ability of this method to reasonably accurately estimate crack depth. The depth estimation from simulation is quite accurate, with error of only a few percent coming from the crack width as described previously. Depth estimation using the measurements show greater error; especially for the K- and Ka-band barium titanate-filled crack measurements, which is most likely due to the

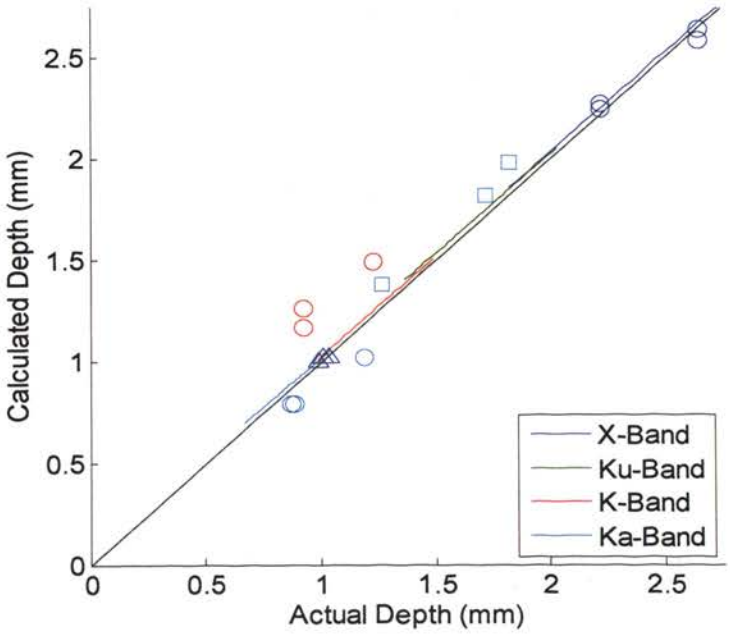

Figure 3.10. Comparison of depth calculated from simulation of barium titanate-filled cracks (lines) and measurement of barium titanate (circles), corn oil (squares), and distilled water (triangles) filled cracks using (2), to actual depth (as measured by micrometer). Repeated measurements of the same crack samples are included.

extrapolation of relative permittivity for these bands. The variations in packing also contribute to the error in barium titanate measurements, as can be seen in the difference between estimated depths for repeated measurements of the same crack. The influence of crack width on the resonant frequency may also be important, and since it was much greater for empty than filled cracks it will likely be greatest for small permittivity materials (e.g., corn oil). The positioning of the waveguide over the crack is another source of error common to the measurements.

Figure 3.11 shows a comparison of the estimated depth and the actual crack depth for the barium titanate-filled cracks in Figure 3.10, using (14) to correct for the crack width ((14) was derived for permittivities near barium titanate, and may not be accurate for the other filling materials). It is observed that for this case the depths calculated from simulation are very accurate, within 0.6% of the actual depths. The accuracy of depth estimation from measurement is not significantly changed, suggesting that other sources of error are more significant than the influence of crack width.

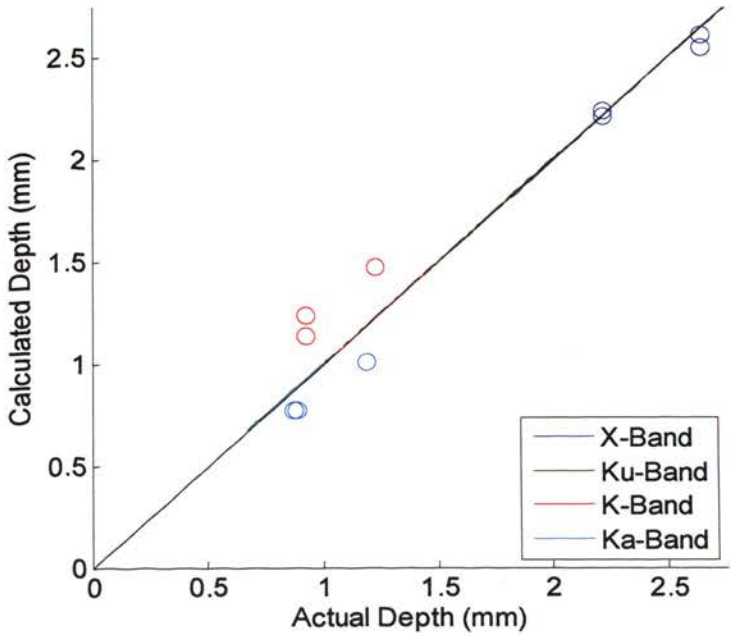

Figure 3.11. Comparison of depth calculated from simulation and measurement of barium titanate-filled cracks to actual depth, as shown in Figure 3.10 but corrected for width using (14).

3.2. FINITE CRACKS

As for finite empty cracks, the behavior of finite filled-cracks can be somewhat similar to long cracks if the crack length is sufficient to support a propagating mode for a portion of the frequencies within the band. Additionally, the filling material makes the cracks electromagnetically longer and the effect of reducing crack length is lessened, as will be shown.

Figure 3.12 shows the simulated frequency dependence of the complex reflection coefficient for cracks with $D = 3$ mm, $W = 2.3$ mm, and six different lengths (starting from $L = a = 23$ mm), filled with a dielectric ($\varepsilon_r = 9$, $\tan\delta = 0.063$) at X-band. It is seen in both the magnitude and phase that the resonant frequency shifts to the right (higher frequencies) as the crack length decreases, as happened for empty cracks and expected from (2). This shift accelerates as the length is reduced. The resonant frequency shifts slower for filled-cracks than for empty cracks; the resonance is still observed even when $L = 8$ mm $\sim a/3$, while for empty cracks it disappeared before $L = a/2$. It is also observed from both the magnitude and phase that the coupling is reduced as the length decreases, as expected since the 23 mm long crack is already undercoupled (from the phase,

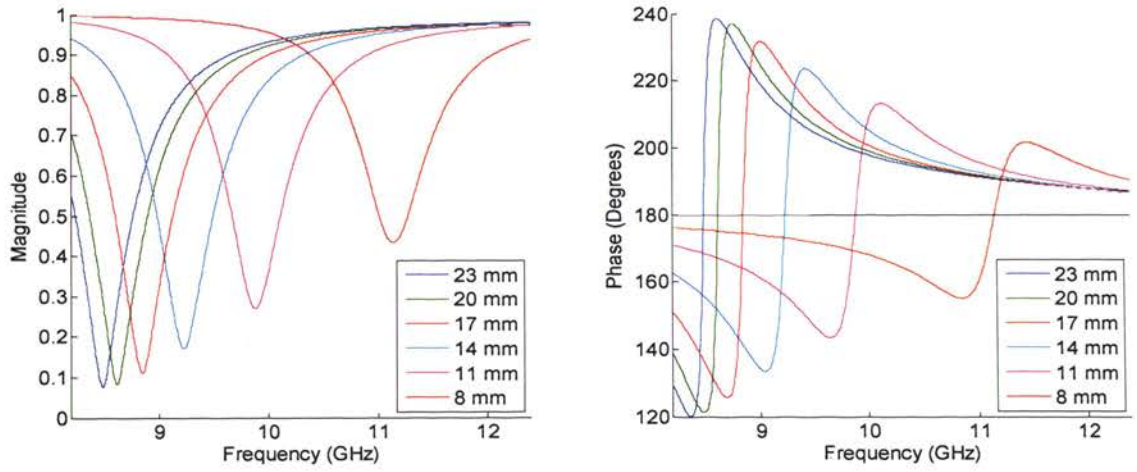

Figure 3.12. Simulated complex reflection coefficient as a function of frequency for filled ($\varepsilon_r = 9$, $\tan\delta = 0.063$) finite cracks in perfect electric conductor with $D = 3$ mm, $W = 2.3$ mm, and six lengths at X-band: a) magnitude and b) phase.

compare to Figure 3.1b) and as the length is reduced even less signal will be coupled into the crack.

Figure 3.13 shows the effect of reduction in crack length from a on depth evaluation, for empty and filled-cracks with $W = 2.3$ mm and depths of 13 and 3 mm, respectively. The different depths were necessary to position the resonant frequency at approximately the same initial ($L = a$) value. Figure 3.13a shows the change in resonant frequency. Although a shift in the resonant frequency occurs in both cases, it is much less for filled than for empty cracks, as observed above, allowing shorter cracks to be evaluated. Figure 3.13b shows the error in depth evaluation using (2) as a function of reduction in crack length. These results suggest that crack depth could be reasonably estimated using (2) as long as the resonant frequency is within the frequency band and crack length is known. The error due to crack length could also be removed, using a correction factor as a function of crack length.

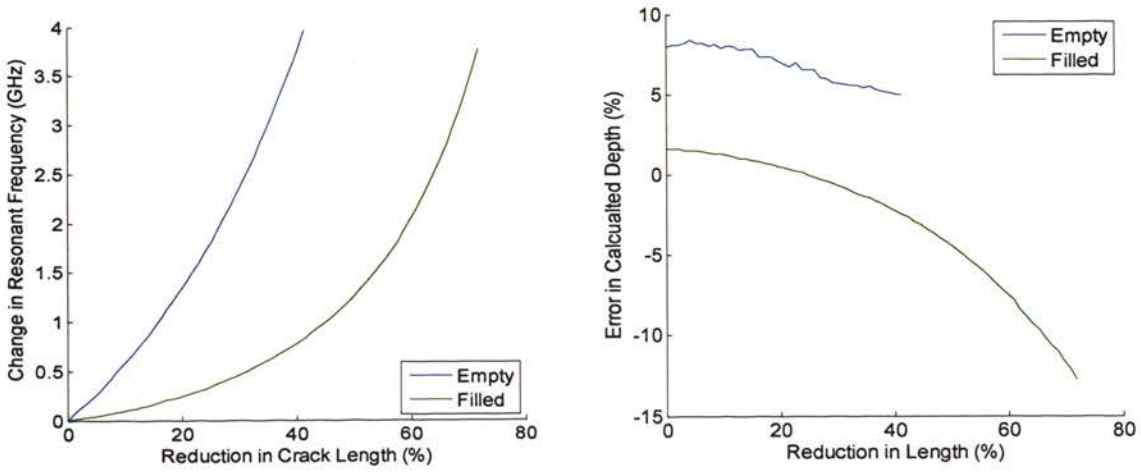

(a) (b)

Figure 3.13. Effect of reduction in crack length from a on depth evaluation for empty ($D = 13$ mm, $W = 2.3$ mm) and filled ($\varepsilon_r = 9$, $\tan\delta = 0.063$, $D = 3$ mm, $W = 2.3$ mm) cracks in perfect electric conductor at X-band: a) change in resonant frequency and b) error in depth estimation using (2).

3.3. PITS

Filled pits have electrically larger dimensions than when empty and may support propagating waves while being small enough to be contained in the probing waveguide aperture. Figure 3.14 shows the simulated magnitude of reflection coefficient and measured reflectometer output for four barium titanate-filled pits with diameter of 2.75 mm and four different depths at Ka-band. Resonances are clearly visible in the simulated magnitude for the three deepest pits, as seen in Figure 3.14a, and a part of the resonant dip is visible for the shallowest pit. This shows that these pits will support at least one propagating mode. The edge of the resonant dip for a second resonance is also visible for the 2.51 mm-deep pit. Simulations (not shown) indicated that these pits will support at least two propagating modes which are excited by the probing waveguide. Consequently, the pit depth cannot be calculated directly from equations for circular waveguides and the relationship would likely have to be developed from simulation or measurement. Figure 3.14b shows measurement results for pits with similar dimensions using the Ka-band reflectometer. As for the simulations, resonances are visible for the three deepest cracks,

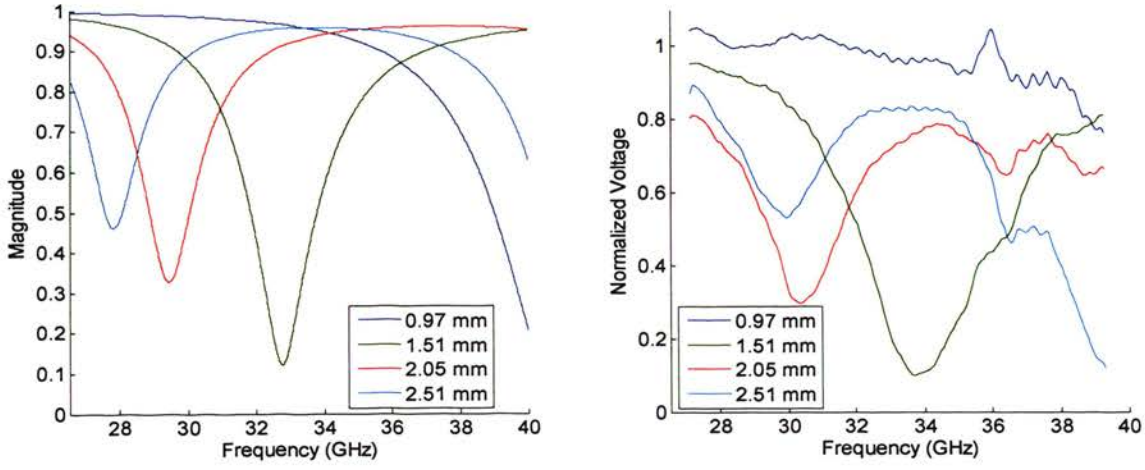

(a) (b)

Figure 3.14. Resonant response as a function of frequency for barium titanate-filled cracks with diameter of 2.75 mm and five depths at Ka-band: a) simulated magnitude of reflection coefficient and b) measured reflectometer output. In b) smoothing and normalization to a no crack measurement (per frequency point) were applied.

and a part of the resonance response is seen for the shallowest. The edge of the second resonant dip is seen for the 2.51 mm-deep crack as well and, in fact, shows a greater drop in signal.

4. DIELECTRIC SLAB-LOADED WAVEGUIDE PROBE

4.1. PROBE DESIGN

The quarter-wavelength method of depth evaluation presented in Sections 2 and 3 has a practical limitation which is the requirement of using high frequencies for very shallow damage depth to become equal to a quarter-wavelength. It is also limited by the requirement that damage length or diameter is large enough to support a propagating mode. A probe was designed to avoid these limitations by providing a resonance within the probe itself. The probe is placed so that the sample being tested (conducting plate and damage) becomes one face of the resonator. Damage in the sample may change the response of the resonance, and analysis of these changes may allow evaluation of the damage depth.

The resonant structure was formed by placing a dielectric insert in the probing waveguide, as shown in Figure 4.1. The shape of the insert is shown in Figure 4.1a. A dielectric insert of this shape has been used before to concentrate the electric field in the center of the waveguide and increase its sensitivity for detecting tiny pits [30] in a non-resonant measurement approach. The dielectric material TMM10I, a ceramic polymer composite designed for stripline and microstrip applications, was used for the insert. The dielectric properties of this material are listed to be $\varepsilon_r' = 9.8 \pm 0.245$ and $\tan \delta = 0.002$ [46] and it can be purchased in a sheet form which readily enables cutting it to the desired

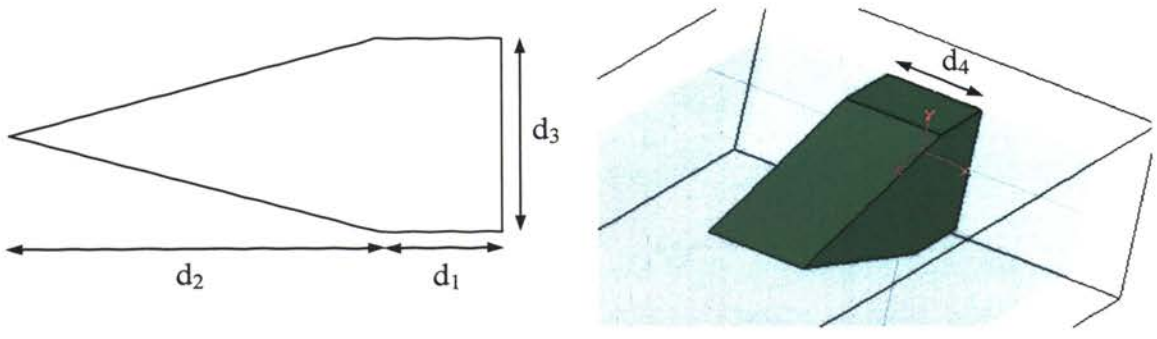

Figure 4.1. Dielectric insert: a) Side-view and b) perspective view in waveguide (to-scale). $d_1 = 2.5$ mm, $d_2 = 7.5$ mm, $d_3 = 4.3$ mm, and $d_4 = 3.175$ mm.

shape. The shape shown in Figure 4.1a is cut out of a sheet with thickness of 3.175 mm to make the insert. The insert is tightly placed along the *b* dimension of the probing rectangular waveguide section, as shown in Figure 4.1b, with the insert centered along the *a* dimension and flush with the waveguide aperture. Due to availability a waveguide section of length 50.8 mm was used. The insert and the waveguide section together constitute what will be referred to as the slab-loaded waveguide probe. The probe was designed to operate at K-band (18-26.5 GHz). This band was chosen for demonstrating the proof-of-concept for damage depth evaluation and also due to the availability of a VNA for coherent reflection coefficient measurements.

Figure 4.2 shows the magnitude and phase of reflection coefficient for the slab-loaded waveguide probe placed against an aluminum plate (no damage) at K-band. The measurement system is calibrated before the probe is attached, since proper calibration loads do not exist for this unique probe and it cannot be calibrated at the aperture. In Figure 4.2a a resonance is observed as a sharp dip in the magnitude near 25.5 GHz. Since no damage is present in this simulation, the resonance occurs solely due to the dielectric insert. The resonance is very sharp, which may be attributed to the low loss nature of the dielectric material used for the insert. In Figure 3.2b there is a significant linear response in the phase, due to signal propagation through the waveguide section, and a sharp change at the resonance (about 25.5 GHz). Figure 4.2c shows this phase response with the linear portion subtracted out. The phase results reported throughout the rest of this section will have a similar subtraction applied. With the signal propagation effects thus removed the resonant response in the phase can be clearly seen. The phase goes through a 360° change so the resonator is overcoupled. The phase variation apart from the resonance response suggests that the linear subtraction applied to the phase does not completely remove all other features.

Figure 4.3 shows the simulated sensitivity of the magnitude of reflection coefficient at resonance to various geometrical parameters of the dielectric slab, as given in Figure 4.1. The magnitude level at the resonance is clearly dependent on d_1, d_2, and d_3, but only weakly dependent on d_4. The non-monotonic behavior is attributed to coupling from the empty waveguide into the resonant section (the section with the dielectric insert), since similar behavior was observed for the coupling of the signal from a probing

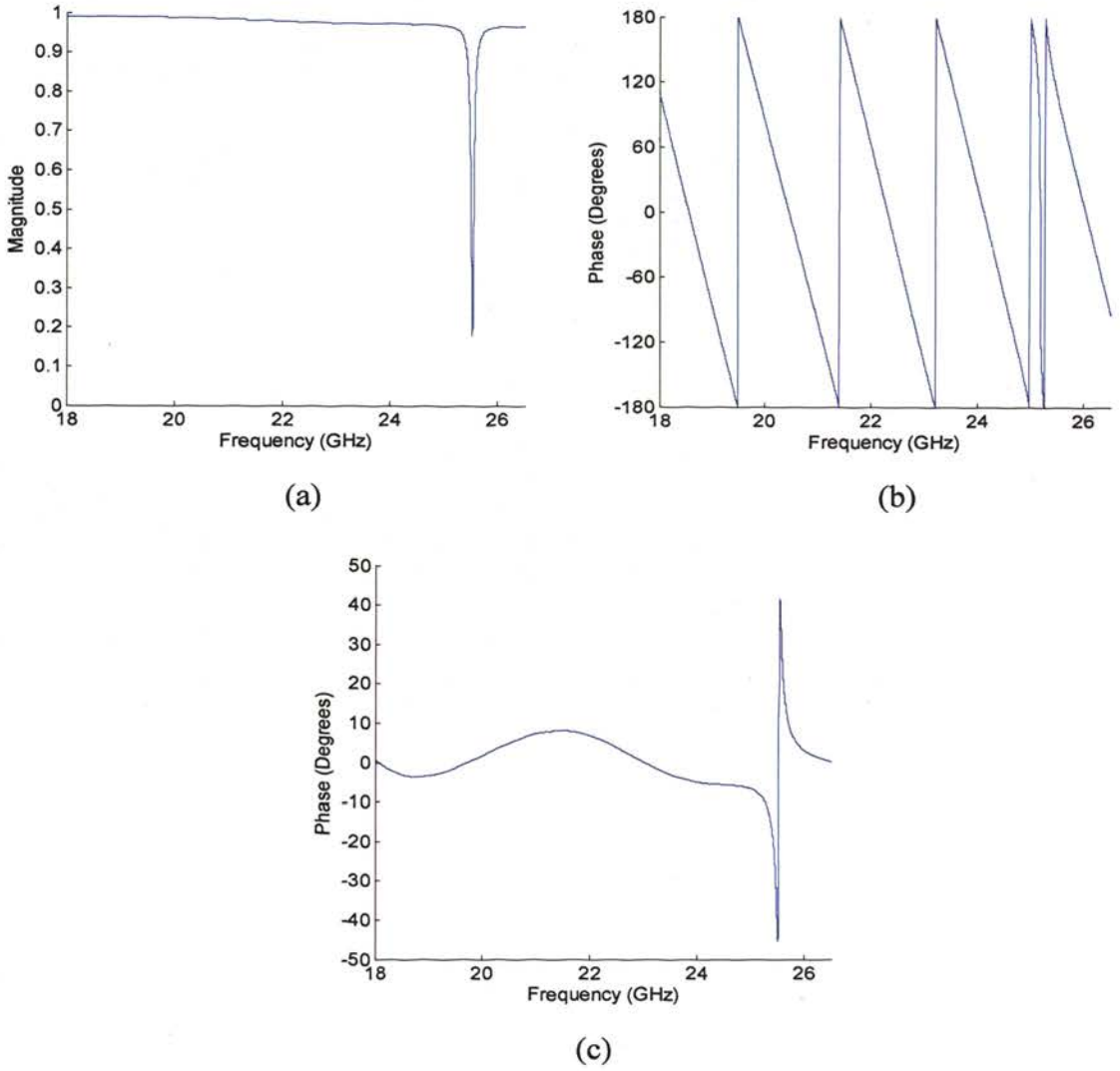

Figure 4.2. Simulated complex reflection coefficient as a function of frequency for slab-loaded waveguide probe and aluminum plate at K-band: a) magnitude, b) uncorrected phase, and c) corrected phase.

waveguide into quarter-wavelength resonant cracks in Sections 2 and 3. The minimums then correspond to critical coupling. This shows that d_1, d_2, and d_3 each affect the coupling from the empty waveguide into the resonant section of the probe. The noise-like variation in Figure 4.3d is due to the discrete frequency steps and does not reflect any physical phenomenon. For all of these cases the magnitude dips to less than 0.4 and, consequently, the resonant frequency can be easily determined from the magnitude.

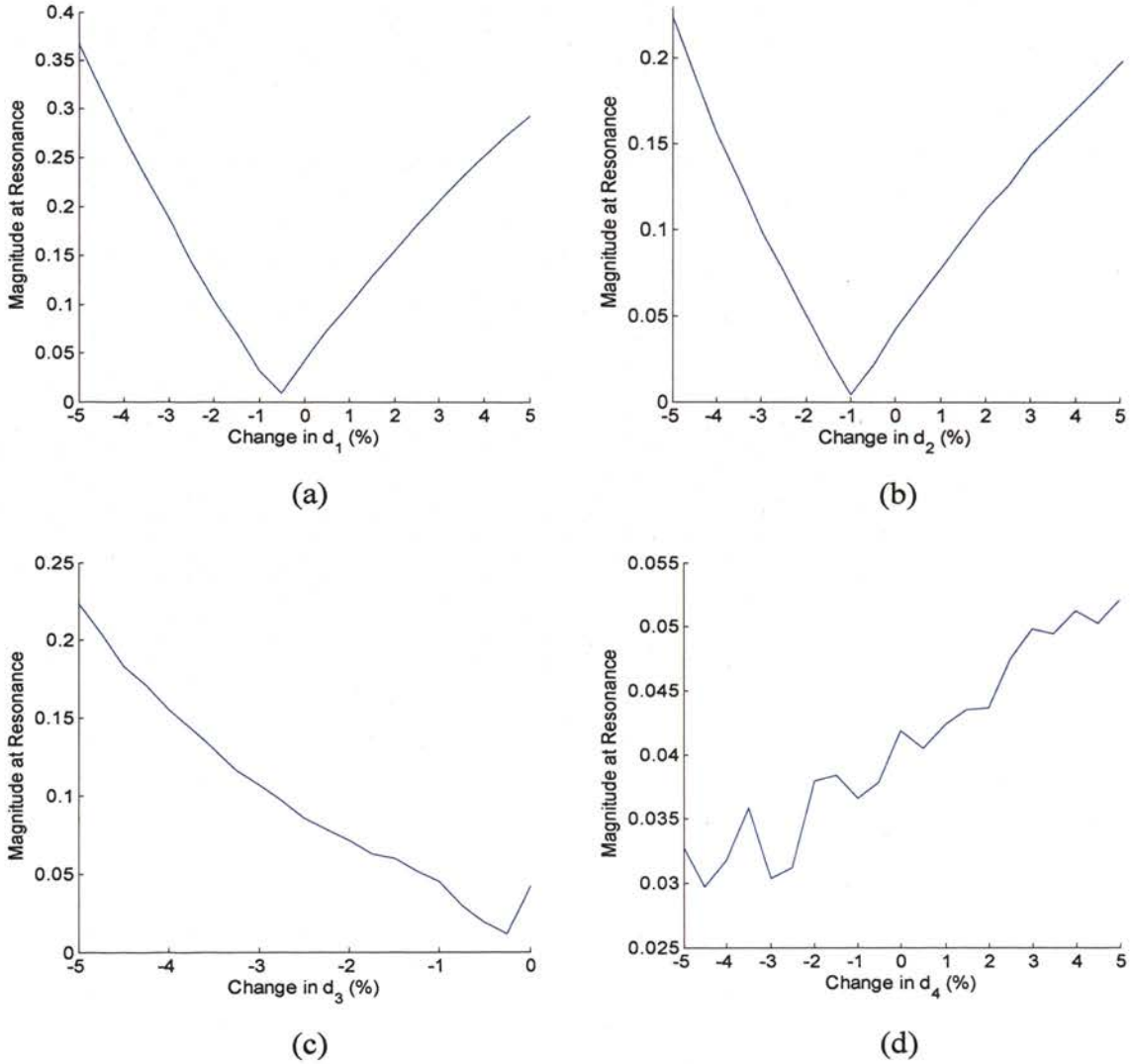

Figure 4.3. Simulated sensitivity of the magnitude level at resonance to geometric parameters of the dielectric insert at K-band: sensitivity to a) d_1, b) d_2, c) d_3, and d) d_4.

Figure 4.4 shows the simulated sensitivity of the resonant frequency to various geometrical parameters of the dielectric slab, as given in Figure 4.1. The resonant frequency is inversely related, in a near-linear fashion, to each parameter. This makes physical sense, since smaller resonators will tend to resonate at higher frequencies. The resonant frequency is most strongly dependent on d_3, with a 5% reduction resulting in a 1.6% shift of the resonant frequency. It is then dependent, in decreasing order of dependence, on d_4, d_1, and d_2, respectively. A shift in the resonant frequency due to the

probe characteristics is not particularly critical since it will be common for reference and damage measurements. The shift may be significant if a direct comparison of simulation and measurement is desired or if the shift is large enough to move the resonance outside of the operating frequency band. These shifts are relatively small so the latter is not expected to occur.

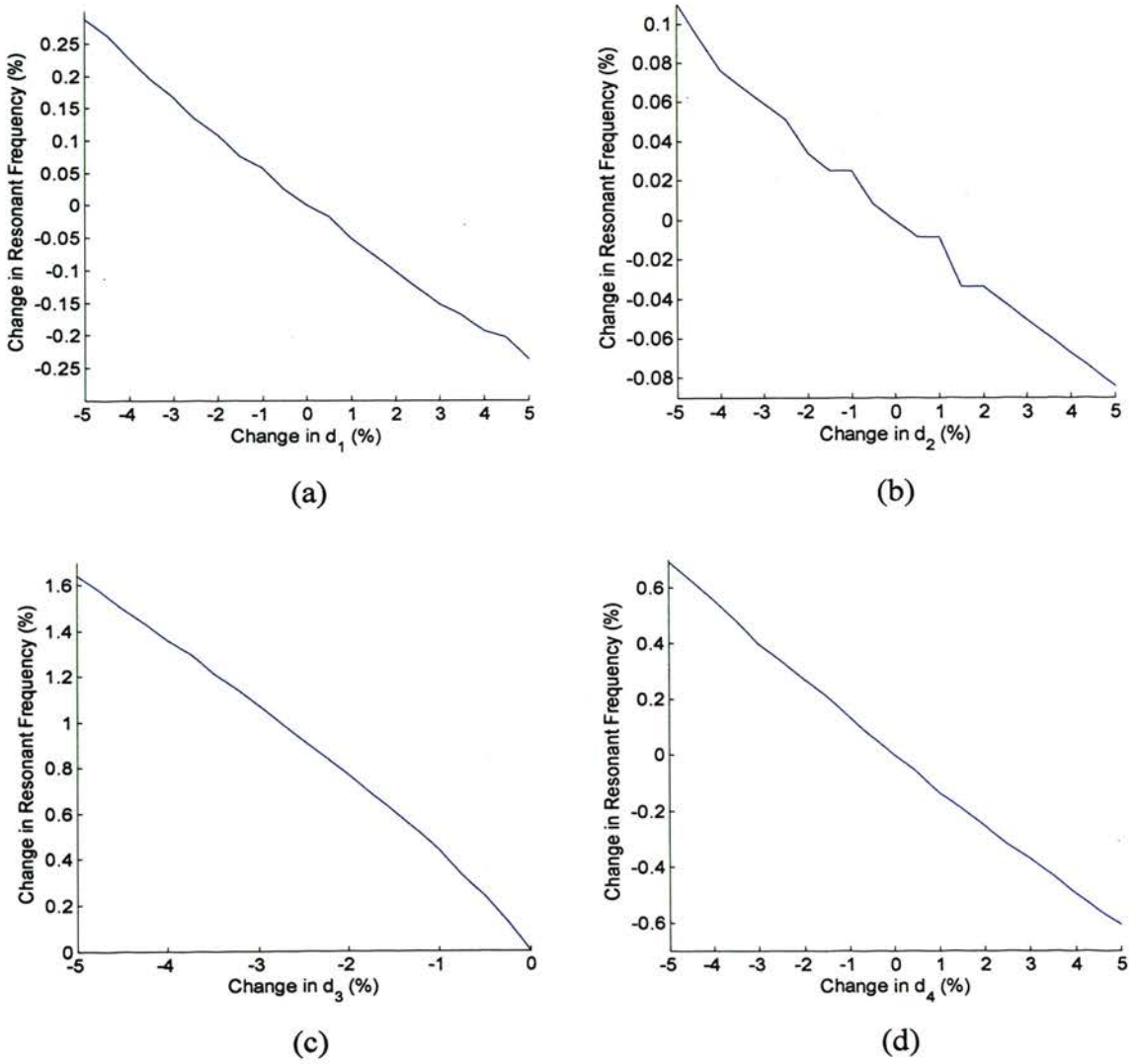

Figure 4.4. Simulated sensitivity of the resonant frequency to geometric parameters of the dielectric insert at K-band: sensitivity to a) d_1, b) d_2, c) d_3, and d) d_4.

4.2. LONG CRACKS

4.2.1. Simulation Results. The consideration of crack lengths extending beyond the waveguide aperture has a significant effect on simulation time and also whether crack length must be considered as a parameter to describe a "long" crack. Figure 4.5 shows the magnitude of reflection coefficient for long cracks with $D = 0.2$ mm, $W = 0.5$ mm and three lengths at K-band. The curves lie on top of one another, with virtually no difference in the reflection coefficient characteristics as a function of crack length. This shows that the reflection coefficient is not sensitive to crack length extending outside the probing waveguide aperture and the simulation geometry can be simplified by setting $L = a$, as shown in Figure 1.1a. This is expected since one of the consequences of the dielectric insert is that the electric field is concentrated in the center of the waveguide, resulting in this probe being less sensitive to variations in crack length than the empty waveguide probes described previously.

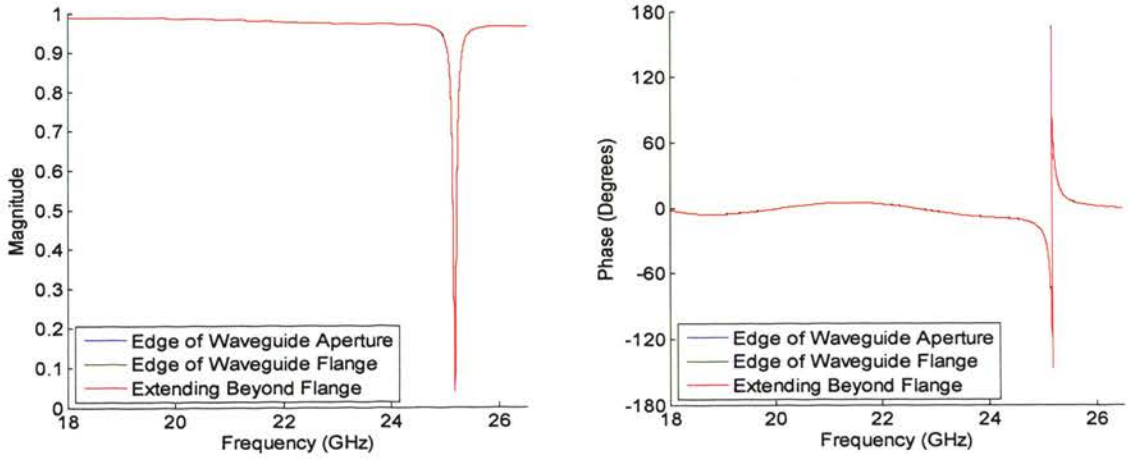

(a) (b)

Figure 4.5. Simulated complex reflection coefficient as a function of frequency for slab-loaded waveguide probe and crack in aluminum with $D = 0.2$ mm, $W = 0.5$ mm and three lengths at K-band: a) magnitude and b) phase.

Figure 4.6 similarly shows the complex reflection coefficient for cracks with $W =$ 0.5 mm and six different depths at K-band, while crack lengths were set to be equal to a.

There is an obvious shift in the resonant frequency as a function of depth in both the magnitude and phase of reflection coefficient, with deeper cracks shifting the resonance further to the left (lower frequencies). There is also a non-monotonic change in the magnitude levels at resonance. If the phase is considered, it can be seen that as the crack depth increases the resonance behavior changes from undercoupled to overcoupled (phase change of less than 360° to phase change of 360°).

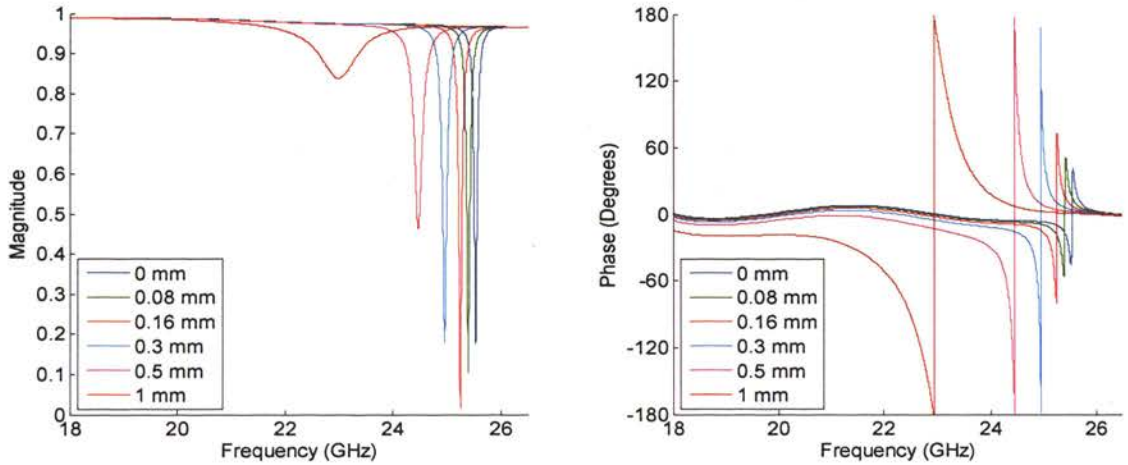

(a) (b)

Figure 4.6. Simulated complex reflection coefficient as a function of frequency for slab-loaded waveguide probe and cracks in aluminum with $W = 0.5$ mm and six depths at K-band: a) magnitude and b) phase.

Figure 4.7 shows simulated characteristics of the resonant response as functions of depth for four crack widths at K-band. Figure 4.7a shows the magnitude of reflection coefficient at the resonant frequency (i.e. magnitude minimum). A non-monotonic behavior is observed, similar to the results shown in Figures 2.4a and 3.2a, with the minimum indicating critical coupling. Figure 4.7b shows the resonant frequency and it is evident that for each width the resonant frequency can be related to a specific depth, which is a very significant feature for depth evaluation. The Q-factors shown in Figure 4.7c are much higher than those seen for crack resonators (see Figures 2.4b and 3.2b),

which may allow more accurate determination of the resonant frequency. For each of these curves, as the depth increases the Q-factor smoothly decreases, with a distinct change in slope at one point (indicated by arrows). By comparison with Figure 4.7a these points correspond to critical coupling. Similar behavior was observed for filled cracks and is shown in Figure 3.2b. A quantization-like feature for the higher Q-factor values is

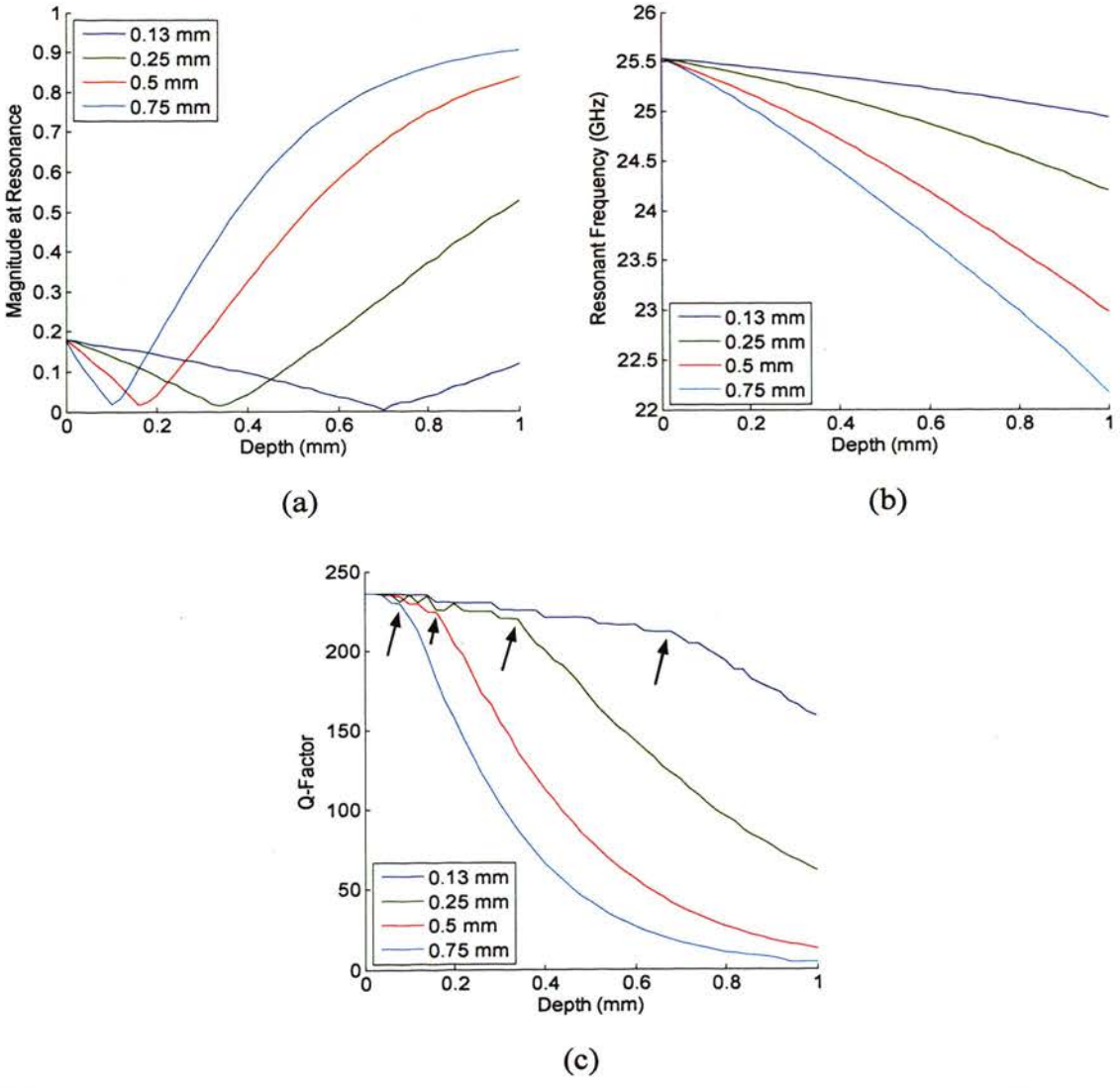

Figure 4.7. Simulated characteristics of resonant response as a function of depth for slab-loaded waveguide probe and cracks in aluminum with four widths at K-band: a) magnitude of reflection coefficient at resonant frequency, b) resonant frequency, and c) Q-factor.

seen in Figure 4.7c, which is due to the fact that discrete frequency points were calculated in these simulation.

4.2.2. Sensitivity Analysis. The sensitivity of this method to variations in the probe position was investigated as well. Figure 4.8 shows the resonant response for a

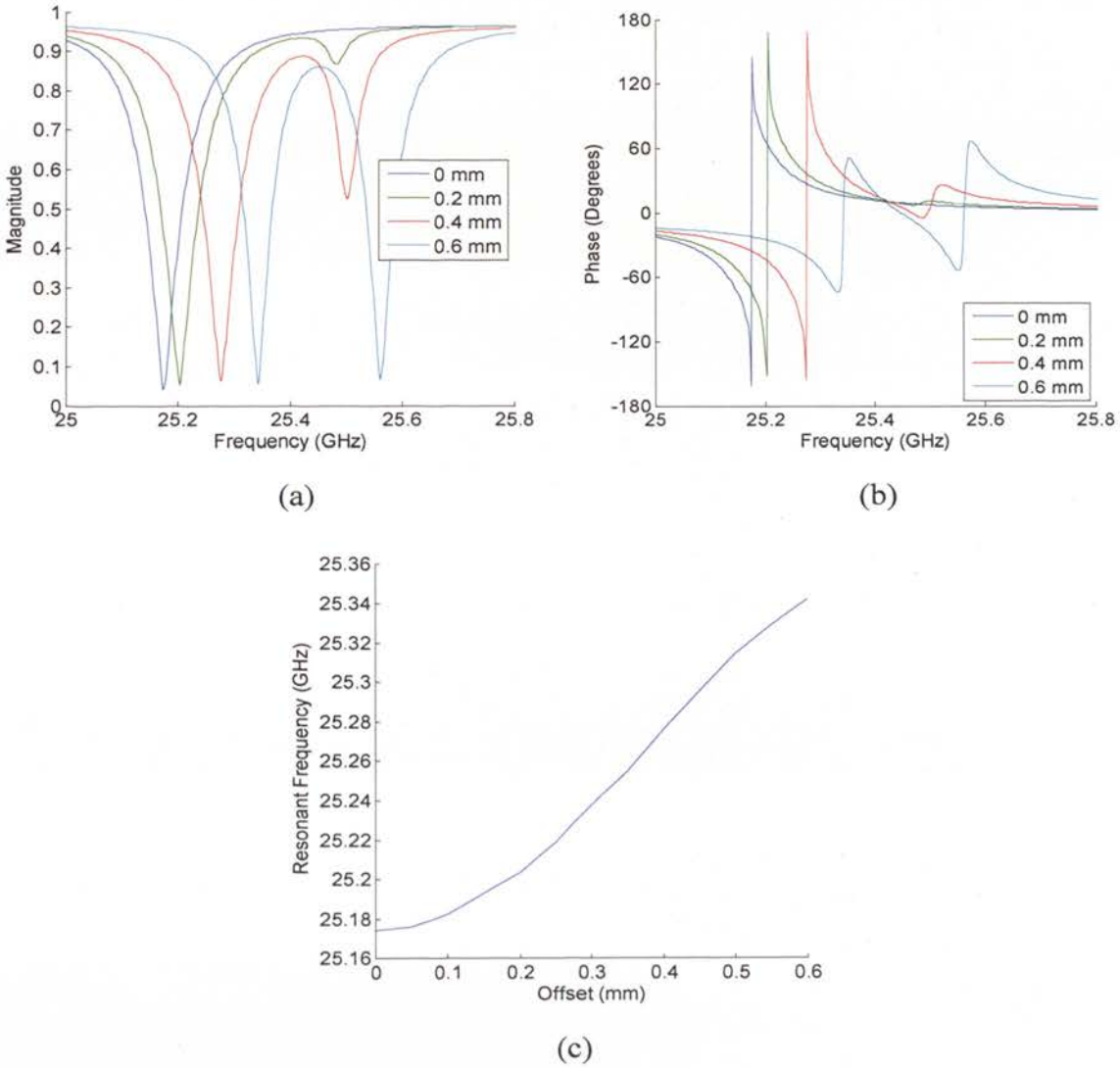

Figure 4.8. Simulated resonant response for slab-loaded waveguide probe and cracks in aluminum with $D = 0.2$ mm and $W = 0.5$ mm with its position varied along b from the center of the probe at K-band: a) magnitude and b) phase of reflection coefficient as a function of frequency for four position offsets and c) resonant frequency as a function of offset.

crack with $D = 0.2$ mm and $W = 0.5$ mm with its position varied along b. Figures 4.8a-b show the magnitude and phase, respectively, of reflection coefficient as a function of frequency for four different offsets of the crack from the center of the probing waveguide along b, only a portion of K-band is shown so the changes in the resonant response can be better viewed. The results show that as the offset increases the initial resonance shifts slightly to the right and a second resonance is observed at a slightly higher frequency. This second resonance may be caused by the excitation of a second mode in the dielectric slab, due to the asymmetry introduced by the geometrical offset in this case. For an offset of 0.6 mm the second resonance has a magnitude dip as large as the first. Figure 4.8c shows the shift of the resonant frequency of the first resonance as a function of the offset. This shift of the resonant frequency is on the order of that produced by variations in depth, so probe position is very critical for accurate depth evaluation using the slab-loaded waveguide probe. However, since the double resonance is an indication that the probe is not centered, the probe can be centered over the crack by varying its position until only one resonance is observed. Alternatively, the minimum resonant frequency could be used to center the probe, as this also occurs at the center position.

Figure 4.9 shows the magnitude of reflection coefficient for six liftoffs (i.e., gaps) of the probe from the conducting plate. A crack length equal to the waveguide flange was used for this simulation. It is observed that the resonance shifts to the right as the liftoff increases and eventually occurs outside of the frequency band for liftoffs greater than 0.05 mm. For a liftoff of 0.1 mm no resonant behavior is visible within the frequency band. Consequently, liftoff can be very critical when using the slab-loaded waveguide probe and care should be taken when measuring to ensure that the probe is in firm contact with the conducting plate.

4.2.3. Dielectric-Filled Cracks. An investigation was undertaken to see if filling the crack with a dielectric material may be used in conjunction with the slab-loaded waveguide probe to improve the depth evaluation characteristics. Figure 4.10 shows characteristics of the resonant response as functions of depth for empty and filled ($\varepsilon_r' = 10$, $\tan\delta = 0.06$) cracks with $W = 0.5$ mm at K-band. Figure 4.10a shows the magnitude of reflection coefficient at the resonant frequency (i.e. magnitude minimum). For cracks

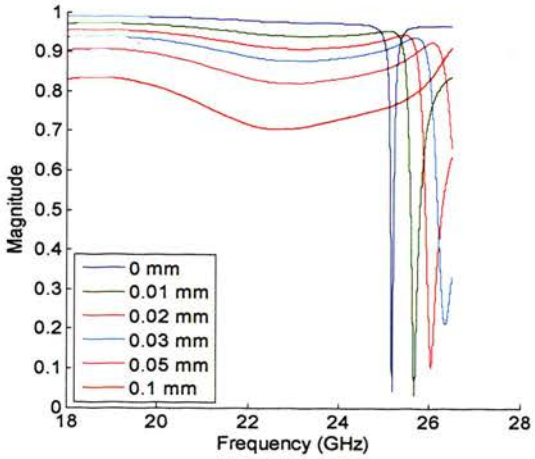

Figure 4.9. Simulated magnitude of reflection coefficient as a function of frequency for slab-loaded waveguide probe and crack in aluminum with $D = 0.2$ mm, $W = 0.5$ mm, and four liftoffs of the probe from the aluminum plate at K-band.

shallower than 0.2 mm (i.e., undercoupled cracks, from Figure 4.6b) filling the crack does not affect the magnitude at resonance significantly; but for deeper cracks the magnitude level is lower for filled cracks, and begins to decrease as a function of depth for depths of 0.7–1 mm. This is likely due to the loss from the dielectric in the crack. Figure 4.10b shows the resonant frequency. For depths less than 0.2 mm filling has no effect on the resonant frequency, but for deeper cracks the frequency shift is greater for filled cracks than for empty ones. Figure 4.10c shows that the Q-factor is also unchanged for depths less than 0.2 mm, but for greater depths the Q-factor is lower for filled cracks. This is expected since additional losses are introduced by the dielectric filling material. These simulations show that dielectric fillings have no effect for the shallowest cracks, the most important and difficult case for evaluation. However, for deeper cracks, a dielectric filling material may be beneficial for increasing the shift of the resonant frequency and the magnitude dip, at the cost of a lower Q-factor.

4.2.4. Measurement Results. A dielectric slab-loaded waveguide probe was prepared as shown in Figure 4.1. Figure 4.11 shows the magnitude of reflection coefficient for cracks with four different widths and various depths. Several resonances are observed; the desired resonance is indicated by the arrows and the resonant behavior is much wider (i.e., lower Q-factor) and has a smaller magnitude dip than predicted by

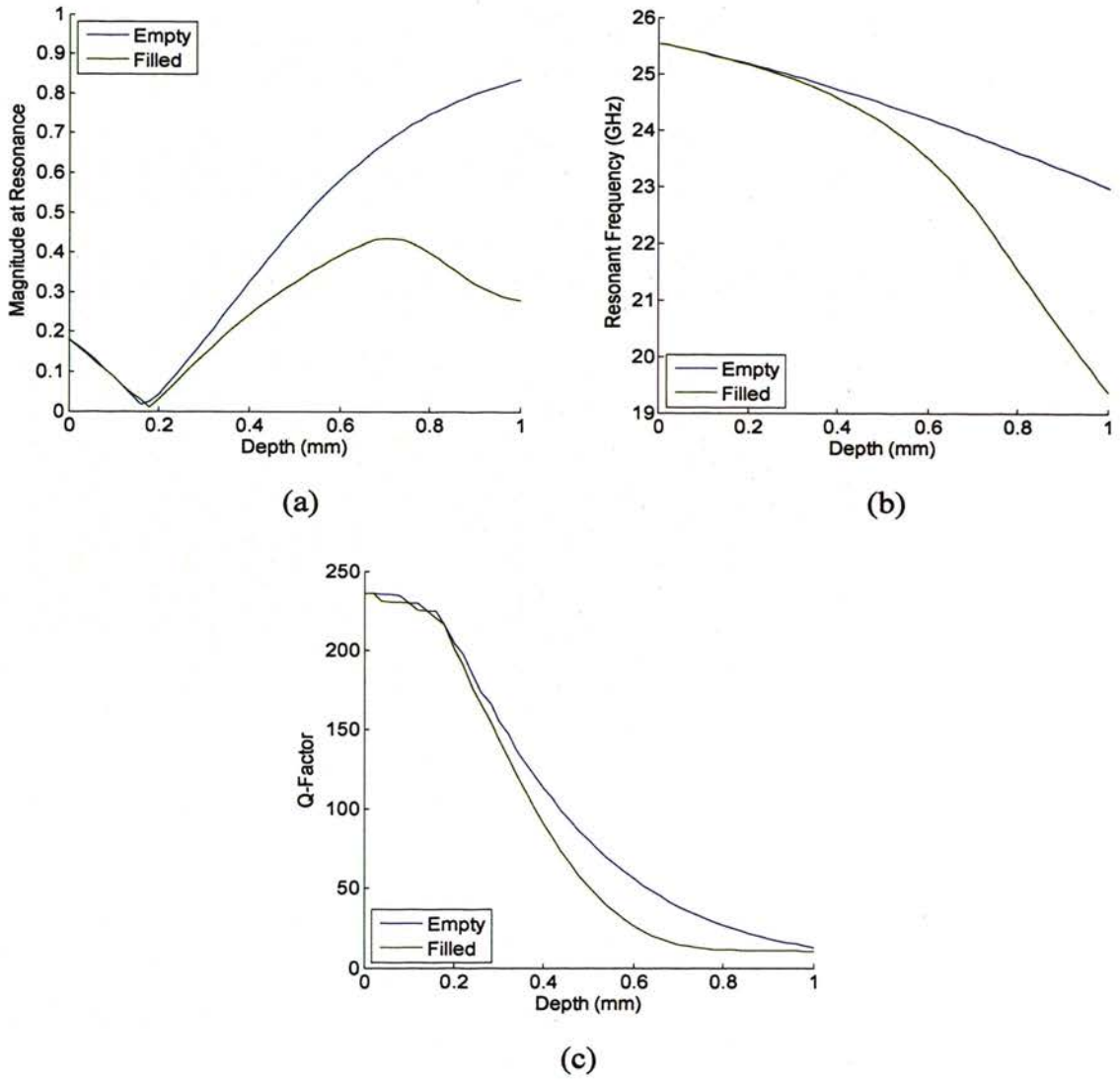

Figure 4.10. Simulated characteristics of resonant response as functions of depth for slab-loaded waveguide probe and empty and filled ($\varepsilon_r' = 10$, $\tan\delta = 0.06$) cracks in aluminum with $W = 0.5$ mm at K-band: a) magnitude at resonant frequency, b) resonant frequency, and c) Q-factor.

simulation. The additional resonances are most likely due to imperfections in the preparation and placement of the dielectric insert. The dominant resonance can easily be identified and the resonance frequency is observed to shift with depth, so some degree of depth evaluation may be possible. It is also worth noting that the magnitude level outside the resonance is much lower than shown by the simulation results (i.e., about 0.7 instead

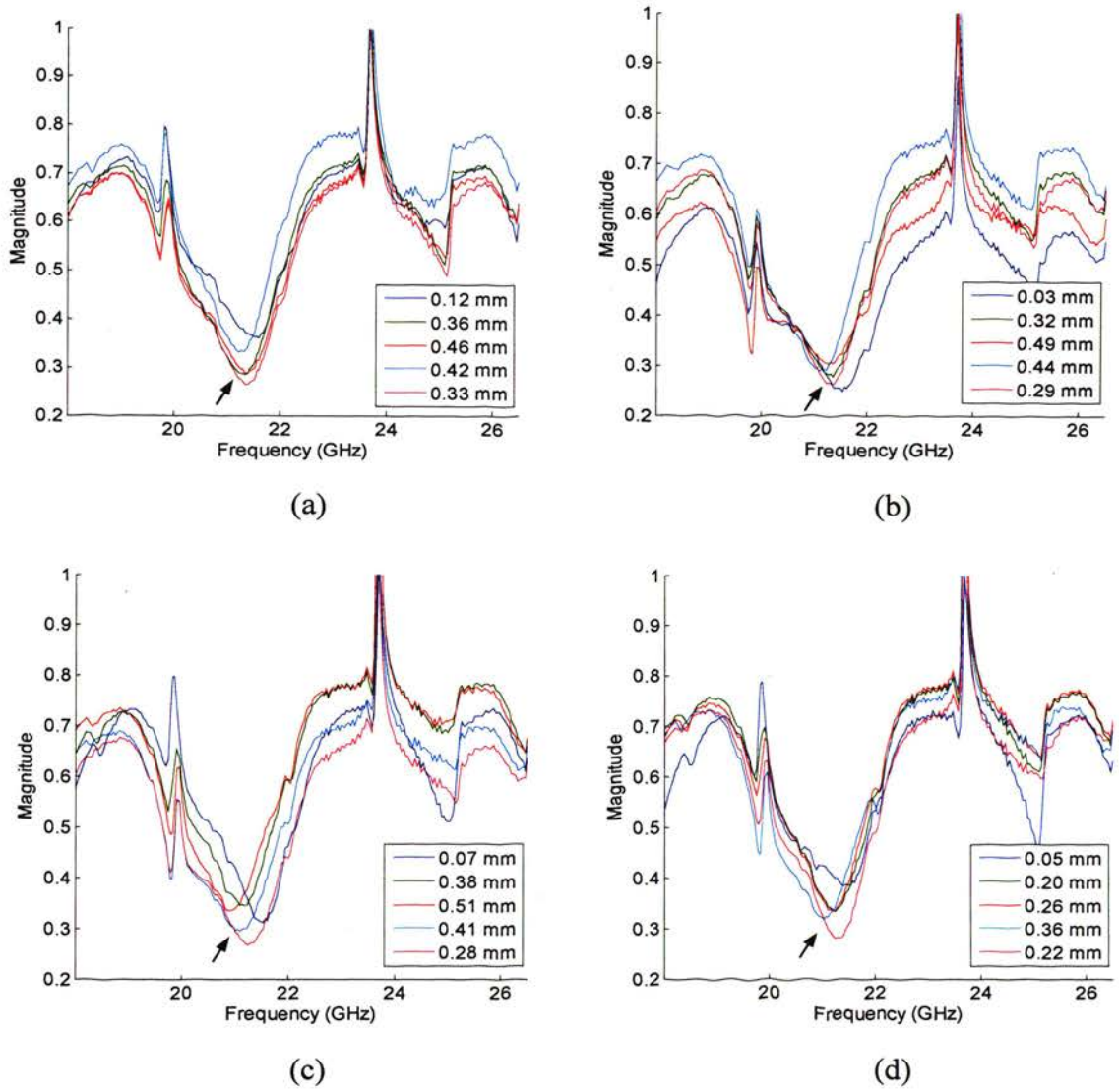

Figure 4.11. Measured magnitude of reflection coefficient as a function of frequency for slab-loaded waveguide probe and cracks with four widths and several depths at K-band: a) $W = 0.51$ mm and five depths, b) $W = 1.02$ mm and five depths, c) $W = 1.52$ mm and five depths, and d) $W = 2.54$ mm and five depths. The desired resonances are indicated by arrows.

of 0.95), which seems to indicate that there are significantly more non-resonance losses in the actual probe than there were in the simulations.

Figure 4.12 shows the resonant frequency, from the measurements in Figure 4.11, as a function of varying crack depth. The results show lower resonant frequencies for

deeper cracks, as expected. However, the correlation is weak, which may be due to error from the imperfections in the probe construction or variations in probe position. If a few outliers are removed, these results suggest that crack depth may be evaluated with roughly 25% error.

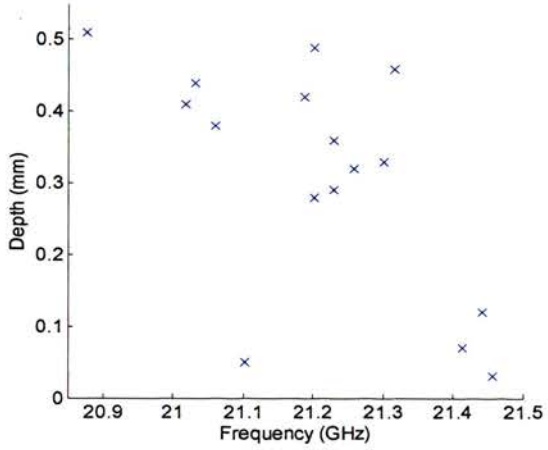

Figure 4.12. Crack depth vs. resonant frequency for slab-loaded waveguide probe and cracks with four widths at K-band.

A second probe was prepared and used to repeat the measurements of the 1.52 and 2.54 mm-wide cracks. Figure 4.13 shows the magnitude of reflection coefficient for these measurements, and can be directly compared to Figures 4.11c-d. It is observed that there are fewer extra resonances in these measurements, and those extra resonances are smaller, which may indicate that this probe was prepared more accurately. The desired resonance is clearly evident, and the resonant frequency shifts with crack depth. The resonant dip in magnitude is still smaller and wider (lower Q-factor) than expected from simulation, but the resonant frequency can still be easily determined. A second resonance is observed to the right of the desired resonant frequency, which is likely due to the offset of the probe position from the center of the crack (see Figure 4.8a).

Figure 4.14 shows the resonant frequency, from the measurements shown in Figures 4.13a-b, as a function of crack depth. The relationship between crack depth and

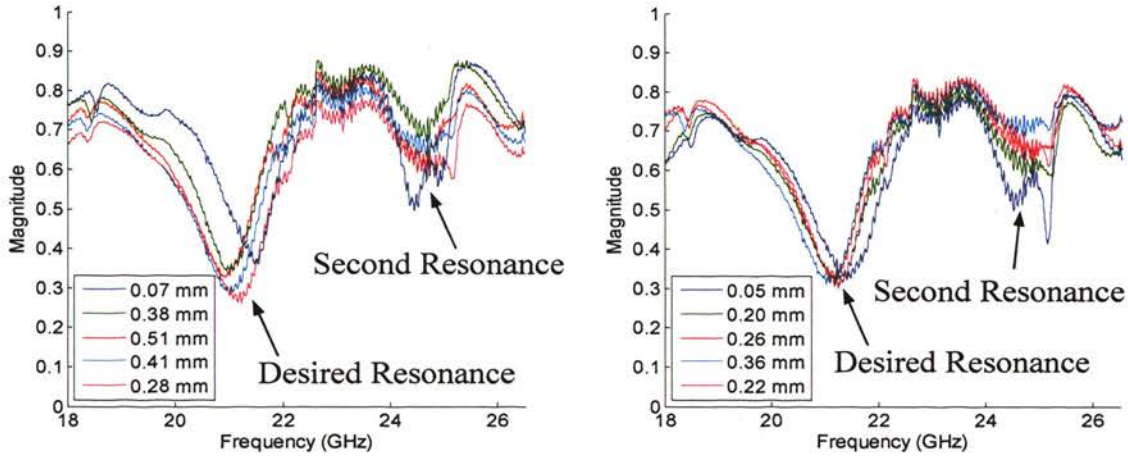

Figure 4.13. Measured magnitude of reflection coefficient as a function of frequency for dielectric slab-loaded waveguide probe and cracks with two widths and several depths at K-band: a) $W = 1.52$ mm and five depths and b) $W = 2.54$ mm and five depths.

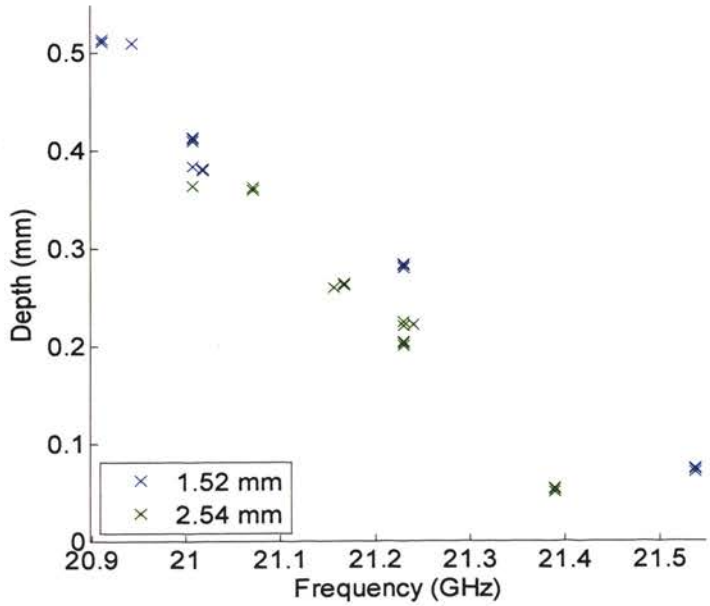

Figure 4.14. Crack depth vs. resonant frequency for slab-loaded waveguide probe and cracks with two widths at K-band. Three measurements of each crack are shown.

resonant frequency is much more clear for this set of measurements than those shown in Figure 4.12. The crack width is also seen to have an effect on the resonant frequency, with a roughly linear relationship between crack depth and resonant frequency. Three measurements of each crack are included in these results and the agreement in resonant frequency within each set of three shows that these measurements are repeatable with respect to probe position.

4.3. FINITE CRACKS

Figure 4.15 shows the resonant response for different crack lengths. Figure 4.15a shows the magnitude of reflection coefficient for six different finite-crack lengths. There is no significant change between the $L = a = 11$ mm and $L = 5$ mm curves. A small shift of the resonant frequency is seen for the $L = 4$ mm curve and the resonance continues to shift as the length becomes shorter, approaching the undamaged conducting plate case as the length goes to zero. Figure 4.15b shows the resonant frequency as a function of crack length. As observed from Figure 4.15a, there is no noticeable change for lengths greater

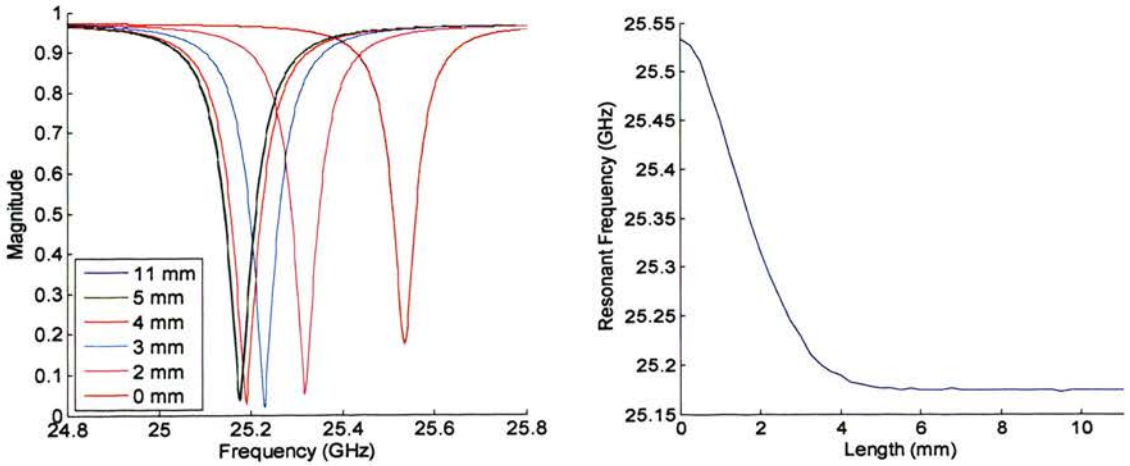

(a) (b)

Figure 4.15. Simulated resonant response for cracks in aluminum with $D = 0.2$ mm, $W = 0.5$ mm, and different lengths at K-band: a) magnitude of reflection coefficient as a function of frequency for six crack lengths and b) resonant frequency as a function of crack length.

than 5 mm, but for smaller lengths the resonant frequency undergoes a significant shift. The dielectric insert width, d_4, of 3.175 mm may be related to the crack length which is significant. If that is correct, only the portion of the crack which is next to the dielectric insert will significantly affect the resonance. These simulations suggest that cracks with $a > L \geq a/3$ may be reasonably considered to be "long" (i.e., $a = L$) for the purpose of depth evaluation.

4.4. PITS

4.4.1. Simulation Results. The concentration of the electric field near the center of the waveguide due to the dielectric insert (as described in [30] and seen in the finite crack results) and the resonance perturbation approach are both expected to be beneficial features for pit depth evaluation. Figure 4.16 shows the simulated complex reflection coefficient for the slab-loaded waveguide probe and pits with two diameters, each with six different depths. Figures 4.16a-b show a small but measurable shift in the resonant frequency in both the magnitude and phase, respectively, for pits with diameter of 1 mm, and the resonant frequency converges to a finite value as the depth increases. This convergence is expected since the pit is much too small (pit diameter $<< a$) to support a propagating mode, and consequently penetration will be limited. Figures 4.16c-d show a much more significant shift for pits with diameter of 2 mm, which is expected since larger pits should perturb the resonance characteristics more significantly. It is also observed that the resonance shifts first to the right, and then to the left, as the depth increases, which could introduce ambiguity in depth evaluation when using the resonant frequency for this purpose.

Figure 4.17 shows characteristics of the resonant response as functions of depth for pits with five different diameters. The Q-factor in Figure 4.17c is calculated from (8). The magnitude at the resonant frequency (Figure 4.17a), resonant frequency (Figure 4.17b), and Q-factor (Figure 4.17c) are all insensitive to the 0.5 mm-diameter pits. They are sensitive to changes in depth for the 1 mm-diameter pits, but only for depths less than 0.4 mm. This may be considered the penetration limit of the non-propagating modes supported by the pit. For the 1.5, 2, and 2.5 mm-diameter pits the magnitude at the resonant frequency, resonant frequency, and Q-factor all appears to be converging to a

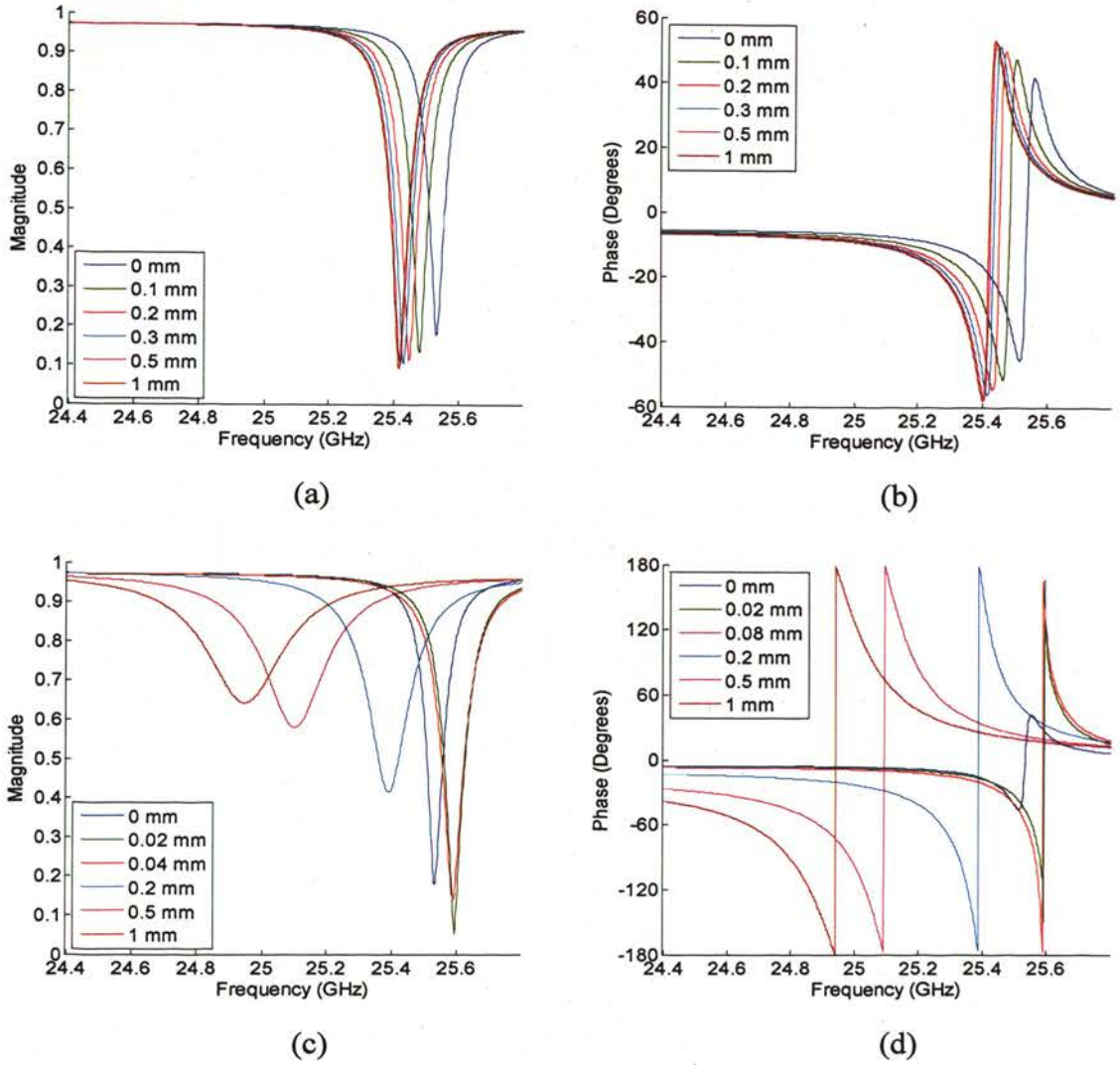

Figure 4.16. Simulated complex reflection coefficient as a function of frequency for pits in aluminum with two diameters and several depths at K-band: a) magnitude and b) phase for pits with diameter of 1 mm and six depths, and c) magnitude and d) phase for pits with diameter of 2 mm and six depths.

value as well, expected since they will only support non-propagating modes. The 1.5, 2, and 2.5 mm-diameter pits also each exhibit non-monotonic behavior with depth for the magnitude at resonance and/or the resonant frequency, as seen in Figures 4.17a-b. The non-monotonic behavior of the resonant frequency could introduce ambiguity in depth evaluation, as mentioned earlier. Figure 4.17c shows that for the 1.5, 2, and 2.5 mm-diameter pits the Q-factor drops as pit depth increases, with larger diameter pits also

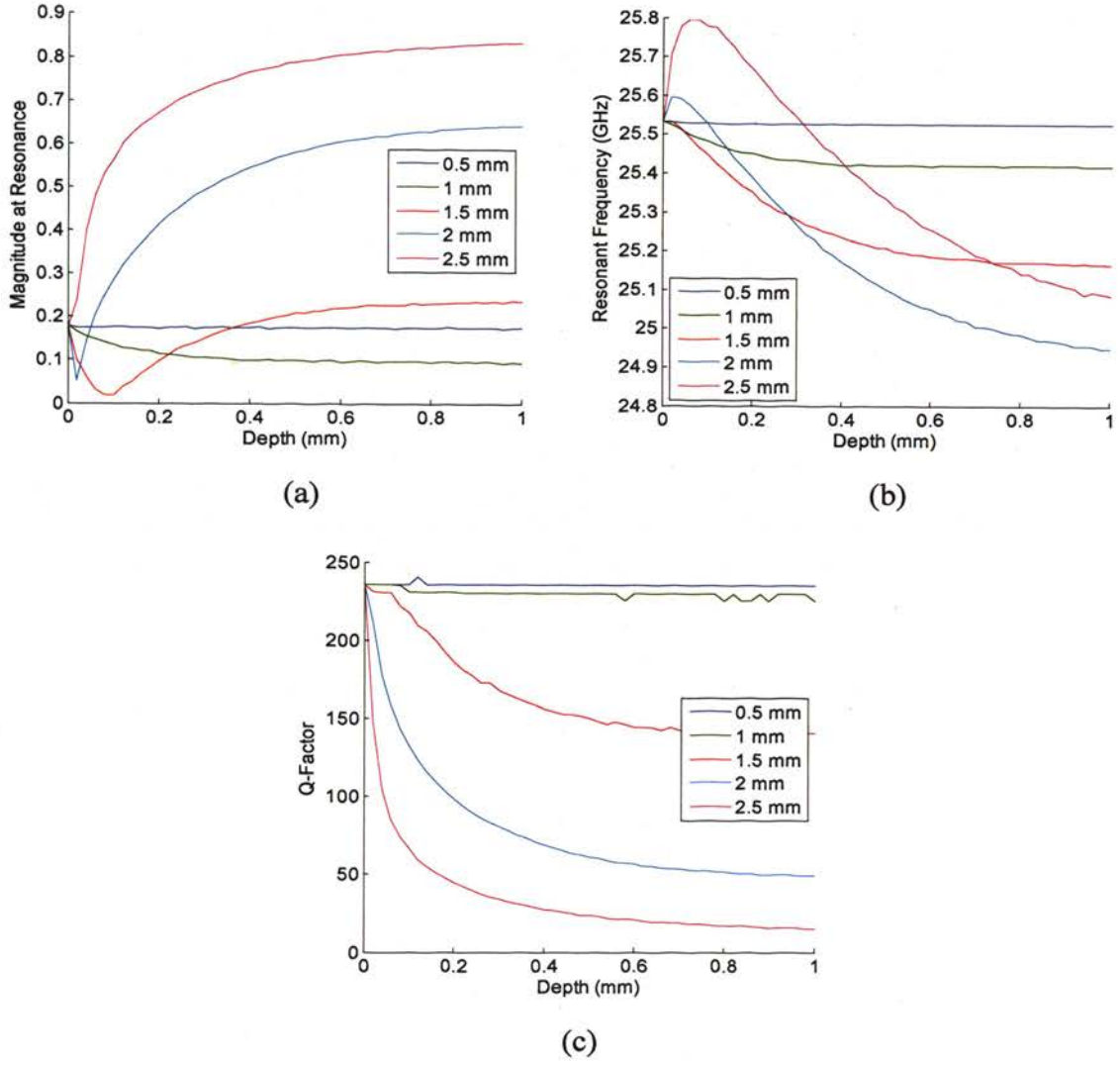

Figure 4.17. Simulated characteristics of resonant response as functions of depth for slab-loaded waveguide probe and pits with five diameters at K-band: a) magnitude at resonant frqeuency, b) resonant frequency, and c) Q-factor.

having lower Q-factors. It is also relatively large, around 230 if no pit is present (depth of zero); compared to a maximum of about 40 for both the empty and filled crack resonators.

Simulations including an offset of the pit 0.2 mm along b from the center of the waveguide showed that two resonances are observed (as for long cracks, see Figure 4.8), and furthermore that the behavior of these two resonances depends on pit diameter.

Figure 4.18 shows the magnitude and phase of reflection coefficient for offset pits with two different diameters, each with six different depths, at K-band. Figures 4.18a-b show that for 1 mm-diameter pits the depth shifts the resonant frequency, as in Figures 4.16a-b, but the shape of the resonant response is also distorted. This distortion is consistent with the interaction of two resonances with resonant frequencies very close to one another.

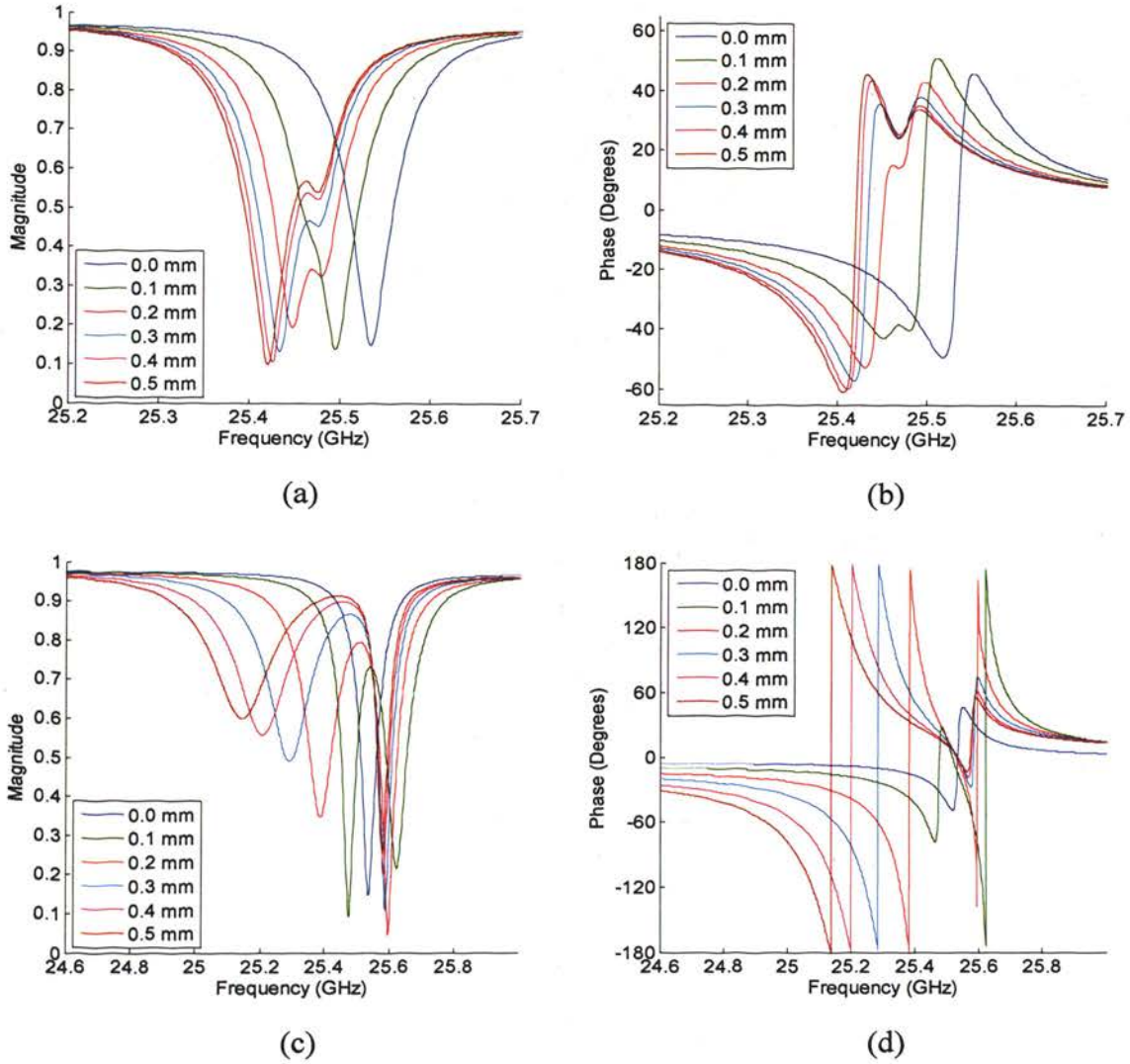

Figure 4.18. Simulated complex reflection coefficient as a function of frequency for pits in a perfect electric conductor with two diameters and six depths at K-band: a) magnitude and b) phase for pits with diameter of 1 mm and c) magnitude and d) phase for pits with diameter of 2 mm. Pits are offset 0.2 mm in the *b* direction from the center of the probe.

Figures 4.18c-d show that two resonant responses are observed for the offset pits with diameter of 2 mm. The resonant frequency of the leftmost (desired) resonance shifts significantly as a function of depth, but the rightmost resonance shifts very little. It is also worth noting that for both diameters the phase to the near-left of the resonances is ordered by depth.

Figure 4.19 shows the phase of reflection coefficient at a single frequency as a function of depth for pits with six diameters, including those in Figures 4.18b and d. Figure 4.19a shows that at 24.5 GHz the phase is clearly related to both depth and diameter for most of the pits. There is no change in the phase as a function of varying depth for the 0.5 mm-diameter pits, as was observed above, and the 1 mm-diameter pits seem to converge to a value around a depth of 0.3 mm. For any other combination of diameter and depth shown in this figure, depth can be uniquely identified using the phase information along with knowledge of the pit diameter. The curves are also sorted by diameter, and for the larger diameter pits the phase depends on depth in a near-linear fashion. Figure 4.19b shows the phase of reflection coefficient for similar conditions to Figure 4.19a, but at a measurement frequency of 25 GHz. A larger change in the phase is

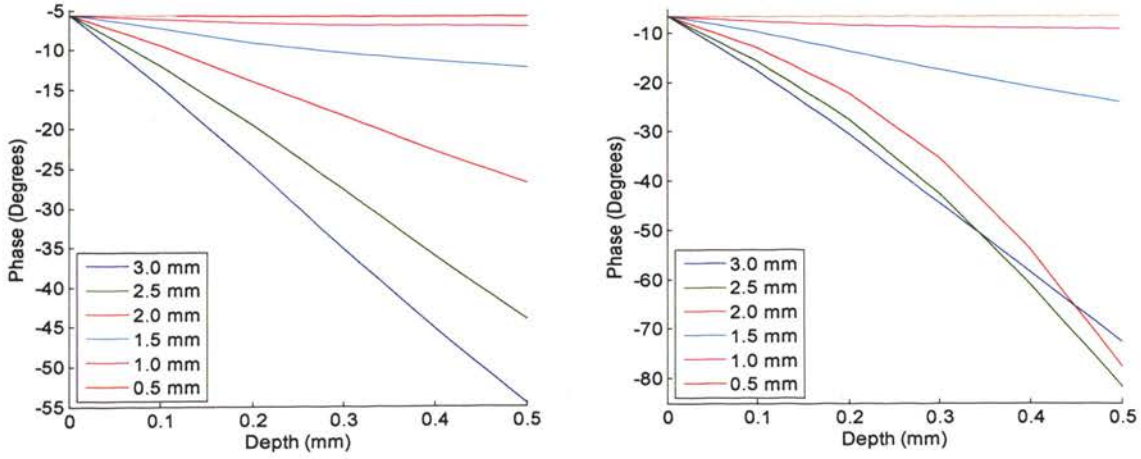

Figure 4.19. Phase of reflection coefficient as a function of pit depth for pits in a perfect electric conductor with six diameters at two frequencies: a) 24.5 GHz and b) 25 GHz (K-band).

observed for this frequency than for 24.5 GHz. However, the effect of diameter is less clear, since the curves are not ordered by diameter for the entire band. This may be due to the interaction of the two resonances, as shown in Figure 4.18. The relationship between phase and depth is also clearly non-linear for the 2 and 2.5 mm-diameter pits. It is apparent from Figures 4.16b and 4.16d that this method could also be applied to pits which are centered in the waveguide.

4.4.2. Measurement Results. A third dielectric insert was machined and used for the following measurements. Figure 4.20 shows the simulated and measured magnitude and phase of reflection coefficient for pits with diameter of 1.02 mm and five depths. A 0.2 mm-offset along *b* from the center of the probe is included in the simulations to simulate variation in the exact position of the probe in measurements. The measured magnitude, shown in Figure 4.20b, has a much wider (lower Q-factor) resonant response than the simulation results shown in Figure 4.20a. Also, there is no second resonance in the measured results, but one is seen in the simulation results. This could indicate that the probe was very well positioned or that the second resonance is outside of the measured frequency band. Regardless, a shift in the resonant frequency is observed and can be related to pit depth. It is also interesting to note that there is a significant variation between the measured 0.24, 0.25 and 0.26 mm curves, which is not expected since the depths are very close and the simulated results show little variation between these three curves. Figures 4.20c-d show the simulated and measured phase for these pits. The simulations show these pits with a smaller phase variation (i.e., undercoupled), but the measurement results show a 360° phase transition (i.e., overcoupled), which allows easier determination of the resonant frequency from phase. The resonant frequencies indicated by the phase are in agreement with those indicated by their respective magnitude measurements. It should also be noted that the phase to the left of the resonances is ordered by depth, for both simulation and measurement.

Figure 4.21 shows the simulated and measured magnitude and phase of reflection coefficient for pits with diameter of 1.52 mm and five depths. A 0.2 mm-offset along *b* from the center of the probe is included in the simulations to simulate variation in the exact position of the probe in measurements. The measured magnitude, shown in Figure 4.21b, again has a much wider (lower Q-factor) resonant response than the simulation

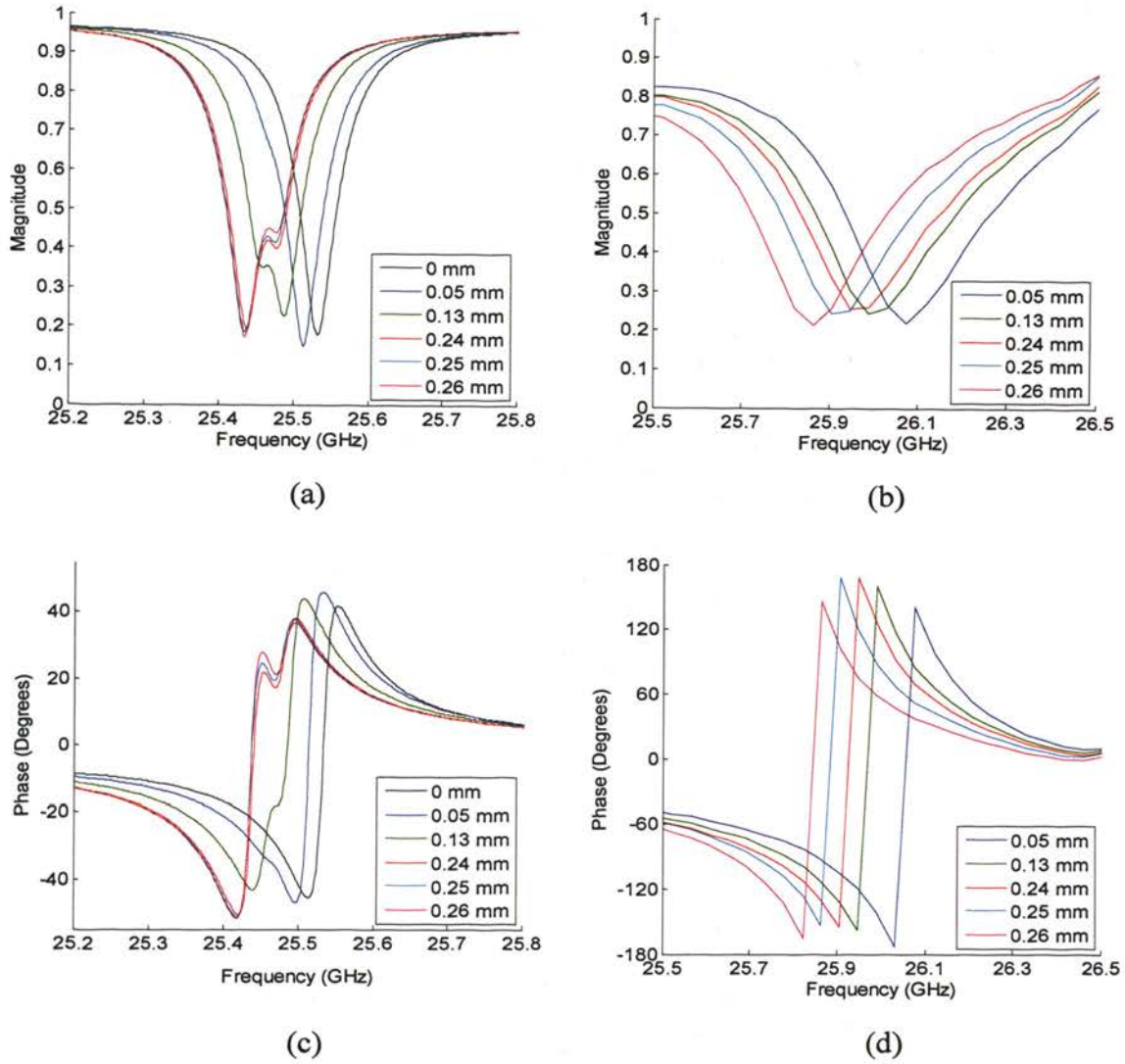

Figure 4.20. Complex reflection coefficient as a function of frequency for slab-loaded waveguide probe and pits in aluminum with diameter of 1.02 mm and five depths at K-band: a) simulated magnitude, b) measured magnitude, c) simulated phase, and d) measured phase. For the simulations the pits are offset 0.2 mm along *b* from the center of the waveguide and an undamaged (depth of zero) case is included for reference.

results shown in Figure 4.21a. Also, as for the 1.02 mm-diameter pits, only one resonance is seen in the measured results, but two are evident in the simulations. Again, this may indicate that the probe was very well positioned or that the second resonance is outside of the measured frequency band. A shift in the resonant frequency is observed which may be related to pit depth. Figures 4.20c-d show the simulated and measured phase for these

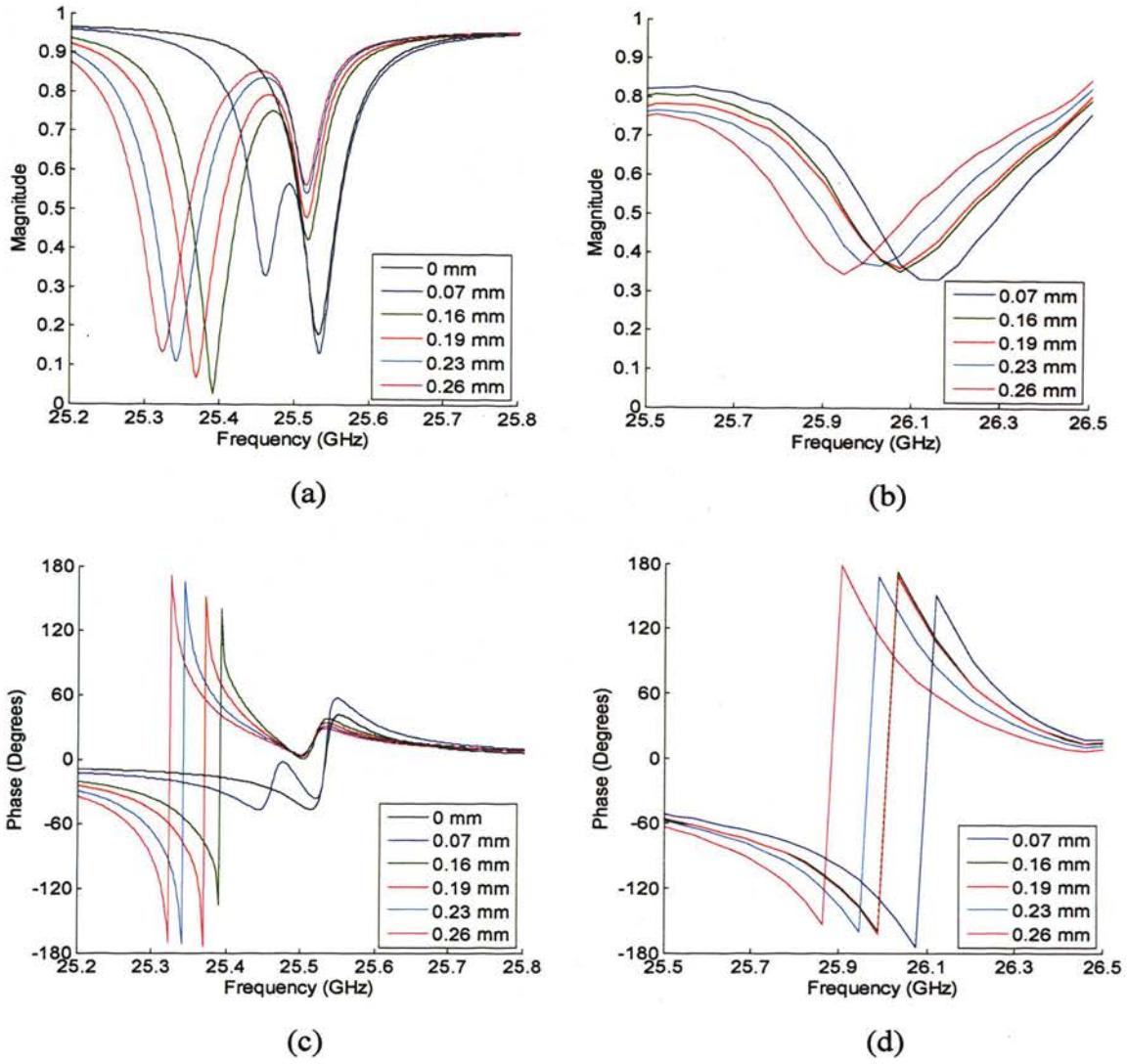

Figure 4.21. Complex reflection coefficient as a function of frequency for slab-loaded waveguide probe and pits in aluminum with diameter of 1.52 mm and five depths at K-band: a) simulated magnitude, b) measured magnitude, c) simulated phase, and d) measured phase. For the simulations the pits are offset 0.2 mm along *b* from the center of the waveguide.

pits. The simulations show that the first resonance is overcoupled and the second resonance in undercoupled (phase transitions of 360° and less than 360°, respectively). The measurement results show an overcoupled situation. The resonant frequencies indicated by the phase are in agreement with those indicated by their respective

magnitude measurements. It is also noted that, once again, the phase to the left of the resonances is ordered by depth for both simulation and measurement.

Figure 4.22 shows the shift of the resonant frequency as a function of depth for the measurements (solid) and simulations (dashed) shown in Figures 4.20a-b and 4.21a-b. For each curve individually the shift is calculated relative to the shallowest pit. If the two deepest pit measurements of the 1.02 mm-diameter curve and the deepest measurement of the 1.52 mm-diameter curve are ignored, then a reasonable match is observed.

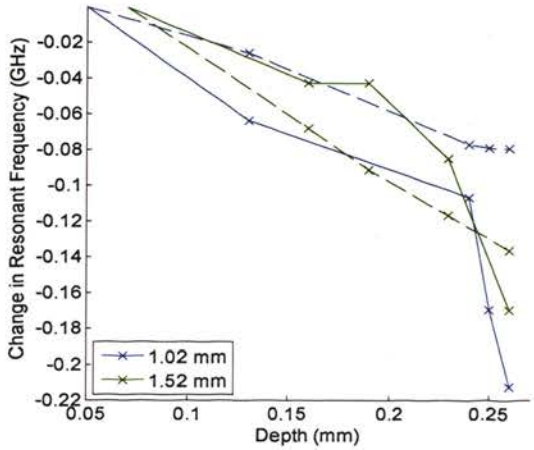

Figure 4.22. Measured (solid) and simulated (dashed) shift of resonant frequency as a function of depth (each curve referenced to its respective shallowest pit) for slab-loaded waveguide probe and pits in aluminum with two diameters at K-band.

A single-frequency phase measurement near the resonance, as shown for simulations in Figure 4.19a-b, may prove to be a more reliable approach for pits than evaluating the resonant frequency. Figure 4.23 shows the phase of reflection coefficient at 25.8 GHz for the measurements shown in Figures 4.20d and 4.21d as well as a set of pits with a diameter of 2.54 mm. Larger depths are clearly associated with greater changes in phase, with a significant change in phase even for small changes in depth. It is also interesting to note that for these measurements the larger diameter pits had a smaller overall change in phase for a similar change in depth, which is in contrast to the simulation results shown in Figure 4.19a. This reversal may be caused by the close

proximity of the measurement frequency to the resonant frequency (consider Figure 4.19b, where the phase change is not fully ordered by diameter for the larger three pit diameters), the multiple resonance behavior of the pits, or some combination of the two.

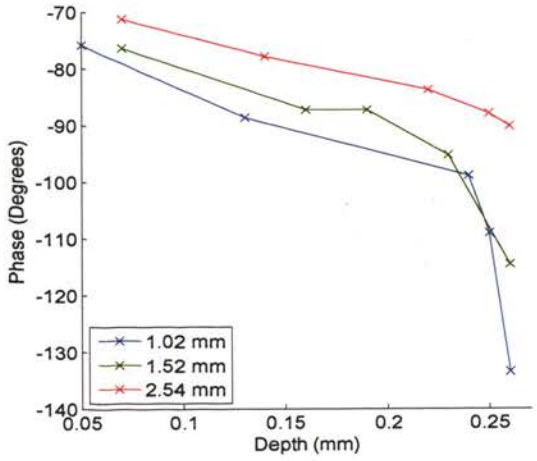

Figure 4.23. Measured phase of reflection coefficient at 25.8 GHz (near resonance) as a function of depth for pits in aluminum with three diameters at K-band.

5. SUMMARY

5.1. EMPTY DAMAGE

It has been shown that a crack, when properly excited (i.e., by a probing rectangular waveguide), can be modeled as a rectangular waveguide. This probing waveguide/crack structure exhibits quarter-wavelength resonance characteristics. Simulation and measurement results showed that the depth of a quarter-wavelength deep short-circuited crack can be evaluated using the measured resonant frequency of the magnitude of reflection coefficient and (2).

Simulations of a lossless case showed that the resonance behavior is evident in only the phase of reflection coefficient. Simulations including conductor losses showed that the magnitude of reflection coefficient may also exhibit resonant behavior if the crack width is small compared to b (e.g., 0.005–0.1 mm at W-band). Variations in the crack width have a significant influence on the resonant frequency, up to 12%, but can be easily corrected for if the crack width is known. Simulations results also indicated that this method is relatively insensitive to relative probe placement.

Simulation results indicated that this approach can be used to evaluate depths of about 1 mm at W-band, and larger depths can be evaluated by using lower frequencies. Measurements were conducted at K-band for cracks with depths of 3-4 mm, and crack depth was estimated to within 20% of the depth measured by micrometer. Relatively large changes in phase (and possibly magnitude) and the use of only the resonant frequency from the reflection coefficient measurements make this approach less sensitive to noise and measurement error than the non-resonant approaches.

A phase change was observed for cracks shallower than a quarter-wavelength, in both simulation and measurement, which is actually the tail end of the resonant response. This phase change may be related to depth for a given crack width and, consequently, could potentially be used for depth evaluation.

Simulations were performed that show that some finite cracks ($a/2 < L < a$) may support propagating modes for some portion of the operating frequency band. It was also shown that if such a mode is supported and the resonant frequency can be evaluated then (2) can be used to estimate depth. For finite cracks with $L < a/2$ a phase change was

observed in simulation that converges to a value as crack depth increases, due to the limited penetration of non-propagating modes into the crack. This phase change may be related to depth if both crack width and length are known and crack depth is less than the maximum signal penetration into the crack. It was also shown that phase, and thus depth evaluation, is sensitive to the position of the crack along a.

Pit measurement results were similar to the smaller finite cracks. Simulation and measurement showed a phase change which converges to a value as depth increases, due to the limited penetration of non-propagating modes. The phase may be related to depth if diameter is known and depth is less than the maximum penetration into the pit. Change in phase due to the presence of pits is small, particularly for small diameters; in such cases the phase may change by only a few degrees.

5.2. FILLED DAMAGE

It was shown that a crack filled with a dielectric material still behaves according to (2) and exhibits a quarter-wavelength resonance. The dielectric filling makes the crack electromagnetically deeper and allows shallower cracks to be evaluated ($D \sim 0.25$ mm at W-band with $\varepsilon_r' = 10$). It was also shown that when the crack is filled with a dielectric material, the resonant frequency may be evaluated from the magnitude of reflection coefficient for a wide range of widths, as a result of the dielectric loss.

For filled cracks, the measurability of the resonance response was considered, and it was found to strongly depend on the loss tangent of the filling material and the crack width. These considerations were described by the coupling between the probing waveguide and crack. The largest magnitude dip was shown to occur near critical coupling and the largest Q-factor near critical coupling or when overcoupled. This is important from the measurement point of view when choosing a filling dielectric material. The filling material (with respect to the relative permittivity) and frequency band should be selected based on the range of depths being evaluated.

The resonant frequency (and thus depth evaluation) was shown to be quite insensitive to crack width and position of the crack within the probing waveguide aperture, and totally insensitive to the loss tangent of the filling material. The error introduced by crack width could be removed with a correction factor if the width is

known. Crack depth evaluation was shown to be very sensitive to the value of relative permittivity of the filling material. Thus, for accurate depth evaluation, the relative permittivity should be known as accurately as possible.

The simulation model was experimentally verified, and measurements over three frequency bands, three dielectric materials, and depths of 0.7–2.7 mm demonstrated the capabilities of this approach to estimate depth. It was also shown that depth can be evaluated using a millimeter wave measurement reflectometer, which is only sensitive to reflected power. Such systems are easier to construct and much less expensive to build or acquire than vector network analyzers.

Resonant frequency of dielectric-filled finite cracks was shown to change less as a result of reductions in the crack length, compared to empty cracks. Dielectric-filled finite cracks were also shown to support propagating modes for smaller lengths. These features allow the quarter-wavelength resonance to be used for a wider range of crack lengths.

Measurements were performed indicating that larger dielectric-filled pits may support propagating modes, and consequently resonate. A shift of the resonant frequency was observed which may be related to the pit depth and, thus, potentially be used for depth evaluation.

5.3. DIELECTRIC SLAB-LOADED WAVEGUIDE PROBE

A dielectric insert was designed and mounted in a K-band waveguide to produce a slab-loaded waveguide probe. This probe was shown to resonate in the absence of damage, and the resonance was shown to evidence reasonable tolerance to the considered geometrical variations in the preparation of the dielectric insert.

A shift of the probe resonance due to the presence of a crack, and related to crack depth, was shown in simulation and measurement. This shift may be used for depth evaluation. It was also shown that the resonance is highly sensitive to probe position and a small offset will cause a second resonance to occur near in frequency to the initial resonance.

The probe was shown to be insensitive to reductions in finite-crack length while $L > a/3$, allowing any such finite cracks to be evaluated in the same manner as "long" cracks.

The probe was shown to be sensitive to pits with diameters of 1 mm or more. A shift of the resonance frequency with respect to depth was observed. A single frequency phase measurement near the resonance was shown allow depth evaluation if the pit diameter was known. Pits were shown to be highly sensitive to probe position, with a shift of the resonant frequency and second resonance resulting from even a small position offset, as was the case for cracks.

5.4. FUTURE WORK

The quarter-wavelength resonance approach for empty cracks may be further developed by additional sensitivity analysis, which may lead to the development of additional correction factors which can improve the accuracy of depth estimation. More accurate measurements of the dielectric permittivity of barium titanate are recommended if additional depth evaluation of cracks filled with that material is intended. Crack evaluation could also be improved by using better packing methods, or better materials for packing. A material with higher permittivity (or permeability) could be used to allow evaluation of shallower depths without the need to increase the operating frequency.

Improvements to the slab-loaded waveguide probe may include redesigning it, or optimizing the current design, for greater sensitivity to damage depth and/or reduced sensitivity to probe position. Techniques could be developed for more accurate positioning of the probe. A more detailed analysis of the electromagnetic behavior of the probe and pits may be beneficial in optimizing this approach; particularly with respect to the excitation of a second resonance (observed when the pit is offset from the center of the probe) and the non-monotonic behavior of the resonant frequency with respect to depth.

Various other approaches presented which do not use the resonant frequency will require the preparation of reference curves, from simulation or measurement, which relate the measured parameter and known damage geometry to depth. Such curves may also be necessary for the resonant frequency of dielectric-filled pits.

All the methods presented could be scaled to higher frequency bands to allow the evaluation of smaller damage (length of finite cracks, diameter of pits, and depth for all cases). Analysis of other damage geometries and the resulting effect on depth evaluation may also be necessary for depth evaluation in practical situations.

BIBLIOGRAPHY

[1] S. K. Burke, "Eddy-Current Inversion in the Thin-Skin Limit: Determination of Depth and Opening for a Long Crack," *Journal of Applied Physics*, vol. 76, no. 5, pp. 3072-3080, 1994.

[2] H. Huang, N. Sakurai, T. Takagi and T. Uchimoto, "Design of an Eddy-Current Array Probe for Crack Sizing in Steam Generator Tubes," *NDT & E International*, vol. 36, no. 7, pp. 515-522, 2003.

[3] S.I. Rokhlin and J.-Y. Kim, "In Situ Monitoring of Surface Fatigue Crack Initiation and Growth from Surface Cavity," *International Journal of Fatigue*, vol. 25, no. 1, pp. 41-49, 2003.

[4] X. Jian, S. Dixon, N. Guo, R.S. Edwards and M. Potter, "Pulsed Rayleigh Wave Scattered at Surface Crack," *Ultrasonics*, vol. 44, Supplement 1, pp. e1131-e1134, 2006.

[5] M.P. Connolly, D.H. Michael and R. Collins, "The Inversion of Surface Potential Measurements to Determine Crack Size and Shape," *Journal of Appied. Physics*, vol. 64, no. 5, pp. 2638-2647, 1988.

[6] Y. Ju, M. Saka and Y. Uchimura, "Evaluation of the Shape and Size of 3D Cracks Using Microwaves," *NDT & E International*, vol. 38, no. 8, pp. 726-731, 2005.

[7] N. Wang and R. Zoughi, "Moment Method Solution for Modeling the Interaction of Open-Ended Coaxial Probes and Surface Cracks in Metals," *Materials Evaluation*, vol. 60, no. 10, pp. 1253–1258, 2002.

[8] Y. Wang and R. Zoughi, "Interaction of Surface Cracks in Metals with Open-Ended Coaxial Probes at Microwave Frequencies," *Materials Evaluation*, vol. 58, no. 10, pp. 1228–1234, 2000.

[9] K. Krzywosz, "Multivariate Regression Algorithm for ID Pit Sizing," *IV Conferencia Panamericana de END April 2007*, Buenos Aires, pp. 1-9, Oct. 2007.

[10] W. Harara, "Pit-Depth Measurement on Large Diameter Pipes by Tangential Radiography Using a Co-60 Gamma-Ray Source," *Russian Journal of Nondestructive Testing*, vol. 40, no. 11. pp. 782-788, 2004.

[11] P.J. Shull, *Nondestructive Evaluation: Theory, Techniques, and Applications*, Marcel Dekker, 2002.

[12] S. Kharkovsky and R. Zoughi, "Microwave and Millimeter Wave Nondestructive Testing and Evaluation, Overview and Recent Advances," *IEEE Instrumentation and Measurement Magazine*, pp. 26-38, April 2007.

[13] R. Zoughi, *Microwave Non-Destructive Testing and Evaluation*, Kluwer Academic Publishers, pp. 123-208, 2000.

[14] A. Bahr, *Microwave Nondestructive Testing Methods*, Gordon and Breach Science Publishers, 1982.

[15] C. Yeh and R. Zoughi, "A Novel Microwave Method for Detection of Long Surface Cracks in Metals," *IEEE Transactions on Instrumentation and Measurement,* vol. 43, no. 5, pp. 719-725, 1994.

[16] C. Yeh and R. Zoughi, "Microwave Detection of Finite Surface Cracks in Metals using Rectangular Waveguide Sensors," *Research in Nondestructive Evaluation*, vol. 6, pp. 35-55, 1994.

[17] C. Yeh, E. Ranu and R. Zoughi, "A Novel Microwave Method for Surface Crack Detection using Higher Order Waveguide Modes," *Materials Evaluation*, vol. 52, pp. 676-681, 1994.

[18] C. Yeh and R. Zoughi, "Sizing Technique for Slots and Surface Cracks in Metals," *Materials Evaluation*, vol. 53, pp. 496-501, 1995.

[19] S.I. Ganchev, R. Zoughi, C. Huber, R.J. Runser and E. Ranu, "Microwave Method for Locating Surface Slot/Crack Tips in Metals," *Materials Evaluation*, vol. 54, pp. 598-603, 1996.

[20] C. Huber, H. Abiri, S.I. Ganchev and R. Zoughi, "Analysis of the 'Crack Characteristic Signal' using a Generalized Scattering Matrix Representation," *IEEE Transactions on Microwave Theory and Techniques*, vol. 45, pp. 477-484, 1997.

[21] C. Huber, H. Abiri, S. Ganchev and R. Zoughi, "Modeling of Surface Hairline Crack Detection in Metals Under Coatings using Open-Ended Rectangular Waveguides," *IEEE Transactions on Microwave Theory and Techniques*, vol. 45, pp. 2049-2057, 1997.

[22] N. Qaddoumi, E. Ranu, J.D. McColskey, R. Mirshahi, and R. Zoughi, "Microwave Detection of Stress Induced Fatigue Cracks in Steel and Potential for Crack Opening Determination," *Research in Nondestructive Evaluation*, vol. 12, pp. 87-103, 2000.

[23] F. Mazlumi, S.H.H. Sadeghi, R. Moini, "Interaction of Rectangular Open-Ended Waveguides with Surface Tilted Long Cracks in Metals," *IEEE Transactions on Instrumentation and Measurement*, vol. 55, pp. 2191 – 2197, 2006.

[24] R. Zoughi, and S. Kharkovsky, "Microwave and Millimeter Wave Sensors for Crack Detection," *Fatigue & Fracture of Engineering Materials & Structures*, vol. 31, no. 8, pp. 695-713, 2008.

[25] H.H. Park, Y.H. Cho and H.J. Eom, "Surface Crack Detection Using Flanged Parallel-Plate Waveguide," *Electronics Letters*, vol. 37, pp. 1526 – 1527, 2001.

[26] F. Mazlumi, S.H.H. Sadeghi and R. Moini, "Interaction of an Open-Ended Rectangular Waveguide Probe With an Arbitrary-Shape Surface Crack in a Lossy Conductor," *IEEE Transactions on Microwave Theory and Techniques*, vol. 54, no. 10, pp. 3706-3711, 2006.

[27] J. Kerouedan, P. Queffelec, P. Talbotl, C. Quendo, S. De Blasi and A. Le Brun, "Detection of Micro-Cracks on Metal Surfaces using Near-Field Microwave Dual-Behavior Resonator Filters," *Measurement Science and Technology*, vol. 19, no. 10, pp. 105701, 10 pages, 2008.

[28] H. Shirai and H. Sekiguchi, "A Simple Crack Depth Estimation Method from Backscattering Response," *IEEE Transactions on Instrumentation and Measurement*, vol. 53, pp. 1249-1254, 2004.

[29] A.D. McClanahan, E.A. Nanni, A.R. Maxon, M.T. Ghasr, S. Kharkovsky, R. Zoughi and D. Palmer, Jr., "Millimeter Wave Depth and Opening Characterization of Surface Damage in Fuselage Skins," *Review of Progress in Quantitative Nondestructive Evaluation Vol. 28A,* Chicago, IL, July 21- July 25, 2008, vol. 1096, AIP Conference Proceedings, edited by D.O. Thompson and D.E. Chimenti, American Institute of Physics, Melville, NY, 2009, pp. 394-401.

[30] M. Ghasr, S. Kharkovsky, R. Zoughi and R. Austin, "Comparison of Near-Field Millimeter Wave Probes for Detecting Corrosion Pit under Paint," *Intrumentation and Measurement Technology Conference May 2004 (IMTC 2004)*, pp. 2240-2244.

[31] D. Hughes, R. Zoughi. R. Austin. N. Wood and R. Engelbart, "Near-Field Microwave Detection of Corrosion Precursor Pitting under Thin Dielectric Coatings in Metallic Substrates," *Proceedings of the Twenty-ninth Annual Review of Progress in Quantitative Nondestructive Evaluation*, vol. 22B, Bellingham, WA, July 14-19, 2002, pp. 462-469.

[32] M. Ghasr, B. Carroll, S. Kharkovsky, R. Zoughi and R. Austin, "Size Evaluation of Corrosion Precursor Pitting using Near-Field Millimeter Wave nondestructive Testing Methods," *Review of Quantitative Nondestructive Evaluation*, vol. 24, pp. 547-553, 2005

[33] M. Ghasr, B. Carroll, S. Kharkovsky, R. Zoughi and R. Austin, "Millimeter Wave Differential Probe for Nondestructive Detection of Corrosion Precursor Pitting," *IEEE Transactions on Instrumentation and Measurement*, vol. 55, no. 5, pp.1620-1627, 2006.

[34] D.M. Pozar, *Microwave Engineering, Third Ed.* Hoboken, NJ: John Wiley & Sons, Inc., 2005, pp. 106-111, 123-124, 269, 271, 275-276, 279-281, 292, 341.

[35] R.W. Beatty and B.C. Yates, "A Graph of Return Loss Versus Frequency for Quarter-Wavelength Short-Circuited Waveguide Impedance Standards," *IEEE Transactions on Microwave Theory and Techniques*, vol. 17, pp. 282-284, 1969.

[36] N. Marcuvitz, *Waveguide Handbook.* London, UK: Peter Peregrinus Ltd., 1951, pp. 307-309.

[37] C.G. Montgomery, R.H. Dicke and E.M. Purcell, *Principles of Microwave Circuits*. London, UK: Peter Peregrinus Ltd., 1987, pp. 187-189.

[38] J. Krupka, J. Breeze, A. Centeno, N. Alford, T. Claussen and L. Jensen, "Measurement of Permittivity, Dielectric Loss Tangent, and Resistivity of Float-Zone Silicon at Microwave Frequencies," *IEEE Transactions on Microwave Theory and Techniques,* vol. 54, no. 11, pp. 3995-4001, 2006.

[39] X. Chen, G. Wang, Y. Duan and S. Liu, "Microwave Absorption Properties of Barium Titanate/Epoxide Resin Composites," *Journal of Physics D: Applied Physics*, vol. 40, pp. 1827-1830, 2007.

[40] M.P. McNeal, S.J. Jang and R.E. Newnham, "Particle Size Dependent High Frequency Dielectric Properties of Barium Titanate," *Proceedings of the Tenth IEEE International Symposium on Applications of Ferroelectrics, 1996 (ISAF '96)*, vol. 2, pp. 837-840, 1996.

[41] K. Bois, L. Handjojo, A. Benally, K. Mubarak and R. Zoughi, "Dielectric Plug-Loaded Two-Port Transmission Line Measurement Technique for Dielectric Property Characterization of Granular and Liquid Materials," *IEEE Transactions on Instrumentation and Measurement*, vol. 48, no. 6, pp. 1141-1148, 1999.

[42] K. Mubarak, "Determination of Fresh Concrete Water–to–Cement (w/c) Ratio using Monopole Probes at Microwave Frequencies," M.S. thesis, Department of Electrical and Computer Engineering, Colorado State University, Fort Collins, Colorado, 1999.

[43] H.P. Schwan and K.R. Foster, "Microwave Dielectric Properties of Tissue," *Biophysical Journal*, vol. 17, pp. 193-197, 1977.

[44] N.I. Furashov, V.E. Dudin, and B.A. Sverdlov, "Study of the Dielectric Properties of Water in the Frequency Range 75–120 GHz," *Radiophysics and Quantum Electronics*, vol. 49, no. 6, pp. 442-452, 2006.

[45] G. Brooker, R. Hennessey, C. Lobsey, M. Bishop, and E. Widzyk-Capehart, "Seeing through Dust and Water Vapor: Millimeter Wave Radar Sensors for Mining Applications," *Journal of Field Robotics*, vol. 24, no. 7, pp. 527-557, 2007.

[46] *TMM® Thermoset Microwave Materials Data Sheet*, Rogers Corporation, Chandler, AZ, 2008.

VITA

Andrew Dale McClanahan was born in St. Louis County, in Missouri on December 26, 1984. He received his BSEE at the University of Missouri – Rolla (now Missouri University of Science and Technology). At UMR, Andrew worked as an undergraduate research assistant at the Applied Microwave Nondestructive Testing Laboratory (*amntl*). He also worked as a student intern with the Nondestructive Testing Group at Marshall Space Flight Center in Huntsville, AL.

Andrew has continued working with *amntl* at the Missouri University of Science and Technology while pursuing his MSEE degree, and received the Chancellor's Fellowship. He received his Masters of Science Degree in Electrical Engineering from the Missouri University of Science and Technology in July 2009.

Andrew enjoys singing and playing the guitar, strategy board games, and studying the Bible.